

(NASA-CR-167990-VOL-1) ANALYTICAL MODELING
OF OPERATING CHARACTERISTICS OF
PREMIXING-PREVAPOORIZING FUEL-AIR MIXING
PASSAGES. VOLUME 1: ANALYSIS AND RESULTS
Final Report (United Technologies Research

883-12353

Unclass
01054

G3/54

NASA CR-167990
R82-915362-40

Analytical Modeling of Operating Characteristics of Premixing-Prevaporizing Fuel-Air Mixing Passages

Vol. I Analysis and Results

Olof L. Anderson
Louis M. Chiappetta
David E. Edwards
John B. McVey



February 1982

Prepared for
NASA Lewis Research Center
Under Contract NAS3-21269

1. Report No.	2. Government Accession No.	3. Recipient's Catalog No.	
4. Title and Subtitle Analytical Modeling of Operating Characteristics of Premixing-Prevaporizing Fuel-Air Mixing Passages		5. Report Date February 1982	
		6. Performing Organization Code	
7. Author(s) O. L. Anderson, L. M. Chiappetta D. E. Edwards, J. B. McVey		8. Performing Organization Report No. R82-915362-40	
		10. Work Unit No.	
9. Performing Organization Name and Address United Technologies Research Center Silver Lane East Hartford, CT 06108		11. Contract or Grant No. NAS3-21269	
		13. Type of Report and Period Covered Final Report (Volume I) User's Manual (Volume II)	
12. Sponsoring Agency Name and Address NASA Lewis Research Center 21000 Brookpark Road Cleveland, OH 44135		14. Sponsoring Agency Code	
15. Supplementary Notes NASA Project Manager - C. J. Marek UTRC Project Manager - O. L. Anderson			
16. Abstract A model for predicting the distribution of liquid fuel droplets and fuel vapor in pre-mixing-prevaporizing fuel-air mixing passages of the direct injection type is reported herein. This model consists of three computer programs; a calculation of the two-dimensional or axisymmetric air flow field neglecting the effects of fuel a calculation of the three-dimensional fuel droplet trajectories and evaporation rates in a known, moving air flow; a calculation of fuel vapor diffusing into a moving three-dimensional air flow with source terms dependent on the droplet evaporation rates. The fuel droplets are treated as individual particle classes each satisfying Newton's law, a heat transfer, and a mass transfer equation. This fuel droplet model treats multi-component fuels and incorporates the physics required for the treatment of elastic droplet collisions, droplet shattering, droplet coalescence and droplet wall interactions. The vapor diffusion calculation treats three dimensional, gas-phase, turbulent diffusion processes. The analysis includes a model for the autoignition of the fuel-air mixture based upon the rate of formation of an important intermediate chemical species during the pre-ignition period. This species is produced both within the vicinity of the fuel droplets and throughout the diffusing fuel vapor-air mixture. The model, as represented by these computer codes, is applied to two premixing fuel-air mixing passage designs and the results are discussed. An application of the autoignition model is also presented.			
17. Key Words (Suggested by Author(s)) Premixing-Prevaporizing Passages Autoignition Model Two-phase Flow Two- and Three-Dimensional Flow Models Computer Program		18. Distribution Statement	
19. Security Classif. (of this report) Unclassified	20. Security Classif. (of this page) Unclassified	21. No. of Pages 143	22. Price*

Analytical Modeling of Operating Characteristics of
Premixing-Prevaporizing Fuel-Air Mixing Passages

Volume I - Analysis and Results

TABLE OF CONTENTS

	<u>Page</u>
1.0 SUMMARY.	1
2.0 INTRODUCTION	2
3.0 ANALYSIS OF AXISYMMETRIC AIRFLOW	4
3.1 General Approach.	4
3.2 Coordinate System	5
3.3 Equations of Motion	7
3.4 Turbulence Model.	9
3.5 Numerical Methods	14
3.6 References.	15
3.7 List of Symbols	17
4.0 ANALYSIS OF FUEL DROPLET BEHAVIOR.	19
4.1 General Approach.	19
4.2 Momentum Equations.	20
4.3 Heat and Mass Transfer Equations.	22
4.4 Evaluation of Thermodynamic and Transport Properties.	25
4.5 Evaluation of Distillate Fuel Effects	31
4.6 High Pressure Effects	34
4.7 Droplet Class and Distribution Functions.	37
4.8 Droplet Collision Model	41
4.9 Droplet Shattering Model.	49
4.10 Droplet-Solid Boundary Interaction Model.	51
4.11 Numerical Methods	53
4.12 References.	54
4.13 List of Symbols	57
4.14 Tables.	61
4.15 Figures	62

TABLE OF CONTENTS (Cont'd)

	<u>Page</u>
5.0 ANALYSIS OF DIFFUSION OF FUEL VAPOR.	68
5.1 General Approach.	68
5.2 Fuel Vapor Diffusion Equation	69
5.3 Numerical Methods	70
5.4 References.	72
5.5 List of Symbols	73
6.0 COMPUTER MODEL CALIBRATION	74
6.1 Calibration of Fuel Droplet Model	74
6.2 Model Sensitivity Study	76
6.3 Calibration of Vapor Diffusion Model.	79
6.4 References.	80
6.5 Tables.	81
6.6 Figures	83
7.0 PARAMETRIC STUDIES	88
7.1 Swirl Tube Premixing Passage.	88
7.2 Series Staged Premixing Passage	90
7.3 Reference	91
7.4 List of Symbols	92
7.5 Figures	93
8.0 ANALYSIS OF AUTOIGNITION	102
8.1 General Approach	102
8.2 Basic Equations	103
8.3 Autoignition Models	105
8.4 Numerical Methods	110
8.5 Results and Discussion	111
8.6 References	113
8.7 List of Symbols	114
9.0 CONCLUDING REMARKS	120
APPENDIX A - LITERATURE SURVEY	122

Analytical Modeling of Operating Characteristics of
Premixing-Prevaporizing Fuel-Air Mixing Passages

Volume I - Analysis and Results

1.0 SUMMARY

A model for predicting the distribution of liquid fuel droplets and fuel vapor in premixing-prevaporizing fuel-air mixing passages of the direct injection type is reported herein. This model consists of three computer programs: a calculation of the two-dimensional or axisymmetric air flow field neglecting the effects of fuel; a calculation of the three-dimensional fuel droplet trajectories and evaporation rates in a known, moving air flow; and a calculation of fuel vapor diffusing into a moving three-dimensional air flow with source terms dependent on the droplet evaporation rates. The air flow calculation can treat compressible swirling flows in arbitrary ducts with arbitrary pressures, temperatures and velocities as initial conditions. The fuel droplets are treated as individual particle classes each satisfying Newton's law, a heat transfer, and a mass transfer equation. Each particle class has a number density such that summation over all particle classes yields the fuel flow rate. This fuel droplet model treats multicomponent fuels and incorporates the physics required for the treatment of elastic droplet collisions, droplet shattering, droplet coalescence and droplet wall interactions. The vapor diffusion calculation treats three-dimensional, gas-phase, turbulent diffusion processes with the turbulence level determined by the air flow calculation and the source terms determined by the droplet evaporation rates.

The analysis includes a model for the autoignition of the fuel-air mixture based upon the rate of formation of an important intermediate chemical species during the pre-ignition period. This species is produced both within the vicinity of the fuel droplets and throughout the diffusing fuel vapor-air mixture. Since chemical reaction rates may depend upon the local mixture temperature, the local mixture temperature is adjusted for the effect of fuel evaporation.

A preliminary calibration of the computer codes and a parametric study showing the effects of the air flow conditions and initial droplet conditions on the evaporation rate are included. The model, as represented by these computer codes, is applied to two premixing fuel-air mixing passage designs and the results are discussed. An application of the autoignition model is also presented.

2.0 INTRODUCTION

One combustion control strategy for meeting Governmental regulations on emissions of pollutants from internal combustion engines which has recently received considerable attention is the use of the premixing, prevaporizing combustion concept whereby uniform, homogeneous fuel-air mixtures are delivered to the combustion chamber in such proportions that the gas temperature-time history permits complete oxidation of the hydrocarbon fuel but does not permit significant production of the oxides of nitrogen. Methods of achieving premixed, prevaporized fuel-air mixtures include external vaporization schemes whereby the fuel is vaporized before being mixed with air and direct injection of a finely atomized spray into the airstream. This effort is concerned with the prediction of the distribution of liquid and vapor fuel produced by the direct injection method.

Distribution of the liquid fuel throughout an airstream is primarily effected through the use of multi-point fuel injection, by imparting velocity components to the fuel droplets which are normal to the airstream velocity components, and by turbulent diffusion of the fuel throughout the airstream. Vaporization of the spray is achieved by heat transfer from the airstream to the droplets and mass transfer of fuel vapor from the droplet surface to the droplet environment. Knowledge of the magnitude of the vaporization time is of particular concern in the case of gas turbine engines wherein fuel is injected into high temperature compressor discharge air due to the requirements that the vaporization time be significantly less than the autoignition time of the fuel-air mixture and that the required passage length be consistent with engine dimension limits. From a design point of view, what is required is an analytical procedure whereby the atomization and initial distribution characteristics which a given fuel injection system will deliver can be evaluated in terms of the fuel distribution and degree of vaporization which can be achieved within a given mixer/vaporizer section length.

For prevaporizing premixing fuel-air passages, autoignition must be prevented because the uncooled engine hardware in this duct can undergo catastrophic failure as a result of the sudden large heat release following autoignition. Clearly, exploitation of the concept requires that the residence time within the fuel preparation passage be long enough to achieve essentially complete vaporization and yet short enough to preclude the occurrence of autoignition. An analysis is required, therefore, to predict if autoignition occurs in premixing passages at simulated gas turbine engine operating conditions.

This report describes the analytical models which were developed to predict the operating characteristics of premixing-prevaporizing fuel-air mixing passages of the direct injection type. The technical approach adopted for developing these models is to separate the problem into three parts each with its own computer code. These three parts are: calculation of the two-dimensional or axisymmetric gas flow field (ADD code), calculation of the three dimensional nonequilibrium heating and

vaporization of the fuel droplets (PTRAK code), and calculation of the three-dimensional turbulent diffusion of fuel vapor in air (VAPDIF code). In applying this approach, it is implicitly assumed that the air flow behavior can affect the fuel droplet behavior, but the fuel droplet behavior does not affect the air flow behavior. This is justified because the mass fraction of fuel droplets and fuel vapor is small. Similarly, it is assumed that the fuel droplet behavior affects the fuel vapor behavior but the fuel vapor behavior does not affect the fuel droplet behavior. This decoupling (or weak interaction) assumption of the problem allows a much simpler solution wherein the air flow behavior, fuel droplet behavior, and vapor diffusion can be analyzed in succession.

This report also describes a model for predicting autoignition in two-phase turbulent flows. It is assumed in the model that autoignition is determined by the rate of formation of an intermediate chemical species, it is also assumed that production of this species has a negligible effect on fuel vapor concentration. Sources of this species are calculated by the PTRAK code within the vicinity of the fuel droplets; additional sources are calculated by the VAPDIF computer program as the fuel vapor diffuses throughout the premixing passage. These sources are then used in the VAPDIF code to determine the local concentration of the rate-controlling species. A criterion is applied to determine if autoignition of the fuel-air mixture has occurred.

Some chemical reaction rates are functions of the local gas temperature. A first-order correction is made to the temperature distribution due to evaporation of the fuel prior to determination of the local rate of production of the intermediate species. Consistent with the weak interaction assumption described earlier, the effect of this temperature correction on the flow field or vaporization rate is assumed to be negligible.

The model, composed of the three computer programs, 1) treats the three dimensional behavior of the fuel droplets and fuel vapor in a moving gas stream, 2) represents a reasonable compromise between rigor and empiricism, and 3) yields practical results with a reasonable expenditure of computer time. This report describes the analytical models incorporated into the computer codes and presents the results of a preliminary calibration of the models, a sensitivity study, and an analysis of two premixing passage designs that illustrate the features of the analytical models incorporated into the computer programs. An application of the autoignition model is also presented.

3.0 ANALYSIS OF AXISYMMETRIC AIRFLOW

3.1 General Approach

The ADD code was developed to solve the internal flow weak interaction problem using a forward marching numerical procedure that does not require an interaction between the inviscid core flow described by the elliptic Euler equations and the wall boundary layers described by the parabolic boundary layer equations. The basic mathematical description and justification of the technical approach is given by Anderson (Ref. 3.1). A more detailed derivation and description of the various features of the computer code is given in Ref. 3.2. Applications of the computer code are given in Refs. 3.3 and 3.4.

This method can be described in the following manner. First, an orthogonal coordinate system is constructed for the duct from the potential flow solution such that the stream function forms the coordinate normal to the wall and the velocity potential forms the coordinate tangent to the wall. Since the potential flow streamlines approximate the real streamlines, the equations of motion may be greatly simplified by assuming that the velocity normal to the potential flow streamlines is small compared to the streamwise velocity. This procedure reduces the governing viscous flow equations to a parabolic system of partial differential equations which can be solved by a forward marching numerical integration procedure. Furthermore, it can be shown (Ref. 3.1) that the resulting solution has the same order of accuracy for viscous flows as the streamline curvature method has for inviscid flows. Thus, the inviscid-flow weak interaction with the wall boundary layer is solved without the need for iterations between different flow fields; i.e., the inviscid core flow and the boundary layer flow.

Symbols used in this section are defined on pages 17-18.

3.2 Coordinate System

The equations of motion are solved in a streamline orthogonal coordinate system (n, s, ϕ) . This coordinate system is generated by first solving for the plane potential flow through a duct with the same cross-section that the annular duct makes with the meridional plane. The normal coordinate n is the stream function and the streamwise coordinate s is the velocity potential. Rotation about the axis of symmetry produces an axisymmetric orthogonal coordinate system uniquely suited to solve the problem.

The (n, s) coordinates are related to the physical coordinates (r, z) through Laplace's equation.

$$\frac{\partial^2 n}{\partial r^2} + \frac{\partial^2 n}{\partial z^2} = 0 \quad (3.2.1)$$

$$\frac{\partial^2 s}{\partial r^2} + \frac{\partial^2 s}{\partial z^2} = 0 \quad (3.2.2)$$

The metric scale coefficients are the same in both directions and are equal to the inverse of the magnitude of the potential flow velocity.

$$v^2 = \left(\frac{\partial n}{\partial r}\right)^2 + \left(\frac{\partial n}{\partial z}\right)^2 = \left(\frac{\partial s}{\partial r}\right)^2 + \left(\frac{\partial s}{\partial z}\right)^2 \quad (3.2.3)$$

Lengths along the streamlines and potential lines are given by

$$dx = ds/v \quad (3.2.4)$$

$$dy = dn/v \quad (3.2.5)$$

and curvatures of streamlines and potential lines are given by

$$\frac{1}{r_s} = \frac{\partial V}{\partial n} \quad (3.2.6)$$

$$\frac{1}{r_n} = \frac{\partial V}{\partial s} \quad (3.2.7)$$

If the duct wall contours $r_w(z)$ are specified, Eqs. (3.2.1) and (3.2.2) are solved using the complex potential and the Schwartz-Christoffel transformation (Ref. 3.5) using the method described in Ref. 3.1).

3.3 Equations of Motion

The ADD code equations, given below, are written in an orthogonal streamline coordinate system where n is the normal coordinate (potential flow stream function) and s is the streamwise coordinate (potential flow velocity potential). The metric scale coefficient is the same in both the n and s directions and is equal to $(1/V)$ where V is the magnitude of the potential flow velocity.

$$\frac{\partial \psi}{\partial n} = \frac{r \rho U_s}{V} \quad (3.3.1)$$

$$\frac{V}{r} \frac{\partial \psi}{\partial n} \frac{\partial U_s}{\partial s} - \frac{V}{r} \frac{\partial \psi}{\partial s} \frac{\partial U_s}{\partial n} - \frac{\rho U_s^2}{r} \frac{\partial r}{\partial s} + \frac{\partial P}{\partial s} = \frac{V}{r} \frac{\partial}{\partial n} \left(\frac{r \tau_{ns}}{V} \right) - \left(\frac{\tau_{ns}}{V} \right) \frac{\partial V}{\partial n} \quad (3.3.2)$$

$$\frac{V}{r} \frac{\partial \psi}{\partial n} \frac{\partial U_\phi}{\partial s} - \frac{V}{r} \frac{\partial \psi}{\partial s} \frac{\partial U_\phi}{\partial n} + \rho \frac{U_s U_\phi}{r} \frac{\partial r}{\partial s} = \frac{V}{r} \frac{\partial}{\partial n} \left(\frac{r \tau_{n\phi}}{V} \right) + \frac{\tau_{n\phi}}{r} \frac{\partial r}{\partial n} \quad (3.3.3)$$

$$\rho U_s^2 \frac{\partial V}{\partial n} - V \rho \frac{U_\phi^2}{r} \frac{\partial r}{\partial n} + V \frac{\partial P}{\partial n} = 0 \quad (3.3.4)$$

$$T \frac{V}{r} \frac{\partial \psi}{\partial n} \frac{\partial I}{\partial s} - T \frac{V}{r} \frac{\partial \psi}{\partial s} \frac{\partial I}{\partial n} = V \frac{\partial}{\partial n} \left(\frac{r q_n}{V} \right) + \frac{\tau_{ns}^2 + \tau_{n\phi}^2}{\mu_E} \quad (3.3.5)$$

$$\tau_{ns} = \mu_E \frac{\partial}{\partial n} (V U_s) \quad (3.3.6)$$

$$\tau_{n\phi} = \mu_E \frac{\partial}{\partial n} \left(\frac{U_\phi}{r} \right) \quad (3.3.7)$$

$$q_n = C_p \frac{\mu_E}{Pr} V \left(\frac{\partial T}{\partial n} \right) \quad (3.3.8)$$

$$P = \rho R T \quad (3.3.9)$$

$$I - I_0 = C_p \ln(T/T_0) - R \ln(P/P_0) \quad (3.3.10)$$

Equations (3.3.1) through (3.3.10) form a set of eight first order partial differential equations and two algebraic equations which may be used to solve for ten unknowns. The boundary conditions for this problem are given by

$$U_s(0,s)=0$$

$$U_\phi(0,s)=0$$

$$q_n(0,s)=0 \quad (3.3.11)$$

$$\psi(0,s)=0$$

for the ID wall and

$$U_s(1,s)=0$$

$$U_\phi(1,s)=0$$

$$q_n(1,s)=0$$

$$\psi(1,s)=\psi(1)$$

(3.3.12)

for the OE wall.

3.4 Turbulence Model

Three turbulence models have been programmed into the ADD code. These turbulence models are: (1) eddy viscosity model (Ref. 3.1), (2) modified eddy viscosity model (Ref. 3.6) which uses the streamline curvature corrections of Eide (Ref. 3.7) and Bradshaw (Ref. 3.8), and (3) two equation turbulence model (Ref. 3.6) which is based on the work of Chen (Ref. 3.9) using the curvature corrections of Launder, et al. (Ref. 3.10).

Eddy Viscosity Model

The eddy viscosity model is essentially an equilibrium model based on Prandtl's mixing length theory (Ref. 3.11). The outer layer and freestream flow have an eddy viscosity which varies with s only. This freestream eddy viscosity is given by:

$$\mu_T = \chi \frac{\rho_\infty U_\infty}{2} \int_0^h \left(1 - \frac{U}{U_\infty}\right) dy \quad (3.4.1)$$

where χ is an empirical constant assumed to be 0.016 (Ref. 3.12) and $\rho_\infty U_\infty$ is taken to be the maximum in the duct. Hence, for thin boundary layers, the integral in Eq. (3.4.1) reduces to $2 \delta^*$ where δ^* is the displacement thickness. Alternately with large freestream distortion, Eq. (3.4.1) can be thought of as:

$$\mu_T = \chi \rho_\infty h (U_\infty - \bar{U}) \quad (3.4.2)$$

where \bar{U} is the average velocity and h is the duct length. Equation (3.4.2) is a typical wake mixing length model.

For the "wall layer", the turbulence model derived by VanDriest (Ref. 3.13) is used.

$$\frac{\mu_T}{\mu_w} = \kappa^2 (y^+)^2 [1 - \exp(-y^+/A^+)]^2 \frac{dU^+}{dy^+} \quad (3.4.3)$$

where U^+ , y^+ are universal boundary layer coordinates given by:

$$U^+ = U / \sqrt{\tau_w / \rho_w} \quad (3.4.4)$$

$$y^+ = \rho_w y \sqrt{\tau_w / \rho} / \mu_w \quad (3.4.5)$$

where the subscript w refers to values at the wall.

The generally accepted values of the empirical constants χ , κ , A^+ are taken to be 0.016, 0.40, 26.0, respectively. For swirling flows U and U^+ are determined from the resultant velocity.

Modified Eddy Viscosity Model

The modified eddy viscosity model is a two layer model where the Prandtl mixing length l is defined by

$$\mu_T = \rho l^2 |e| \quad (3.4.6)$$

In the wall region, the mixing length is given by

$$\frac{\rho_w U^+ l}{\mu_w} = \kappa Y^+ [1 - \exp(-Y^+/A^+)] \quad (3.4.7)$$

In the outer region or wake region including the freestream, the mixing length is Eq. (3.4.6)

$$\mu_T = \rho l (U_\infty - \bar{U}) \quad (3.4.8)$$

where

$$l = \chi h \quad (3.4.9)$$

Eide and Johnston (Ref. 3.7), modified the mixing length in the wall layer by a factor F given by

$$F = l/l_0 = 1 + \beta_s R_{is} + \beta_\phi R_{i\phi} \quad (3.4.10)$$

where β_s and β_ϕ are empirical constants and R_{is} and $R_{i\phi}$ are the Richardson numbers for streamline curvature and swirl defined by

$$S_s = \frac{U_s}{r_s} / \left(\frac{\partial U_s}{\partial Y} + \frac{U_s}{r_s} \right) ; R_{is} = 2 S_s (1 + S_s) \quad (3.4.11)$$

$$S_\phi = \frac{U_\phi}{r} / \left(\frac{\partial U_\phi}{\partial Y} + \frac{U_\phi}{r} \right) ; R_{i\phi} = 2 S_\phi (1 + S_\phi) \quad (3.4.12)$$

Eide estimated that $\beta_s = \beta_\phi = 6.0$.

The outer region of the flow field is governed by large scale mixing. Using the suggestion of Bradshaw (Ref. 3.8) for a bulk Richardson number, the outer layer mixing length is modified by a factor \bar{F}

$$\bar{F} = 1 + (\bar{\alpha}_s \bar{R}_{is} + \bar{\alpha}_\phi \bar{R}_{i\phi})(2\gamma/h-1) \quad (3.4.13)$$

where

$$\bar{R}_{is} = -h/r_s \quad (3.4.14)$$

$$\bar{R}_{i\phi} = \frac{h \bar{U}_\phi}{r \bar{U}_s} \quad (3.4.15)$$

Bradshaw estimates values of $\bar{\alpha}_s = \bar{\alpha}_\phi = 6.5$.

Two Equation Turbulence Model

The two equation turbulence model programmed into the ADD code is based on the work of Chen (Ref. 3.9) with the curvature corrections of Launder (Ref. 3.10). In the ADD code coordinates, these equations are given by

$$\frac{r\rho U_s}{v} \frac{\partial k}{\partial s} + \frac{r\rho U_n}{v} \frac{\partial k}{\partial n} - \frac{\partial}{\partial n} \left[\left(\mu + \frac{\mu_T}{\sigma_\epsilon} \right) r \frac{\partial k}{\partial n} \right] = \frac{r S_k}{v^2} \quad (3.4.16)$$

$$\frac{r\rho U_s}{v} \frac{\partial \epsilon}{\partial s} + \frac{r\rho U_n}{v} \frac{\partial \epsilon}{\partial n} - \frac{\partial}{\partial n} \left[\left(\mu + \frac{\mu_T}{\sigma_\epsilon} \right) r \frac{\partial \epsilon}{\partial n} \right] = \frac{r S_\epsilon}{v^2} \quad (3.4.17)$$

where the source terms are given by

$$S_k = P - \rho \epsilon - 2\mu \frac{k}{v^2} \quad (3.4.18)$$

$$S_\epsilon = C_1 P \frac{\epsilon}{k} - C_2 \rho \frac{\epsilon^2}{k} - 2C_3 \mu \frac{\epsilon}{v^2} \quad (3.4.19)$$

$$P = \mu_T \left\{ \left[\frac{\partial}{\partial n} (v U_s) \right]^2 + \left[\frac{\partial}{\partial n} \left(\frac{U \phi}{r} \right) \right]^2 \right\} \quad (3.4.20)$$

$$\mu_T = C_\mu \rho \frac{k^2}{\epsilon} \quad (3.4.21)$$

$$R_T = \frac{\rho}{\mu} \frac{k^2}{\epsilon} \quad (3.4.22)$$

$$R_{it} = 2 \frac{k^2}{\epsilon} \left[\frac{U \phi}{r^2} \cos^2 \theta v \frac{\partial}{\partial n} (r U \phi) + 2 \frac{U_s}{r_s^2} v \frac{\partial}{\partial n} (r_s U_s) \right] \quad (3.4.23)$$

$$\mu_E = \mu + \mu_T \quad (3.4.24)$$

$$\frac{1}{r_s} = - \frac{\partial v}{\partial n} \quad (3.4.25)$$

$$\cos \theta = v \frac{\partial r}{\partial n} \quad (3.4.26)$$

The empirical constants are given by:

$$C_1 = 1.35 \quad (3.4.27)$$

$$C_2 = 1.8 \left\{ 1 - (.4/1.8) \exp \left[-R_T^2 / 36 \right] \right\} \left\{ 1 - .2 R_T \right\} \quad (3.4.28)$$

$$C_3 = \exp(-.5 Y^+) \quad (3.4.29)$$

$$C_\mu = .09 \left\{ 1 - \exp(-.0115 Y^+) \right\} \quad (3.4.30)$$

ORIGINAL PAGE IS
OF POOR QUALITY

$$\sigma_k = 1.0 \quad (3.4.31)$$

$$\sigma_\epsilon = 1.3 \quad (3.4.32)$$

Finally, the boundary conditions are given by

$$k(0) = \epsilon(0) = 0 \quad (3.4.34)$$

$$k(1) = \epsilon(1) = 0 \quad (3.4.35)$$

3.5 Numerical Methods

With the relationship between μ_E and the mean flow specified, Eq. (3.3.1) through (3.3.10) can be solved by a forward marching numerical integration scheme. Equations (3.3.1) through (3.3.10) are first linearized by expanding all dependent variables in a Taylor series expansion in the marching direction (s), and terms of $O(\Delta s^2)$ are dropped. Finite difference equations are then obtained using the two point centered difference scheme of Keller (Refs. 3.14, 3.15). The resulting matrix equations are (10 x 10) block tridiagonal and are solved by block factorization using the method of Varah (Ref. 3.16).

The numerical solution is second order accurate in the n direction, first order in the s direction, and linearly stable. The Δs step size is limited not by linear stability conditions but by the required accuracy in the Taylor series expansion in s .

3.6 References

- 3.1 Anderson, O. L.: Calculation of Internal Viscous Flows in Axisymmetric Ducts At Moderate to High Reynolds Numbers. Int. J. of Computers and Fluids, Vol. 8, No. 4, December 1980.
- 3.2 Anderson, O. L.: User's Manual for a Finite Difference Calculation of Turbulent Swirling Compressible Flow in Axisymmetric Ducts with Struts and Slot Cooled Walls. Vol. I & II, USAAMRDL-TR-74-50.
- 3.3 Barber, T. J., P. Raghuraman, and O. L. Anderson: Evaluation of An Analysis for Axisymmetric Internal Flows in Turbomachinery Ducts. ASME Winter Meeting, Flow in Primary Non-Rotating Passages in Turbomachines, December 2-7, 1979.
- 3.4 Vatsa, V. N., M. J. Werle, and O. L. Anderson: Solution of Slightly Under-expanded Axisymmetric Co-Flowing Jet Flows. AIAA 18th Aerospace Sciences Meeting, AIAA-80-006, January 1980.
- 3.5 Kober, H.: Dictionary of Conformal Representations. Dover Publications, Inc., New York, 1957.
- 3.6 Anderson, O. L., and D. Edwards: Modifications to an Analysis for Axisymmetric Turbulent Swirling Flows. NASA Report (to be published).
- 3.7 Eide, S. A. and J. P. Johnston: Predictions of the Effects of Longitudinal Wall Curvature and System Rotation on Turbulent Boundary Layers. National Science Foundation Grant GK 16450A1, Report No. PU-19, 1974.
- 3.8 Bradshaw, P.: Effects of Streamline Curvature on Turbulent Flow. AGARDograph No. 19, August 1973.
- 3.9 Chen, K-Y: Predictions of Channel and Boundary Layer Flows with a Low-Reynolds Number Two-Equation Model of Turbulence. AIAA 18th Aerospace Sciences Meeting, AIAA-80-0134, January 1980.
- 3.10 Launder, B. E., C. H. Pridden, and B. I. Sharma: The Calculation of Turbulent Boundary Layers on Spinning and Curved Surfaces. Trans. ASME J. of Fluids Eng., p. 231, March 1977.
- 3.11 Schlichting, H.: Boundary Layer Theory. 6th Ed., McGraw-Hill, New York (1968).
- 3.12 Clauser, F.: The Turbulent Boundary Layer Advanced Applied Mathematics, Vol. 4, pp. 1-51, 1956.

References (Cont'd)

- 3.13 Van Driest, E. F.: On Turbulent Flow Near a Wall. *Journal of Aeronautical Sciences*, Vol. 23, No. 11, 1956.
- 3.14 Keller, H. B.: A New Difference Scheme for Parabolic Problems. *Numerical Solution of Partial Differential Equations - II SYNSPADE 1970*. Academic Press, New York.
- 3.15 Keller, H. B.: Accurate Difference Methods for Linear Ordinary Differential Systems Subject to Linear Constraints. *SIAM J., Numerical Analysis*, Vol. 6, No. 1, March 1968.
- 3.16 Varah, J. M.: On the Solution of Block Tridiagonal Systems Arising from Certain Finite Difference Equations. *Mathematics of Computation*, Vol. 26, No. 120, October 1972.

3.7 List of Symbols

A^+	Van Driest constant (26.0)
C_p	Specific heat of air
C_v	Constant in Two Equation Turbulence Model
e	Rate of Strain
F	Ratio mixing length to flat plate mixing length
\bar{F}	Ratio free stream mixing length to wake mixing length
h	Duct height
I	Entropy
k	Turbulence kinetic energy
l	Mixing length
l_o	Mixing length flat plate
n	Normal coordinate (stream function)
p	Static pressure
P	Turbulence production
r	Radius
r_s, r_n	Radius of curvature
R	Gas constant
R_{is}, \bar{R}_{is}	Richardson numbers for streamline curvature
R_{it}	Turbulent Richardson number
$R_{i\phi}, \bar{R}_{i\phi}$	Richardson number for swirl
R_t	Turbulent Reynolds number

List of Symbols (Cont'd)

s	Streamwise coordinate (velocity potential)
T	Temperature
U_s, U_ϕ, U_n	Velocity components
U_∞	Maximum velocity
\bar{U}	Average velocity
U^+	Universal velocity
U^*	Friction velocity
V	Reciprocal of metric coefficient (potential flow velocity)
X, Y	Distance along s and n coordinates
Y^+	Universal distance from wall
z	Axial distance
α_s, α_ϕ	Empirical constants
β_s, β_ϕ	Empirical constants
δ^*	Displacement thickness
ϵ	Turbulence dissipation
κ	Prandtl constant (.41)
μ	Molecular viscosity
μ_E	Effective viscosity
μ_T	Turbulent viscosity
ρ	Density
$\tau_{ns}, \tau_{n\phi}$	Stress
χ	Clauser constant (.016)
ψ	Stream function

4.0 ANALYSIS OF FUEL DROPLET BEHAVIOR

4.1 General Approach

The behavior of the fuel spray is calculated using the Particle Tracking (PTRAK) computer program which is described in this section.

The analysis assumes lean equivalence ratios, i.e., that the mass fraction of fuel is small. Under these conditions, the air flow behavior can be solved first using the analysis described in Section 3.0 and incorporated into the ADD code. The pressure, temperature and velocity field are then stored on a data file and used in the fuel droplet analysis. Thus the air flow behavior can effect the fuel droplet behavior, but the fuel droplet behavior does not effect the air flow behavior.

The spray is divided into a number of classes (up to 1250). In each class, droplet diameter, velocity components, and position in the flowfield are specified; these parameters may differ among the various classes. The PTRAK model calculates the trajectory, vaporization rate, and temperature variation of each class of droplets. Large droplets may shatter into smaller droplets. Droplets from two classes may coalesce into larger entities. Droplets may collide with the duct walls and either rebound or undergo additional vaporization due to heat transfer to the droplet from the wall. The fuel may be either a pure compound or a distillate liquid. As a result of these processes, a distribution of fuel vapor sources is calculated for use in the vapor diffusion computer program (see Section 5.0).

Symbols used in this section are defined on pages 57-60.

4.2 Momentum Equations

The equations of motion for the fuel droplet trajectories presently coded into the PTRAK computer program are given below. It should be noted that these equations of motion are written in the orthogonal streamline coordinate system used by the ADD code. The additional terms on the right hand side are acceleration terms generated by the curvilinear coordinate system. V_s , V_n , and V_ϕ are the fuel droplet velocities and s , n , ϕ are the coordinates of the fuel droplet in the ADD code coordinate system. The drag of the fuel droplet is written in terms of a drag coefficient, C_D .

$$\frac{dV_s}{dt} = \frac{\rho C_D A}{2m} \Delta U (U_s - V_s) - V_n^2 \frac{\partial V}{\partial s} + \frac{V_\phi^2}{r} \frac{\partial r}{\partial s} + V_n V_s \frac{\partial V}{\partial s} \quad (4.2.1)$$

$$\frac{dV_n}{dt} = \frac{\rho C_D A}{2m} \Delta U (U_n - V_n) - V_s^2 \frac{\partial V}{\partial n} + \frac{V_\phi^2}{r} \frac{\partial r}{\partial n} + V_s V_\phi \frac{\partial V}{\partial s} \quad (4.2.2)$$

$$\frac{dV_\phi}{dt} = \frac{\rho C_D A}{2m} \Delta U (U_\phi - V_\phi) - \frac{V_n V_\phi}{r} V \frac{\partial r}{\partial s} - \frac{V_s V_\phi}{r} V \frac{\partial r}{\partial n} \quad (4.2.3)$$

$$\frac{ds}{dt} = V V_s \quad (4.2.4)$$

$$\frac{dn}{dt} = V V_n \quad (4.2.5)$$

$$\frac{d\phi}{dt} = \frac{V_\phi}{r} \quad (4.2.6)$$

where the cross-sectional area of the fuel droplet is given by

$$A = \pi D^2 / 4 \quad (4.2.7)$$

The drag coefficient is determined from correlations reported by Dickerson and Schuman (Ref. 4.1):

$$\begin{aligned} C_D &= 27 Re_D^{-0.84} & 0 < Re_D \leq 80. \\ C_D &= 0.271 Re_D^{0.217} & 80 < Re_D \leq 10^4 \\ C_D &= 2.0 & Re_D > 10^4 \end{aligned} \quad (4.2.8)$$

where the droplet Reynolds number is based on film properties and the relative velocity.

$$Re_D = \rho_m D \Delta U / \mu_m \quad (4.2.9)$$

$$\Delta U = \left\{ (U_s - v_s)^2 + (U_\phi - v_\phi)^2 + (U_n - v_n)^2 \right\}^{1/2} \quad (4.2.10)$$

Equations (4.2.1) through (4.2.6) constitute an initial value problem where v_{s0} , v_{n0} , $v_{\phi 0}$, s_0 , n_0 , ϕ_0 are specified.

4.3 Heat and Mass Transfer Equations

In the case of a (single component) droplet vaporizing in a gas stream of uniform temperature, the droplet temperature history can be described in terms of a heat-up period, during which time the droplet temperature changes, and an "equilibrium vaporization" period, during which time the droplet temperature remains constant. The physical processes of major significance during these periods are the transport of heat to the droplet and the transport of vapor away from the droplet surface. The net difference between the energy flux to and away from the droplet accounts for changes in the droplet temperature.

The rigorous mathematical treatment of the droplet vaporization and heating problem requires the solution of time-dependent partial differential equations for the diffusion of mass and energy for conditions both within the droplet and in the surrounding gas-phase. Understandably, a great amount of insight into the behavior of a droplet can be obtained from such an approach. However, there are several reasons why such a procedure is not incorporated into the PTRAK code. First, solutions to the set of partial differential equations would have to be obtained for hundreds of droplet classes throughout the premixing passage; computer run times would become unacceptably large. Second, it is not clear whether sufficient information is available for calculating heat and mass transfer coefficients for droplets in forced convection (due to the relative velocity between the droplet and the air). Third, there is a paucity of data useful for verifying a model of this complexity especially if the model includes the effects of distillate fuels on heat and mass transfer rates.

Instead of using a rigorous mathematical treatment of the droplet heat and mass transfer processes in the development of the PTRAK program, an existing semi-empirical model was extended for use with distillate fuels. The model described herein is based largely on the work of El Wakil, et.al (Ref. 4.2) and Priem and Heidmann (Ref. 4.3).

There are three assumptions that make the mathematical treatment of droplet heat and mass transfer quite tractable. The first is the quasi-steady assumption by which the transport processes are assumed to be steady at every instant; that is, at each time t during droplet vaporization and heating, the fluid and thermodynamic conditions of the droplet and gas system adjust instantaneously to steady-state conditions. The quasi-steady assumption is not an equilibrium assumption. With a quasi-steady assumption, the droplet temperature and vaporization rate may change with time. With an equilibrium assumption, the droplet temperature is constant (and equal to its wet bulb value); an equilibrium (constant) vaporization rate does not exist but it can be shown that the ratio of vaporization rate to droplet diameter is nearly constant at equilibrium.

The second assumption is that conditions within the droplet are uniform. This permits the governing partial differential equations for determining droplet

ORIGINAL PAGE IS
OF POOR QUALITY

temperature and mass (or diameter) to be reduced to extremely simple forms for quick solution.

The third assumption is that both the droplet and its surroundings are spherically symmetric. Obviously, the relative velocity between the droplet and the gas causes the droplet to change shape and alter the characteristics of the velocity, thermal, and mass diffusion boundary layers. Correlations developed for vaporizing droplets in a forced convection environment provide the appropriate transport coefficients.

Using these assumptions, the governing partial differential equations for the gas phase are reduced to a set of steady-state, ordinary differential equations with known solutions. These solutions, together with the simple equations for the liquid phase, are combined in a forward-marching time integration procedure (the time-equivalent of the spatial integration of the droplet equations of motion. Sec. 4.2).

The geometry of the system under consideration is shown in Fig. 4-1. The droplet is surrounded by a boundary layer of uniform thickness and properties. At the outer edge of this boundary layer, gas conditions correspond to those of the flow field calculated by the ADD code and will be referred to as the "air" conditions. The convention adopted in Ref. 4.2 and retained here is that the thickness of the boundary layer is equal to the instantaneous droplet radius. For a complete development of the equations for vaporization and heating rate, the reader is referred to Ref. 4.2 and 4.3. The vaporization rate expression has been modified (Ref. 4.4) to account for a finite amount of fuel vapor in the gas outside of the boundary layer. The effect of this "back diffusion" term is negligible for lean systems; it has been retained for use in the PTRAK code but is presently rendered inoperable.

The equation for the vaporization rate is:

$$\dot{w}_L = A_S \tilde{K} p_{f,s} a' \quad (4.3.1)$$

where

$$a' = \frac{p_a}{p_{f,s}} \ln \left(\frac{p_a - p_{f,\infty}}{p_a - p_{f,s}} \right) \quad (4.3.2)$$

The term $p_{f,\infty}$ is the partial pressure of fuel vapor outside of the boundary layer. ($p_{f,\infty} = 0$ in the present version of PTRAK.) The determination of the mass transfer coefficient is presented in the next section. The droplet heating rate equation is:

$$\frac{dT_L}{dt} = \frac{\dot{q}_s - \dot{w}_L \lambda}{\frac{\pi}{6} D^3 \rho_L C_{PL}} \quad (4.3.3)$$

where the total amount of heat arriving at the droplet surface is:

$$\dot{q}_s = hA_s(T_o - T_L) \frac{z}{e^z - 1} \quad (4.3.4)$$

and the parameter z is:

$$z = \frac{\dot{w}_L C_{p_f}}{hA_s} \quad (4.3.5)$$

The droplet surface area, A_s , is calculated from:

$$A_s = \pi D^2 \quad (4.3.6)$$

The determination of the heat transfer coefficient, h , is presented in the next section. Equation (4.3.3) states that some of the heat arriving at the droplet surface is used to vaporize an amount of fuel, \dot{w}_L , while the remainder is used to heat the droplet. At equilibrium, \dot{q}_s is equal to $\dot{w}_L \lambda$ and the droplet temperature (the wet-bulb temperature) is constant (for a pure fluid). Equation (4.3.4) is the product of the forced-convection heat transfer rate for a nonvaporizing system, $hA_s (T_o - T_L)$, and a correction term for the energy carried away from the droplet due to mass transfer (i.e., "blowing" of the boundary layer), $z/(e^z - 1)$. This term approaches unity for a zero mass transfer rate and zero for an infinite mass transfer rate (no energy reaching the droplet surface).

At any instant, the droplet mass is given by

$$m_L = \frac{\pi}{6} D^3 \rho_L \quad (4.3.7)$$

Then, since

$$\frac{dm_L}{dt} = -\dot{w}_L \quad (4.3.8)$$

and assuming that $\rho_L = \rho_L(T_L)$ only, Equations (4.3.3), (4.3.7) and (4.3.8) and be combined to yield:

$$\frac{dD}{dt} = -\frac{2}{\pi D^2 \rho_L} \left[\dot{w}_L + \frac{\pi D^3}{6} \frac{d\rho_L}{dT_L} \frac{dT_L}{dt} \right] \quad (4.3.9)$$

where $d\rho_L/dT_L$ is evaluated as described in the next section.

4.4 Evaluation of Thermodynamic and Transport Properties

In this section, the procedures used to calculate the heat and mass transfer coefficients are presented together with the techniques used to calculate the required thermal properties. The discussion contained herein is limited to flow situations in which the local static pressure is well below the critical pressure of either the fuel or the air. Most of these procedures are also used in the high pressure model for droplet heating and vaporization. The discussion of the effect of high pressure is deferred until Section 4.6.

(1) Mass Transfer Coefficient:

The mass transfer coefficient, \tilde{K} , is obtained from a correlation of the form developed by Ranz and Marshall (Ref. 4.5) for droplet vaporization:

$$Nu_m = \frac{\tilde{K} D T_m R_0}{D_m \mathcal{M}_m} = a + b Re_D^{1/2} Sc^{1/3} \quad (4.4.1)$$

The first term represents the mass transfer due to free convection while the second term represents the mass transfer due to forced convection. Experimental data are required to calibrate suitably the coefficients (a,b). No useful data on the vaporization rates of fuel sprays are currently available; therefore the only recourse at present is to use the Ranz and Marshall results which were obtained for the vaporization of water droplets:

$$a = 2.0$$

$$b = 0.6$$

These coefficients have been incorporated into the PTRAK computer program.

(2) Heat Transfer Coefficient:

A companion expression was developed by Ranz and Marshall for the heat transfer coefficient, h :

$$Nu_h = \frac{hD}{k_m} = a' + b' Re_D^{1/2} Pr^{1/3} \quad (4.4.2)$$

For reasons similar to those presented during the discussion of \tilde{K} , the coefficients have been assigned the values:

$$a' = 2.0$$

$$b' = 0.6$$

ORIGINAL PAGE IS
OF POOR QUALITY

in the PTRAK code.

(3) Dimensionless Transport Numbers:

The Reynolds, Schmidt, and Prandtl numbers are defined as:

$$Re_D = \rho_m D \Delta U / \mu_m \quad (4.4.3)$$

$$Sc = \mu_m / (\rho_m D_m) \quad (4.4.4)$$

$$Pr = \mu_m C_{pm} / k_m \quad (4.4.5)$$

The thermal coefficients used in these parameters are evaluated at a mean boundary layer film condition.

(4) Mean Film Conditions

At any instant during the evaluation of the vaporization and heating rates, it is assumed that the appropriate properties are constant throughout the film surrounding the droplet (Fig. 4.1). In this manner, the differential equations for heat and mass transfer can be integrated to yield Eq. (4.3.1) and (4.3.4).

The mean temperature, T_m , used in the PTRAK code is the log mean value (as suggested in Ref. 4.2).

$$T_m = \frac{T_a - T_L}{\ln(T_a/T_L)} \quad (4.4.6)$$

In the development of the droplet vaporization and heating models used in the PTRAK program, it was assumed that the air temperature varied from 400K to 900K. If it is also assumed that the fuel temperature is typically 300K or greater, then $T_a/T_L \leq 3$. As a result, the log mean temperature will differ by no more than ten percent from the arithmetic mean temperature, $1/2 (T_a + T_L)$. (If the model were used with much higher gas temperatures, such as a fuel droplet might encounter in a combustion chamber, then the difference between alternative definitions of mean temperature can be quite substantial.)

It is also assumed that the fuel vapor and the air thermal coefficients are obtained at a mean fuel vapor concentration (mole fraction):

$$Y_m = \frac{1}{2} (Y_{f,\infty} + Y_{f,s}) \quad (4.4.7)$$

The mole fraction is also equal to the ratio of partial pressure to local static pressure so that:

$$Y_{f,\infty} = p_{f,\infty} / p_0 \quad (4.4.8)$$

$$Y_{f,s} = p_{f,s} / p_0 \quad (4.4.9)$$

As noted earlier, it is assumed in the present version of the PTRAK code that $P_{f,\infty}$ is zero. The partial pressure of fuel vapor at the droplet surface, $p_{f,s}$, is assumed to be equal to the vapor pressure of the fuel at the droplet temperature, T_L .

The mean molecular weight of the mixture at the mean condition is:

$$\bar{m}_m = Y_m \bar{m}_f + (1 - Y_m) \bar{m}_0 \quad (4.4.10)$$

The mean mass fraction of the fuel vapor is

$$C_m = Y_m \bar{m}_f / \bar{m}_0 \quad (4.4.11)$$

The five mean thermal properties that must be evaluated are density (ρ_m), molecular viscosity (μ_m), thermal conductivity (k_m), heat capacity ($C_{p,m}$), and diffusion coefficient (D_m). It is assumed that no pressure gradient exists across the boundary layer. Then from the ideal gas equation of state:

$$\rho_m = p_0 \bar{m}_m / (R_0 T_m) \quad (4.4.12)$$

(see also the discussion in Section 4.6). The mean molecular viscosity is evaluated as a mole weighted average:

$$\mu_m = Y_m \mu_f + (1 - Y_m) \mu_0 \quad (4.4.13)$$

where the viscosities, μ_a and μ_f are evaluated at T_m . (A mole weighted average is used because viscosity is a manifestation of momentum transfer due to molecular collisions and the frequency of collisions is proportional to molecular concentration). Similarly, since heat transfer by conduction is a function of the frequency of molecular collisions, the mean thermal conductivity is:

ORIGINAL PAGE IS
OF POOR QUALITY

$$k_m = Y_m k_f + (1 - Y_m) k_a \quad (4.4.14)$$

where the thermal conductivities are evaluated at T_m .

The heat capacity is a measure of the ability of a system to store energy so that the mean heat capacity (following Ref. 4.2) is:

$$C_{pm} = C_m C_{pf} + (1 - C_m) C_{pa} \quad (4.4.15)$$

where the heat capacities (defined in terms of energy/mass/degree) are evaluated at T_m .

The major components of the gas in the film surrounding the droplet are those of air under flow conditions likely to be found in premixing passages. The use of Eqs. (4.4.13), (4.4.14) and (4.4.15) in lieu of more exact expressions for mixtures of fuel vapor and air would have only a small effect on the calculated heat and mass transfer rates. The diffusion coefficient, D_m , cannot be estimated as simply, however, with the same level of precision. As suggested in Ref. 4.2 the diffusion coefficient is obtained using the kinetic theory result (Ref. 4.6):

$$D_m = \frac{0.002628 \sqrt{T_m^3 \frac{m_f + m_a}{2 m_f m_a}}}{\rho_a \sigma_m \Omega^*} \quad (4.4.16)$$

where

$$\sigma_m = 1/2 (\sigma_a + \sigma_f) \quad (4.4.17)$$

$$\Omega^* = \Omega^* (T^*) \quad (4.4.18)$$

$$T^* = T_m / (\epsilon/k)_m \quad (4.4.19)$$

$$\left(\frac{\epsilon}{k}\right)_m = \sqrt{\left(\frac{\epsilon}{k}\right)_f \left(\frac{\epsilon}{k}\right)_a} \quad (4.4.20)$$

The collision integral function, Ω^* , is tabulated in Table 4.1. The force constants for air are:

$$\sigma_a = 3.689 \text{ \AA}$$

$$\left(\frac{\epsilon}{k}\right)_a = 84K$$

Force constants are not available for typical jet fuels. It is recommended that the force constants for the molecule, (C_9H_{20}) (the heaviest paraffin reported in Ref. 4.6) be used:

$$\sigma_f = 8.448$$

$$\left(\frac{\epsilon}{k}\right)_f = 240 \text{ K}$$

(5) Fuel Properties Required in the Model

Fourteen properties for each fuel must be determined for use in the PTRAK model in the most general problem. The equations described in the preceding discussion account for most of the required properties. The remaining properties are needed for special features of the model that will be described below.

Five of the properties are constants. These are the fuel molecular weight (m_f), critical pressure (P_{cf}), critical temperature (T_{cf}) and the force constants (σ_f) (ϵ/k_f). The force constants are generally not available for jet fuels; at present, the constants presented above are recommended.

There are four vapor phase properties. Three of these are input to the model in the form of polynomial expressions:

$$\text{Property} = \sum_{N=1}^4 A_N T_m^{N-1} \quad (4.4.21)$$

where "property" is the fuel vapor molecular viscosity (μ_f), the thermal conductivity (k_f) or the heat capacity (C_{pf}). The fourth parameter is the vapor pressure ($P_{f,s}$) which must be evaluated using a procedure described in Sec. 4.5; it will be shown therein that the vapor pressure will be calculated using an expression of the form:

$$\ln p_{f,s} = \alpha_n + \frac{\beta_n}{T_L} \quad (4.4.22)$$

where the "constants" (α_n , β_n) are determined in accordance with Sec. 4.5.

Five properties of the liquid phase must also be calculated. The liquid density (ρ_L) and heat capacity (c_{pL}) are calculated from:

$$\rho_L \text{ (or } C_{pL}) = \sum_{N=1}^4 A_N T^{N-1} \quad (4.4.23)$$

The liquid molecular viscosity (μ_L) is determined from:

$$\ln \mu_L = \sum_{N=1}^4 A_N T^{N-1} \quad (4.4.24)$$

The semi-logarithmic form is used because the liquid viscosity is a strong function of temperature. Often, an alternative expression of the form

$$\ln \left[\ln \left(\frac{\mu_L}{\rho_L} + C \right) \right] = A \ln T_L + B \quad (4.4.25)$$

is used for calculating viscosity (Ref. 4.7). The form of Eq. (4.4.24) was selected for use in the PTRAK code since it represents the data adequately and its coefficients are determined more conveniently than those used in Eq. (4.4.25). The correlation for surface tension (S_L) reported in Ref. 4.7 is used:

$$S_L \left(\frac{m_f}{\rho_L} \right)^{2/3} = 2.12 (T_{c_f} - 6 - T_L) \quad (4.4.26)$$

In this expression, the liquid density is evaluated at T_L . The heat of vaporization (λ) is calculated using the Clausius-Clapeyron equation (e.g., Ref. 4.8, p. 104) which relates λ to the slope of the vapor pressure curve:

$$\frac{d \ln p_{f,s}}{dT} = \frac{-\lambda m_f}{R_0 T_L^2} \quad (4.4.27)$$

Then, using Eq. (4.4.21) in Eq. (4.4.27)

$$\lambda = \frac{-\beta_n R_0}{m_f} \quad (4.4.28)$$

where the coefficient, β_n may vary throughout the vaporization process as described in Sec. 4.5.

(6) Air Properties Required by the Model

Eight air properties are used in the model. Five of these are constants: air molecular weight (m_a), critical pressure (P_{c_a}), critical temperature (T_{c_a}), and the force constants [σ_a , $(\epsilon/k)_a$]. The other three parameters are molecular viscosity (μ_a), thermal conductivity (k_a) and heat capacity (c_{p_a}) which are determined from polynomial expressions having the form of Eq. (4.4.22). It may be noted that a greater level of sophistication in accounting for the temperature dependence of the physical properties of the fluid is used in the PTRAK code than in the ADD code. The reasons for this are that the mean temperature (T_m) in the droplet film may be substantially different from the air temperature (T_a) and that the mean temperature may vary--due to changes in the liquid temperature--even if the air temperature is uniform throughout the flow field. Both the air molecular viscosity and thermal conductivity increase by nearly a factor of two as the temperature increases from 400K to 900K.

4.5 Evaluation of Distillate Fuel Effects

The vaporization model developed as part of the PTRAK computer program is applicable to both distillate and pure fuels. For the present discussion, a distillate fuel is a liquid mixture consisting of two or more compounds that may differ chemically and physically. The most important property of the fuel for determining the vaporization rate is the vapor pressure because of its influence on the fuel vapor concentration gradient, the physical basis for the vaporization model. If it is assumed that at any instant, the droplet-air system is in thermodynamic equilibrium, then the vapor pressure of the liquid is equal to the partial pressure (and, hence, molar concentration) of the fuel vapor at the surface of the droplet.

For a pure substance, such as water or a single hydrocarbon compound, the vapor pressure is a function only of the temperature of the liquid. Thus, as a liquid of this type vaporizes, its vapor pressure will vary only if its temperature is varying. For a distillate fuel, the vaporization situation is more complicated since the vapor pressure is determined by the contributions of each vaporizing constituent. To illustrate this complexity, assume that the droplet temperature can somehow remain constant. Then the vapor pressure of the distillate liquid tends to decrease with time as the more volatile (higher vapor pressure) components vaporize so that the vapor pressure of a distillate fuel is a function of both droplet temperature and composition.

The dependence of the vapor pressure of a distillate fuel on temperature and composition at a pressure of one atmosphere is given by the standard distillation curve such as the curve for a Jet-A type of fuel given in Fig. 4.2. It is seen in Fig. 4.2 that the fuel temperature must increase as the more volatile components are vaporized at constant pressure. Similarly, another constant value of pressure could be used to obtain a distillation curve which would be qualitatively similar to the curve presented in Fig. 4.2. Thus, the distillation curve is simply an isobar of a pressure-temperature-composition surface.

Because both the droplet temperature and composition must be known at any instant to determine the vapor pressure of the droplet, it is necessary that each droplet in the system be tracked individually. In the PTRAK code, each class of droplets (a class has homogeneous properties in this context) is treated separately. Thus, in principle the composition of each droplet is known at every instant from the distillation curve and the percent of initial mass evaporated. (For droplet classes undergoing coalescence, specification of the droplet "history" requires further assumptions.)

A distillate fuel contains many constituents. It is not practical from a computational standpoint to keep track of each component and calculate its contribution to the vapor pressure. The method used in the vaporization model is based upon the work of Cox (Ref. 4.9) and is a standard procedure used in chemical engineering practice (e.g., Ref. 4.10). In Cox's method it is assumed that, at any instant

during the vaporizing process, the behavior of the distillate fuel is the same as that of some pure substance; that is, its vapor pressure is a function of the liquid temperature only. Different pure substances characterize the vaporization process at each instant. It is assumed that the vapor pressure of a hydrocarbon distillate fuel can be determined from the typical distillation curve for the fuel and the vapor pressure vs. temperature curves for the normal paraffin series of hydrocarbons (C_nH_{2n+2}). This family of vapor pressure curves is shown in Fig. 4.3. It should be noted that Cox used a temperature scale that allowed the vapor pressure for water to be plotted as a linear function of the temperature axis; this vapor pressure curve can be approximated by:

$$\ln p_{f,s} = a_n + \frac{\beta_n}{T_L} + \gamma_n T_L + \delta_n T_L^2 \quad (4.5.1)$$

However, for purposes of this analysis it is more convenient and sufficiently accurate to approximate Eq. (4.5.1) by:

$$\ln p_{f,s} = a_n + \frac{\beta_n}{T_L} \quad (4.5.2)$$

where the subscript n refers to the carbon number of the paraffin which serves as the parameter specifying the composition of the distillate at any instant of time.

Cox's procedure operates as follows. At a particular instant during the vaporizing process, the percent of fuel that has vaporized is calculated for each droplet.

$$P_e = 100 \left[1 - \frac{(\rho_L D_L^3)_{t=t}}{(\rho_L D_L^3)_{t=0}} \right] \quad (4.5.3)$$

(This calculation requires that the computer program has stored the initial values of droplet diameter and density.) The distillation curve (e.g., Fig. 4.2) is entered with the fraction of fuel vaporized as a parameter and the distillation temperature, T_D , is found. This is the temperature that is just sufficient to produce a vapor pressure of one atmosphere at the specified fraction of fuel vaporized. Of course, the droplet temperature is not necessarily equal to the distillation temperature nor is the droplet always vaporizing into surroundings maintained at one atmosphere. To find the correct vapor pressure, one locates the paraffin curve in the Cox chart that passes through the point at a pressure of one atmosphere and the instantaneous value of distillation temperature. It is then assumed that this vapor pressure curve characterizes the vaporization process at the specified instant. The instan-

taneous value of vapor pressure is found by moving along the vapor pressure curve to a temperature equal to the current value of droplet temperature. The vapor pressure is then used to calculate a new value of vaporization rate, droplet temperature, etc. (see Section 4.4) and then a new value of fraction of fuel vaporized. The entire process is repeated until all of the fuel has vaporized.

Implementation of the Cox procedure in the PTRAK code is carried out by using the form of the vapor pressure curves given by Eq.(4.5.2) and inputting two sets of values of pressure and temperature for each curve in the family. From these data, α_n and β_n (Eq. 4.5.2) can be calculated--it is assumed that α and β vary continuously with some parameter such as the carbon number. Thus, the Cox chart is established by two isobars, one of which is taken to be atmospheric pressure (i.e., the pressure used to determine the distillation curve):

$$T_{L1} = F_1(n, 1 \text{ atm}) \quad (4.5.4)$$

$$T_{L2} = F_2(n, p_2) \quad (4.5.5)$$

where p_2 is any pressure other than atmospheric pressure. For example, Eq. (4.5.4) is solved for n with T_{L1} equal to the instantaneous value of distillation temperature. Next, Eq. (4.5.5) is solved for T_{L2} at this value of n . Then, Eq. (4.5.2) is applied twice (once at T_{L1} and p_1 equal to 1 atm, again at T_{L2} and p_2) so that α_n and β_n are determined.

Of course, data for any group of compounds may be used to generate a Cox chart if that group is appropriate to the multi-component fuel being analyzed. The only restriction on the method of utilizing the Cox procedure that has been incorporated into the PTRAK computer program is that the two isobars must be continuous functions of a variable that describes the group of compounds in some fashion. Note that the Cox chart for a pure substance is simply a single vapor pressure curve in the form of Eq. 4.5.2. To avoid the use of additional input options, this is accomplished simply by inputting data for Eqs. (4.5.4) and (4.5.5) as described in Volume II of his report and supplying a distillation curve of the form shown in Fig. 4.4.

4.6 High Pressure Effects

The model for fuel droplet vaporization and heating is designed to be applicable to a wide range of gas temperature (400 to 900 K) and gas pressure (3 to 40 atm). As the pressure of a gas increases (while its temperature remains constant), the density calculated by the ideal equation of state

$$\rho = p\bar{m}/(R_0T) \quad (4.6.1)$$

begins to differ from the actual density. Furthermore, as the pressure increases, the temperature of a vaporizing fuel droplet increases (due to increased convective heat transfer) and may approach the critical temperature of the fuel (Ref. 4.11). At the critical point, there is no distinction between the liquid and vapor phases. These two effects of increasing ambient pressure may lead to significant differences between experimentally determined vaporization rates and rates estimated using simpler droplet vaporization models such as incorporated in the PTRAK code. Two approaches for modeling the droplet heating and vaporization process at high ambient pressure were evaluated for use in this analysis. In the first approach (and the one ultimately incorporated into the PTRAK computer program), mass transfer models are derived from the diffusion equation:

$$\frac{DC}{Dt} = \mathcal{D} \nabla^2 C \quad (4.6.2)$$

which is solved after making simplifying assumptions such as steady flow, spherical symmetry, and ideal gas behavior (e.g., Ref. 4.2 to 4.4). An analogous energy equation is also used to derive heat transfer models. The effect of forced convection is introduced by modifying the appropriate transfer coefficient by application of experimental data. Pressure effects are included either by using thermal and transport coefficients that may have a pressure dependence or by obtaining solutions to Eq. (4.6.2) in terms of partial pressures or concentrations; however, the latter requires that the gas-phase behave ideally.

A second and more rigorous approach begins with the use of the set of differential equations applicable to both the liquid and gas (air plus fuel vapor) phase (e.g., Ref. 4.12 and 4.13). This set of equations includes an equation of state suitable for use at high pressure. It was not within the scope of the present effort to modify the computer program used to calculate the air flow field (the ADD code). However, since the ADD code uses the ideal equation of state (Eq. 4.6.1), it was necessary to assess the departure of air from ideal behavior at elevated pressures. To do this, the density of air was calculated by both Eq. (4.6.1) and the Redlich-Kwong equation (Ref. 4.14).

$$\left[p + \frac{a}{T^{1/2}(v+b)v} \right] (v-b) = \frac{R_0 T}{\bar{m}} \quad (4.6.3)$$

where $v = 1/\rho$ and a and b are constants depending on only the critical properties of the gas (at least for simple molecules). Use of the Redlich-Kwong equation is justified by Shah and Thodos (Ref. 4.15) who compared various equations of state for both argon and n-heptane with experimental data and determined that the Redlich-Kwong equation gave superior results. The discrepancies were largest for n-heptane. Indeed, it appears that as the molecular structure becomes more complicated, corrections must be applied to the "constants" a and b (Ref. 4.16). In the present study, Eq. (4.6.1) and (4.6.3) were used to calculate the density of the air over the range of temperature and pressure cited above and the results agreed within 1.2 percent of each other. This good agreement is not surprising since the air temperatures used (400 to 900 K) are much greater than the critical temperature of air (about 133 K). At temperatures greatly in excess of the critical temperature, the molecules are energetic enough that all gases behave as dilute (and, hence, ideal) gases. Furthermore, the Redlich-Kwong equation was developed for gases above the critical temperature.

The good agreement between the ideal and Redlich-Kwong equations of state means that it is not necessary to modify the ADD code to incorporate the effects of high pressure. However, the gas in the film surrounding the droplet is not air but is a mixture of air and fuel vapor (and the mean film temperature may be below the fuel critical temperature). It is conditions in this film which control the vaporization rate. If the film consists entirely of a hydrocarbon fuel vapor (such as JP-4 whose critical temperature is about 590 K and whose critical pressure is about 31 atm) then significant discrepancies between the densities calculated using Eq. (4.6.1) and Eq. (4.6.3) result. At 400 K the density calculated from Eq. (4.6.3) is about ten times greater than the density calculated from Eq. (4.6.1) for JP-4 vapor. (Even the applicability of the Redlich-Kwong equation at such low subcritical temperatures is questionable based upon the work reported in Ref. 4.15.)

The only position in the vapor film at which the vapor could constitute 100 percent of the mass is at the droplet surface and this can only occur if the droplet is at the boiling point of the fuel at the local pressure. Experience at UTRC in applying vaporization analyses to problems of fuel-air mixing in gas turbine engines indicates that a droplet is not likely to reach its boiling point. A droplet reaches a steady-state temperature determined by the maximum vaporization rate compatible with the imposed heat flux (the wet-bulb temperature), but the droplet vapor pressure at this temperature is considerably less than the compressor discharge pressure which, for modern engines, is in the neighborhood of the critical pressure of fuels of interest. It should be noted that there are conditions where extremely high fuel vapor pressure can exist. Calculations by Wieber (Ref. 4.11) indicate that in spray combustion the droplet temperature can approach the critical temperature (which is obviously always at least as great as the boiling point); however, these results are based on rocket combustion chamber conditions (temperatures about 3000 K and pressures to 150 atm) which are considerably in excess of the flow conditions to which the present model is designed to apply.

If it is assumed that the fuel vapor concentration in the film surrounding the droplet is never more than 50 percent (by mass), then for representative conditions the densities calculated using Eq. (4.6.1) and (4.6.3) are always within 5 percent of each other. The discrepancy diminishes to less than two percent at high temperatures for JP-4 fuel. (Treatment of this mixture of air and fuel vapor using the Redlich-Kwong equation was made in accordance with the rules for determining a and b described in Ref. 4.17).

As a consequence of these calculations, it is apparent that the use of a modified equation of state is not required in this application. Faeth and Chanin (Ref. 4.18) suggest an approach to the droplet vaporization process applicable to intermediate pressures (about one half the critical pressure) which uses the ideal equation of state but which includes real, high pressure, thermodynamic effects through the use of fugacity coefficients which are used to specify the boundary conditions between the liquid and vapor phase of the fuel. The use of such a model presumes the availability of fugacity data and other thermal data which are currently unavailable for distillate fuels. Rosner and Chang (Ref. 4.19) have considered a vaporizing droplet whose temperature is near its critical point. The diffusion equation includes the ratio of the liquid to gas phase density. The analysis is applicable to a droplet in quiescent air and thus requires a forced convection correction. A numerical solution is required. It was judged that simplifying the numerical complexity by solving the problem for a droplet in a quiescent medium and then applying a semi-empirical correction for forced convection to avoid solving a coupled mass transfer and boundary layer calculation would reduce the accuracy of the overall approach because of the inaccuracies of the forced convection correction. Also, the method would consume significant machine computation time. For these reasons, this approach was rejected.

Because none of the alternative approaches offered significant advantages, the first approach was selected for use in the development of the droplet vaporization and heating models for the PTRAK computer program. Alternative correlations to Ranz and Marshall expressions are used for obtaining mass and heat transfer coefficients in the high pressure regime. Following the suggestion of Faeth and Chanin (Ref. 4.18), these alternative correlations are used for gas pressures that exceed one-half the critical pressure of either the fuel or the air. A correlation suggested by Canada (Ref. 4.20) for determining the heat transfer coefficient has been incorporated into the model:

$$Nu_h = \frac{hD}{k_m} = 2 + \frac{0.556 Re_D^{1/2} Pr^{1/3}}{\sqrt{1 + \frac{1.237}{Re_D Pr^{2/3}}}} \quad (4.6.4)$$

It has been assumed that an analogous correlation exists for mass transfer:

$$Nu_h = \frac{\tilde{K} D T_m R_0}{\sigma_m \bar{m}_m} = 2 + \frac{0.556 Re_D^{1/2} Sc^{1/3}}{\sqrt{1 + \frac{1.237}{Re_D Sc^{2/3}}}} \quad (4.6.5)$$

4.7 Droplet Class and Distribution Functions

The system of eight equations Eqs. (4.2.1) through (4.2.6) and Eq. (4.3.3) and (4.3.9) for the eight dependent variables

r, ϕ, z	location in space	
V_r, V_ϕ, V_z	velocity in space	
D	droplet diameter	(4.7.1)
T	droplet temperature	

uniquely determines the state of a droplet at any instant of time when these eight dependent variables are specified as initial conditions. In principle it is possible to solve this set of equations for each of the individual droplets. However, the number of droplets can be substantially reduced by treating each droplet as though it were a cloud of n fuel droplets the mean properties of which are equal to the properties of the individual droplet. This section describes the procedures whereby the state of the liquid fuel is described by the behavior of a relatively few number of individual droplets.

Phase Space

Phase space is nine dimensional space with abscissas given by the eight dependent variables, \vec{r} , \vec{V} , D , T_L and the ordinate given by the number of droplets n_I in the I^{th} class which satisfies the following conditions

$$\left. \begin{aligned} -\frac{\Delta \vec{r}}{2} < \vec{r}_I < \frac{\Delta \vec{r}}{2} \\ -\frac{\Delta \vec{V}}{2} < \vec{V}_I < \frac{\Delta \vec{V}}{2} \\ -\frac{\Delta D}{2} < D_I < \frac{\Delta D}{2} \\ -\frac{\Delta T_L}{2} < T_{LI} < \frac{\Delta T_L}{2} \end{aligned} \right\} \quad (4.7.2)$$

At any instant of time, the distribution of n_I over phase space uniquely determines the state of the cloud of fuel droplets.

Droplet Class (Lagrangian Sense)

A droplet class is defined in the Lagrangian sense by specifying the number of droplets n_I which satisfy conditions (4.7.2) at time $t = 0$. This is equivalent to specifying the initial conditions for the droplet (4.7.1) and assigning a number n_I to each droplet. In the absence of droplet collisions, the number of droplet classes in phase space at any given time determines the state of the entire cloud of droplets.

It should be noted that in this Lagrangian system, more than one droplet class may be at the same location in phase space. When droplets collide or shatter, part or all of the droplets of one class may disappear and a corresponding amount of fuel is assigned to another class. Hence the number density n_I of a given class may change discontinuously.

Distribution Function

The distribution function distributes the number of droplets over phase space. With a small finite number of droplets, it is often convenient to use an integer function called the binomial distribution function with probability of 1/2. This function is given by:

$$f(I, IL) = \frac{(IL)!}{I!(IL-I)!} \left(\frac{1}{2}\right)^{IL}, \quad I = 0, IL \quad (4.7.3)$$

and has the following properties:

$$\sum_{I=0}^{IL} f(I, IL) = 1.0 \quad (4.7.4)$$

As $IL \rightarrow \infty$, the binomial function approaches the normal (Gaussian) distribution function. As an example, define the diameter axis in phase space by (see Fig. 4.5)

$$D_I = D_0 + \Delta D \cdot I \quad (4.7.5)$$

Then the mean diameter and variance of the cloud of droplets is given by

$$\bar{D} = \sum_{I=0}^{IL} f_I D_I = D_{IL/2} \quad (4.7.6)$$

$$\sigma_D = \frac{1}{2} \sqrt{IL} \Delta D \quad (4.7.7)$$

An analogous procedure may be used to distribute fuel droplets over the other coordinates in phase space. The composite distribution function for all of phase space is formed by the product of the binomial distributions for the eight coordinates in phase space, i.e.,

$$F_I = f_r \cdot f_\phi \cdot f_z \cdot f_{v_r} \cdot f_{v_\phi} \cdot f_{v_z} \cdot f_D \cdot f_T \quad (4.7.8)$$

R82-915362-40

The composite distribution function F_I has the property that

$$\sum_{I=0}^{IN-1} F_I = 1.0 \quad (4.7.9)$$

where $IN-1$ is the total number of classes. F_I may be interpreted as the fraction of droplets in the I^{th} class.

Rosin-Rammler Distribution

The Rosin-Rammler distribution function is one of several distribution functions commonly used to characterize the droplet size distribution typically produced by gas turbine fuel injectors (e.g., Ref. 4.21). This distribution function may be used as an alternative to the binomial distribution function Eq. (4.7.8). The Rosin-Rammler distribution is defined as the fraction of droplets greater than size D and is given by

$$R_R = \exp\left[-\left(\frac{D}{D_0}\right)^m\right] \quad (4.7.10)$$

where m is an empirical parameter (typically $1.5 \leq m \leq 3.0$). Hence from the definition of the distribution function (4.6.2) we have

$$f_R = -\frac{dR_R}{dD} dD = m \frac{dD}{D} \left(\frac{D}{D_0}\right)^{m-1} \exp\left[-\left(\frac{D}{D_0}\right)^m\right] \quad (4.7.11)$$

and for a finite number of classes, the Rosin-Rammler distribution function is given by

$$f_{R(I,IL)} = \frac{\left(\frac{D_I}{D_0}\right)^m \exp\left[-\left(\frac{D_I}{D_0}\right)^m\right] \frac{\Delta D}{D_0}}{\sum_{I=0}^{IL} \left(\frac{D_I}{D_0}\right)^m \exp\left[-\left(\frac{D_I}{D_0}\right)^m\right] \frac{\Delta D}{D_0}} \quad (4.7.12)$$

Number Density

The number density is defined as the number of droplets per unit time per unit volume of phase space; the total number of droplets is related to the fuel flow rate by

$$\dot{W}_L = \sum_{I=0}^{IN-1} n_I m_I = n \sum_{I=0}^{IN-1} f_I m_I \quad (4.7.13)$$

Droplet Class (Eulerian Sense)

The equations of motion for the cloud of fuel droplets is solved in the Lagrangian sense, i.e., the fuel droplets are followed in time and the droplet class is defined by its initial conditions. Both the air flow equations and the diffusion equation are solved in the Eulerian sense; i.e., attention is fixed on a point in space and the change in flow in time (or point to point in space) is determined. Therefore, in order for the fuel droplet equations to interact with the air flow and gas flow, droplet classes in the Eulerian sense must be defined. This procedure is necessary because more than one class defined in the Lagrangian sense may be in the same element of volume of phase space.

A droplet class defined in the Eulerian sense is the number of droplets in a given volume of phase space (Eq. 4.7.2) at a given instant of time. Hence the number density of droplet classes defined in the Eulerian sense may change with time.

The solution of the gas diffusion equation requires only two definitions of class in the Eulerian sense; the amount of fuel evaporated per unit volume of space per unit time, and the amount of fuel striking the wall per unit area per unit time. If dV and dA are the differential volume and area respectively, then

$$\dot{w}_f(\bar{r}) = \sum n_I m_I \quad \text{for} \quad \frac{-dv}{2} < \bar{r} < \frac{dv}{2} \quad (4.7.14)$$

and

$$\dot{w}_{fw}(\bar{r}) = \sum n_I m_I \quad \text{for} \quad \frac{-dA}{2} < \bar{r} < \frac{dA}{2} \quad (4.7.15)$$

where the summation takes place for only those droplets which satisfy the conditions stated. In addition, the state of the cloud of fuel droplets may be described by the Sauter mean diameter

$$SMD = \frac{\sum_{I=0}^{IN-1} F_I D_I^3}{\sum_{I=0}^{I,I-1} F_I D_I^2} \quad (4.7.16)$$

4.8 Droplet Collision Model

It has been theorized that the rate of vaporization of a fuel spray may be affected by droplet coalescence which can occur upon collision of two droplets. Coalescence would cause a greater number of smaller droplets to be transformed into a smaller number of larger droplets; because vaporization time is roughly proportional to the square of droplet diameter, the spray vaporization rate is diminished by coalescence. Whether coalescence occurs in sprays of the type of interest herein is in doubt. Experience gained at UTRC by examining holograms of sprays has shown no indication of droplet growth as distance from the injector face increases. In the case of extremely dense sprays such as those existing near the face of the nozzle of a high-thrust, high-pressure ratio gas turbine engine main burner, coalescence may be of significance in the spray development region. However, it is doubtful that experimental techniques for acquiring data in regions of extremely high droplet number density will be available in the near future. Experimental data do indicate that coalescence does not occur for all collisions based upon unreported experiments conducted at UTRC. In these experiments, droplets of alcohol intersected at right angles droplets of fuel oil. The incident droplets had the same diameter (about 100 to 200 microns). After collision, the droplets coalesced into an unstable configuration which shattered into two large droplets of approximately equal size and -- in some cases -- one or two very small droplets. (It should be noted that the study of droplet coalescence was not the purpose of these experiments.)

If coalescence is to occur, some energy must be dissipated during the collision to form a stable, larger droplet. For droplets of water falling through a mist of droplets of the same diameter, Swinbank (Ref. 4.22) has estimated that the relative kinetic energy of the colliding droplets is less than one percent of the required surface energy for droplets with diameters of 250 microns. (These energies would be somewhat less for hydrocarbon fuels because the surface tension is less for these substances than it is for water.) Swinbank conducted experiments with various fluids and observed no coalescence but his droplet diameters were less than 4 microns.

Coalescence does occur in liquid-liquid dispersions such as used in the manufacture of latex paint. As the fraction of the dispersed phase increases, the average droplet size increases until there is equilibrium between the rate of coalescence and the rate of shattering of the subsequent coalesced mass (Ref. 4.23).

A review of several papers (Ref. 4.24) stated that "no observed case of a droplet collision resulting in coalescence has been reported." However, in the case of a relatively large droplet passing through a dispersion of smaller droplets, other workers cited in Ref. 4.24 have concluded "that every drop-droplet collision results in ... coalescence." (Note: "drop" refers to the larger droplet and "droplet" refers to the smaller droplets.) In other words, collisions between droplets of about the same size do not result in coalescence; collisions between droplets of widely differing sizes do result in coalescence.

It appears that some of the uncertainty concerning whether droplets coalesce is due to problems of definition. Some workers (such as cited in Ref. 4.24) are interested in collision efficiency; that is, the probability that a droplet will collide with other droplets in a given volume. Implicit in this approach is the notion that each collision results in coalescence. Yet the previous discussion indicates that not all collisions result in coalescence. Some Russian workers have performed experiments in which a large droplet (400 μm) traverses a cloud of smaller droplets (12-13 μm) which have been doped with a special dye (Ref. 4.25). If the large droplets were spaced far enough apart so as not to interfere with each other, the collection efficiency was about 90 percent; if the large droplets were close enough to cause disturbances in the cloud that did not dampen sufficiently prior to the traverse by the next large droplet, the collection efficiency was about 40 percent. A collection efficiency of 100 percent corresponds to a concentration of dye in the collected fluid indicating the coalescence of one large droplet and one small droplet.

On the other hand, the experiments in Ref. 4.26 assume that collision efficiency and coalescence are highly correlated. In these tests, the droplets were charged electrically to simulate conditions occurring in rain cloud formation. Collision efficiency was highest for droplets of equal size and equal (but opposite) charge. For any charge, the collision efficiency was highest for droplets of equal size. Thus, electrical charge appears to have an important effect on coalescence.

The droplet collision and coalescence problem is too poorly understood and far too complicated to warrant anything other than the simplest model. The model presented herein is developed in the spirit of Swinbank's approach (Ref. 4.22).

Assumptions

In the collision model a number of assumptions are made in order to reduce the number of combinations of collisions which are considered and to avoid the definitions of new classes. These assumptions are:

1. Only binary collisions are considered because binary collisions are the most numerous.
2. Only collisions between two different classes are considered since it is assumed that all droplets of a given class move with the same velocity.
3. Only collisions between the two classes with the largest number density are considered because it is assumed that they are the most numerous.
4. Only collisions between classes in the same element of volume are considered.
5. If a collision occurs a certain fraction of droplets will coalesce, a certain fraction will rebound elastically, and the remainder will proceed unaffected.

6. To prevent the proliferation of classes, no new classes are created. Rather, the properties of the two classes involved in the collision are revised.

Number of Collisions

In a given volume of space ΔV , let the Jth class be the class with the largest number density and the Kth class be the class with the next largest number density. Then the distance between droplets in the Jth class is given by

$$l_J = \left(\frac{\Delta V}{n_J} \right)^{1/3} - D_J \quad (4.8.1)$$

and the number of collisions of class J with class K is

$$n_{\text{collJK}} = \frac{D_K}{l_J} n_K \quad (4.8.2)$$

Likewise for the Kth class

$$l_K = \left(\frac{\Delta V}{n_K} \right)^{1/3} - D_K \quad (4.8.3)$$

$$n_{\text{collKJ}} = \frac{D_J}{l_K} n_J \quad (4.8.4)$$

Then for binary collisions

$$n_{\text{coll}} = \text{MIN}(n_{\text{collJK}}, n_{\text{collKJ}}) \quad (4.8.5)$$

Probability of Coalescence

The probability of coalescence is based on the suggestion of Swinbank (Ref. 4.22) and is assumed to be proportional to the kinetic energy of the collision. The magnitude of the relative velocity of the collision between the Jth and Kth classes is given by

$$V_{JK} = \left| \bar{V}_J - \bar{V}_K \right| \quad (4.8.6)$$

If two droplets coalesce, mass is conserved and the new droplet mass is given by

$$\bar{m} = m_j + m_k \quad (4.8.7)$$

Likewise the resulting droplet temperature is given by

$$\bar{T}_L = \frac{m_j C_{PLJ} T_{LJ} + m_k C_{PLK} T_{LK}}{m_j C_{PLJ} + m_k C_{PLK}} \quad (4.8.8)$$

and the density

$$\bar{\rho}_L = \rho_L(\bar{T}_L) \quad (4.8.9)$$

Thus the coalesced droplet will have a diameter

$$\bar{D} = \left(\frac{\rho_{LJ} D_{LJ}^3 + \rho_{LK} D_{LK}^3}{\bar{\rho}_L} \right)^{1/3} \quad (4.8.10)$$

The work required to expand the Jth and Kth droplet to \bar{D} is equal to the work required to overcome the surface tension force and is given by

$$W_j = S \pi (\bar{D}^2 - D_j^2) \quad (4.8.11)$$

$$W_k = S \pi (\bar{D}^2 - D_k^2) \quad (4.8.12)$$

Hence the total work which must be dissipated to produce the coalesced droplet is

$$W_c = S \pi \bar{D}^2 - W_j - W_k \quad (4.8.13)$$

Since this energy is dissipated by the collision process, then the probability of droplet coalescence is a function of the kinetic energy of the colliding droplets due to their relative motion.

$$\epsilon_j = m_j |v_{jK}|^2 / 2 \quad (4.8.14)$$

$$\epsilon_k = m_k |v_{kJ}|^2 / 2 \quad (4.8.15)$$

Hence the kinetic energy available is

$$\epsilon_c = \text{MIN}(\epsilon_J, \epsilon_K) \quad (4.8.16)$$

The probability of coalescence is then defined as that fraction of the total number of colliding droplets that undergo collisions energetic enough to dissipate the required surface energy:

$$P_c = C \epsilon_c / W_c \leq 1 \quad (4.8.17)$$

where C is an empirically determined constant. Hence the number of droplets that collide and coalesce is given by

$$n_c = P_c n_{\text{coll}} \quad (4.8.18)$$

and the number of droplets that collide and rebound elastically is given by

$$n_{\text{RB}} = (1 - P_c) n_{\text{coll}} \quad (4.8.19)$$

The number of droplets not involved in a collision is $(n_J - n_{\text{coll}})$ from the J th class and $(n_K - n_{\text{coll}})$ from the K th class. The number of droplets that existed in the J th and K th classes prior to the collision is given by

$$n_1 = n_J + n_K \quad (4.8.20)$$

After the collision, the number of droplets is given by

$$\begin{aligned} n_2 &= P_c n_{\text{coll}} && \text{(number coalesced)} \\ &+ (1 - P_c) n_{\text{coll}} && \text{(number elastically rebounding - Jth class)} \\ &+ (1 - P_c) n_{\text{coll}} && \text{(number elastically rebounding - Kth class)} \\ &+ (n_J - n_{\text{coll}}) && \text{(number not involved - Jth class)} \\ &+ (n_K - n_{\text{coll}}) && \text{(number not involved - Kth class)} \\ &= n_J + n_K - P_c n_{\text{coll}} && \end{aligned} \quad (4.8.21)$$

Hence the total number of droplets is reduced by the amount

$$n_2 = n_1 - P_c n_{\text{coll}} \quad (4.8.22)$$

Elastic Collisions

For nonrotating droplets moving in a three-dimensional space (see Fig. 4.6), the dynamics of a collision can be reduced to a one dimensional problem by resolving forces along the line of centers. If V_{J1} and V_{K1} are the velocities before a collision and V_{J2} and V_{K2} are the velocities after a collision, then along the vector \vec{r}_c (see Fig. 4.6)

$$V_{CJ2} = \frac{m_K V_{CK1} (1-e) + (m_J - e m_K) V_{CJ1}}{m_J + m_K} \quad (4.8.23)$$

$$V_{CK2} = \frac{m_J V_{CJ1} (1-e) + (m_J - e m_K) V_{CK1}}{m_J + m_K} \quad (4.8.24)$$

where e is the coefficient of restitution (Ref. 4.27). For perfectly elastic collisions $e = 1$ and for perfectly inelastic collisions $e = 0$.

Class Properties After Collision

From Eqs. (4.8.20) and (4.8.21) it can be seen that the collision of two classes affects conditions in five classes. In order to avoid creating new classes after every collision, the Jth and Kth class are redefined with new properties which are weighted averages. Since the fuel flow rate of liquid droplets is preserved through a collision,

$$\begin{aligned} \dot{W}_{LJK} &= n_{J1} m_{J1} + n_{K1} m_{K1} = P_c n_{coll} \bar{m} + (1 - P_c) n_{coll} m_J + (n_J - n_{coll}) m_J \\ &\quad + (1 - P_c) n_{coll} m_K + (n_K - n_{coll}) m_K \end{aligned} \quad (4.8.25)$$

In the present discussion, it is assumed that the Jth class was the more numerous class prior to the collision. All of the coalesced droplets are arbitrarily assigned to this class. Then the mass and number densities in the Jth and Kth classes can be determined from Eqs. (4.8.26) through (4.8.30):

$$n_{J2} m_{J2} = P_c n_{coll} \bar{m} + (1 - P_c) n_{coll} m_{J1} + (n_{J1} - n_{coll}) m_{J1} \quad (4.8.26)$$

$$n_{K2} m_{K2} = (1 - P_c) n_{coll} m_{K1} + (n_{K1} - n_{coll}) m_{K1} \quad (4.8.27)$$

$$n_{J2} = n_{J1} \quad (4.8.28)$$

$$n_{K2} = n_{K1} - P_c n_{coll} \quad (4.8.29)$$

$$n_2 = n_1 - P_c n_{coll} \quad (4.8.30)$$

The new distribution functions can be defined by

$$f_{J2} = n_{J2} / n_2 \quad (4.8.31)$$

$$f_{K2} = n_{K2} / n_2 \quad (4.8.32)$$

The remaining properties of the new J class are given by

$$\bar{V}_{J2} = \frac{P_c n_{coll} \bar{m} \bar{V}_c + (1 - P_c) n_{coll} m_{J1} \bar{V}_{J2} + (n_{J1} - n_{coll}) m_{J1} \bar{V}_{J1}}{P_c n_{coll} \bar{m} + (1 - P_c) n_{coll} m_{J1} + (n_{J1} - n_{coll}) m_{J1}} \quad (4.8.33)$$

$$T_{LJ2} = \frac{P_c n_{coll} \bar{m} \bar{C}_{PL} \bar{T}_L + (1 - P_c) n_{coll} m_{J1} C_{PL} + T_{LJ1} + (n_{J1} - n_{coll}) m_{J1} C_{PL} T_{LJ1}}{P_c n_{coll} \bar{m} C_{PL} + (1 - P_c) n_{coll} m_{J1} C_{PL} + (n_{J1} - n_{coll}) m_{J1} C_{PL}} \quad (4.8.34)$$

Likewise for the Kth class

$$\rho_{LJ2} = \rho_L (T_{LJ2}) \quad (4.8.35)$$

$$D_{J2} = \left(\frac{6 m_{J2}}{\rho_{LJ2}} \right)^{1/3} \quad (4.8.36)$$

$$\bar{V}_{K2} = \frac{(1 - P_c) n_{coll} m_{K1} \bar{V}_{K2} + (n_{K1} - n_{coll}) m_{K1} \bar{V}_{K1}}{(1 - P_c) n_{coll} m_{K1} + (n_{K1} - n_{coll}) m_{K1}} \quad (4.8.37)$$

$$T_{LK2} = \frac{(1 - P_C) n_{coll} m_{K1} C_{PL} T_{LK1} + (n_{K1} - n_{coll}) m_{K1} C_{PL} T_{LK1}}{(1 - P_C) n_{coll} m_{K1} C_{PL} + (n_{K1} - n_{coll}) m_{K1} C_{PL}} \quad (4.8.38)$$

$$P_{LK2} = P_L(T_{LK2}) \quad (4.8.39)$$

$$D_{K2} = \left(\frac{6 m_{K2}}{\rho_{LK2}} \right)^{1/3} \quad (4.8.40)$$

ORIGINAL PAGE IS
OF POOR QUALITY

4.9 Droplet Shattering Model

Under certain circumstances, the aerodynamic and friction forces acting on a droplet will cause enough instabilities in the liquid so that a larger droplet shatters into smaller droplets. Examination of the literature (Refs. 4.28-4.29) indicates that large droplets ($\sim 10^4 \mu\text{m}$ diameter) subjected to high aerodynamic forces (as produced using shock tubes) are most likely to undergo breakup. It is not clear whether the relatively small droplets injected into the low Mach number fuel preparation section of a gas turbine can be shattered in this manner. Nevertheless, a droplet breakup model has been included in the computer program.

The droplet shattering model used in the analysis is based on a model proposed by Wolfe and Andersen (Ref. 4.28). In this model it is assumed that the breakup of the liquid droplets is controlled by rate processes; hence, the droplet must be subjected to stresses for a period of time before breaking into a finer ensemble of droplets. Breakup is assumed to occur because of deformation of the initially spherical droplet due to aerodynamic forces (bag breakup) and to stripping of liquid from the droplet surface due to friction forces (shear breakup). The time required for droplet breakup to occur is given by:

$$t_B = \frac{D}{[A^2 + B\tilde{P}]^{1/2} - A} \quad (4.9.1)$$

where:

$$A = \frac{16\mu_L}{\rho_a D} \quad (4.9.2)$$

$$B = 2/\rho_L \quad (4.9.3)$$

and

$$\tilde{P} = k_1 \frac{1}{2} \rho_m c_D |\Delta U|^2 - k_2 S/D \quad (4.9.4)$$

The values of the constants k_1 and k_2 are the empirically determined values of Wolfe and Andersen

Breakup Mode	k_1	k_2
Aerodynamic Drag	0.333	2.0
Friction Drag	0.667	4.0

The values of the breakup time are computed at each step in the trajectory for each droplet class; the minimum of the aerodynamic or friction breakup time is compared with the residence time accumulated by the droplet class subsequent to its being subjected to breakup forces. The zero time reference point for

breakup time is taken to be that previous instant of time at which the calculated breakup time undergoes a large step decrease in magnitude; this would correspond to the instant of time at which the droplet was injected into the airstream.

The diameter of the droplets produced after the shattering process (D_2) is given by an equation suggested by Wolfe and Andersen:

$$D_2 = \left[\frac{k_3 \mu_L S^{3/2} D^{1/2}}{\rho_0^2 \rho_L^{1/2} |\Delta U|^4} \right]^{1/3} \quad (4.9.5)$$

A value of k_3 equal to 136 as suggested by Wolfe and Andersen is used in the model. The number of droplets in the class undergoing shattering is adjusted by:

$$n_2 = n \left(\frac{D_2}{D} \right)^3 \quad (4.9.6)$$

so that the mass in this class is conserved.

4.10 Droplet-Solid Boundary Interaction Model

The trajectory calculation used in the PTRAK computer program is used to determine whether a droplet has struck a wall of the fuel preparation section passage. A fraction of the incident particles will rebound elastically from the wall; the other particles will adhere to the wall and may undergo evaporation.

The probability of rebound PRBJ for the Jth class is the fraction of incident particles that rebound elastically. Two mutually-exclusive probability functions are available in the model:

$$0.0 \leq PRB_J = C_1 \leq 1.0 \quad (4.10.1)$$

or

$$0.0 \leq PRB_J = 1 - C_2 (I/W)_J \leq 1.0 \quad (4.10.2)$$

where C_1 and C_2 are input constants. The parameter, I/W , is the ratio of droplet kinetic energy to deformation energy for the Jth class.

In class J, the magnitude of the droplet velocity is V_J so that the droplet kinetic energy that must be dissipated at the wall is:

$$I = \frac{1}{2} \rho_{LJ} V_J^2 \frac{\pi D_J^3}{6} \quad (4.10.3)$$

If the droplet (upon striking the wall) flattens into a hemisphere of diameter D_J , then conservation of mass requires

$$D_J' = 2^{1/3} D_J \quad (4.10.4)$$

The total surface area of the flattened droplet is

$$A_J' = \frac{1}{2} \pi (D_J')^2 + \frac{1}{4} \pi (D_J')^2 = \frac{3}{4} \pi (D_J')^2 \quad (4.10.5)$$

whereas the droplet surface area prior to deformation is

$$A_J = \pi D_J^2 \quad (4.10.6)$$

so that the work (energy) of deformation is

$$W = S(A' - A) = S\pi D_J^2 \left(\frac{3}{4} 2^{2/3} - 1 \right) \quad (4.10.7)$$

Thus--

$$(I/W)_J \cong 0.4 \rho_{LJ} D_J v_J^2 / S \quad (4.10.8)$$

The I/W ratio may be interpreted to mean that a certain amount of kinetic energy must be dissipated on impact in order that sufficient deformation of the droplet occur to cause it to stick to the wall.

For the fraction PRBJ of the droplets that rebound elastically, the droplet properties are identical to those of the incident droplets except that the normal velocity component is $-V_J n$. The fraction $1 - \text{PRBJ}$ of droplets striking the wall remain thereon and may evaporate. It must be remembered that the overall problem for the fuel mixer is a steady-state problem. The droplet transients are only important for relating droplet lifetime to spatial locations within the mixer flowfield. Thus, it is not necessary to consider the rate of fuel evaporation from the wall (as described, say, in Ref. 4.31). Rather, it is only necessary to determine how much fuel has evaporated at location X on the wall; this amount will serve as a boundary condition in the fuel vapor diffusion equation.

Any fuel that does not evaporate but remains on the wall as a film will (in time) reach a steady-state temperature equal to the wall temperature, $T_w(x)$. To determine the fate of this fuel, the percentage of fuel evaporating from the wall is guessed and the distillation temperature is found from the distillation curve. The Cox chart is then used to calculate the vapor pressure at $T_w(x)$ (see Sec. 4.5). If the vapor pressure is higher than the local ambient pressure, the guessed value of fuel evaporated is too high; if the vapor pressure is less than the local pressure, the guessed value is too low. The guessed value is adjusted until the vapor pressure and local pressure agree.

4.11 Numerical Methods

The set of equations Eqs. (4.2.1) through 4.2.6) and Eqs. (4.3.3) and (4.3.9) are solved using a predictor corrector method which is second order accurate in Δt . This algorithm may be described in functional form as follows:

$$\bar{V}_{I+1}^{p+1} = \bar{V}_I + \bar{E}(\bar{r}_m, \bar{V}_m, \bar{T}_{Lm}, D_m) \Delta t^{p+1} \quad (4.11.1)$$

$$\bar{r}_{I+1}^{p+1} = \bar{r}_I + \bar{F}(\bar{r}_m, \bar{V}_m, \bar{T}_{Lm}, D_m) \Delta t^{p+1} \quad (4.11.2)$$

$$\bar{T}_{LI+1}^{p+1} = \bar{T}_{LI} + \bar{G}(\bar{r}_m, \bar{V}_m, \bar{T}_{Lm}, D_m) \Delta t^{p+1} \quad (4.11.3)$$

$$\bar{D}_{I+1}^{p+1} = \bar{D}_I + \bar{H}(\bar{r}_m, \bar{V}_m, \bar{T}_{Lm}, D_m) \Delta t^{p+1} \quad (4.11.4)$$

$$\bar{V}_m^{p+1} = \frac{1}{2} (\bar{V}_{I+1}^{p+1} + \bar{V}_I) \quad (4.11.5)$$

$$\bar{r}_m^{p+1} = \frac{1}{2} (\bar{r}_{I+1}^{p+1} + \bar{r}_I) \quad (4.11.6)$$

$$\bar{T}_{Lm}^{p+1} = \frac{1}{2} (\bar{T}_{LI+1}^{p+1} + \bar{T}_{LI}) \quad (4.11.7)$$

$$\bar{D}_m^{p+1} = \frac{1}{2} (\bar{D}_{I+1}^{p+1} + \bar{D}_I) \quad (4.11.8)$$

$$\Delta t^{p+1} = \frac{\Delta S/V}{V_{sm}} \quad (4.11.9)$$

The initial guess for the variables at station I+1 are the corresponding values at station I. Then the differential equations are evaluated at the mid point. The iteration continues until

$$\left| \frac{\Delta t^{p+1} - \Delta t^p}{\Delta t^p} \right| < \epsilon \quad (4.11.10)$$

4.12 References

- 4.1 Dickerson, R. A. and M. D. Schuman: Rate of Aerodynamic Atomization of Droplets, *J. Spacecraft and Rockets*, January - February 1965, pp. 99-100.
- 4.2 El Wakil, M. M., O.A. Uyehara and P. S. Myers: A Theoretical Investigation of the Heating Up Period of Injected Fuel Droplets Vaporizing in Air, *NACA Technical Note 3179*, May 1954.
- 4.3 Priem, R. J. and M. F. Heidmann: Propellant Vaporization as a Design Criteria for Rocket-Engine Combustion Chambers. *NASA Technical Report R-67*, 1960.
- 4.4 Chinitz, W.: A Theoretical Model of the Spray Vaporization Processes, *United Technologies Research Center Report No. R76-110750-1*, February 1976.
- 4.5 Ranz, W. E. and W. R. Marshall, Jr.: Evaporation from Drops, Pt. I, *Chemical Engineering Progress*, Vol. 48, No. 3, March 1952, pp. 141-146.
- 4.6 Hirschfelder, J. O., C. F. Curtiss and R. B. Bird: *Molecular Theory of Gases and Liquids* (New York; Wiley, 1954), pp. 538-439, 1110-1113, and 1126-1127.
- 4.7 Barnett, H. C. and R. R. Hibbard: Properties of Aircraft Fuels, *NACA Technical Note 3276*, August 1956.
- 4.8 Moore, W. J.: *Physical Chemistry*, 3rd ed., (Englewood Cliffs, New Jersey; Prentice-Hall, 1965).
- 4.9 Cox, Edward R.: Pressure-Temperature Chart for Hydrocarbon Vapors, *Industrial and Engineering Chemistry*, Vol. 15, No. 6, 1923, pp. 592-593.
- 4.10 Perry, John H., ed.: *Chemical Engineers Handbook*, 3rd ed. (New York; McGraw-Hill, 1950), p. 564.
- 4.11 Wieber, P. R.: Calculated Temperature Histories of Vaporizing Droplets to the Critical Point, *AIAA Journal*, Vol. 1, No. 12, December 1963, pp. 2764-2770.
- 4.12 Rosner, D. E. and W. S. Chang: Transient Evaporation and Combustion of a Fuel Droplet Near its Critical Temperature, *Combustion Science and Technology*, Vol. 7, 1973, pp. 145-158.
- 4.13 Prakash, S. and W. A. Singnano: Theory of Convective Droplet Vaporization with Unsteady Heat Transfer in the Circulating Liquid Phase, *Int. J. Heat and Mass Transfer*, Vol. 23, No. 3, 1980, pp. 253-268.

References (Cont'd)

- 4.14 Redlich, O. and J. N. S. Kwong: On the Thermodynamics of Solutions, Part V - An Equation of State - Fugacities of Gaseous Solutions, Chemical Reviews, Vol. 44, 1949, pp. 233-244.
- 4.15 Shah, K. K. and G. Thodos: A Comparison of Equations of States, Industrial and Engineering Chemistry, Vol. 57, No. 3, March 1965, pp. 31-37.
- 4.16 Simonet, R. and E. Behar: A Modified Redlich-Kwong Equation of State for Accurately Representing Pure Components Data, Chemical Engineering Science, Vol. 31, 1976, pp. 37-43.
- 4.17 Reid, R. C. and T. K. Sherwood: The Properties of Gases and Liquids, 2nd ed. (New York; McGraw-Hill, 1966).
- 4.18 Faeth, G. M. and S. Chanin: Investigation of Critical Burning of Fuel Droplets, NASA CR-134793, February 1975.
- 4.19 Rosner, D. E. and W. S. Chang: Transient Evaporation and Combustion of a Fuel Droplet Near its Critical Temperature, Combustion Science and Technology, Vol. 7, 1973, pp. 145-158.
- 4.20 Canada, G. S.: High Pressure Combustion of Liquids Fuels, NASA CR-134540, January 1974.
- 4.21 Swithenbank, J. J. M. Beer, D. S. Taylor, D. Abbott and G. C. McCreath: A Laser Diagnostic Technique for the Measurement of Droplet and Particle Size Distribution, AIAA Paper No. 76-49, AIAA 14th Aerospace Sciences Meeting, Washington, D.C., January 26-28, 1976.
- 4.22 Swinbank, W. C.: Collisions of Cloud Droplets, Nature, No. 4051, June 21, 1947, pp. 849-850.
- 4.23 Delichatlos, M. A. and R. F. Probst: The Effect of Coalescence on the Average Drop Size in Liquid-Liquid Dispersions. Industrial and Engineering Chemistry, Fundamentals, Vol. 15, No. 2, 1976, pp. 134-138.
- 4.24 Pitcher, J. M., et.al: Injection and Combustion of Liquid Fuels, Battelle Memorial Institute, WADC Technical Report 46-344, March 1957, pp. 6.21-6.24.
- 4.25 Soldator, B. L. and L. E. Parlov: The Interaction of Collector Drops with a Water Aerosol, Advances in Aerosol Physics, B. S. Fedosser, editor (Jerusalem; Israel Program for Scientific Translation, 1971) pp. 60-66.

References (Cont'd)

- 4.26 Krasnogorskaya, N. V.: Experimental Investigation of the Collision Efficiency of Charged Droplets of Comparable Size, Advances in Aerosol Physics, op cit., pp. 61-67.
- 4.27 Housner, G. W. and D. E. Hudson: Applied Mechanics - Dynamics, 2nd ed. (Princeton, New Jersey; D. Van Nostrand, 1959).
- 4.28 Wolfe, H. E. and W. H. Andersen: Kinetics, Mechanism and Resultant Droplet Sizes of the Aerodynamic Breakup of Liquid Drops. Aerojet-General Report No. 0395-04 (18) SP, April 1964.
- 4.29 Dickerson, R. A. and T. A. Coultas: Breakup of Droplets in an Accelerating Gas Flow, AIAA 2nd Propulsion Joint Specialists Conference, Paper No. 66-711, Colorado Springs, Colorado, June 13-17, 1966.
- 4.30 Ranger, A. A. and J. A. Nicholls: Aerodynamic Shatter of Liquid Drops, AIAA Sixth Aerospace Sciences Meeting, Paper 68-83, New York, NY, January 22-24, 1968.
- 4.31 Gerstein, M. and M. N. Mansour: The Vaporization Behavior of a Fuel Drop on a Hot Surface, AFOSR TR-78-0010, November 1977.

4.13 List of Symbols

A	Droplet cross-sectional area (cm^2)
A_s	Droplet surface area (cm^2)
C	Mass fraction of gaseous fuel (dimensionless)
C_D	Drag coefficient of droplet (dimensionless)
C_p	Specific heat at constant pressure ($\text{cal}/\text{gm}/^\circ\text{K}$)
C_v	Specific heat at constant volume ($\text{cal}/\text{gm}/^\circ\text{K}$)
D	Droplet diameter (cm)
\mathcal{D}	Mass diffusivity (cm^2/sec)
e	Coefficient of restitution (dimensionless)
f, F	Droplet cloud distribution function (dimensionless)
h	Droplet heat transfer coefficient ($\text{cal}/\text{cm}^2/^\circ\text{K}/\text{sec}$)
I	Droplet kinetic energy ($\text{gm cm}^2/\text{sec}^2$)
k	Thermal conductivity ($\text{cal}/\text{cm}/^\circ\text{K}/\text{sec}$)
\tilde{K}	Mass transfer coefficient ($\text{gm}/\text{cm}^2/\text{atm}/^\circ\text{K}$)
ℓ	Distance between droplets (cm)
m	Droplet mass (gm)
\bar{M}	Molecular weight (dimensionless)
n	Normal coordinate (dimensionless)
n	Droplet total number density (1/sec)
n_I	Droplet number density Ith class (1/sec)
n_{coll}	Number density of collisions (1/sec)
n_{RB}	Number density of elastic collisions (1/sec)

List of Symbols (Cont'd)

Nu_h	Nusselt number for heat transfer (dimensionless)
Nu_m	Nusselt number for mass transfer (dimensionless)
P_c	Probability of coalescence (dimensionless) Or, critical pressure (atm)
P_e	Percent of liquid evaporated (dimensionless)
P	Pressure (atm)
P_f	Vapor pressure (atm)
P_r	Prandtl number $c_p \mu/k$ (dimensionless)
PRB	Probability of rebound (dimensionless)
q_s	Heat transfer rate (cal/sec)
r	Radius from axis of symmetry (cm)
\vec{r}	Position vector for droplet (cm)
Re_D	Droplet Reynolds number (dimensionless)
R_o	Universal gas constant (82.0575 cm ³ .atm/mole/°K)
R_r	Rosin-Rammler function (dimensionless)
s	Streamwise coordinate (dimensionless)
S	Surface tension (dyne/cm)
Sc	Schmidt number ($\nu/\rho/D$) (dimensionless)
SMD	Sauter mean diameter (cm)
t	Time (sec)
t_B	Droplet breakup time (sec)
T	Temperature (°K)
T_c	Critical temperature (°K)

List of Symbols (Cont'd)

T_D	Distillation temperature ($^{\circ}\text{K}$)
U_s, U_n, U_{ϕ}	Air velocity components (cm/sec)
v	Volume (cm^3)
V_s, V_n, V_{ϕ}	Droplet velocity components (cm/sec)
V	Metric scale coefficient (1/cm)
\vec{V}	Droplet velocity vector (cm/sec)
$\overset{\circ}{w}_L$	Vaporization rate gm/sec
w_f	Evaporation rate per volume ($\text{gm}/\text{cm}^3/\text{sec}$)
$\overset{\circ}{w}_{fw}$	Evaporation rate per area ($\text{gm}/\text{cm}^2/\text{sec}$)
W	Work done by surface tension (dyn cm)
$\overset{\circ}{W}_L$	Liquid fuel flow rate (gm/sec)
Y	Mole fraction (dimensionless)
z	Blowing parameter (dimensionless)
α'	Mass transfer parameter (dimensionless)
α_n, β_n	Cox chart parameters for vapor pressure
ϵ/k	Force constant ($^{\circ}\text{K}$)
λ	Heat of vaporization (cal/qm)
μ	Molecular viscosity (gm/cm/sec)
ρ	Density (gm/cm^3)
σ	Force constant (\AA)
σ_D	Variance in binomial distribution (μm)

List of Symbols (Cont'd)

Subscripts

a	Air properties
f	Gaseous fuel properties
L	Liquid fuel properties
m	Mean (air + fuel vapor film) properties
s	Conditions at droplet surface
0	Initial conditions
1	Conditions before collision
2	Conditions after collision
I, J, K	I, J, K th class
∞	Conditions far from the droplet surface (at outer edge of film)

ORIGINAL PAGE IS
OF POOR QUALITY

TABLE 4.1

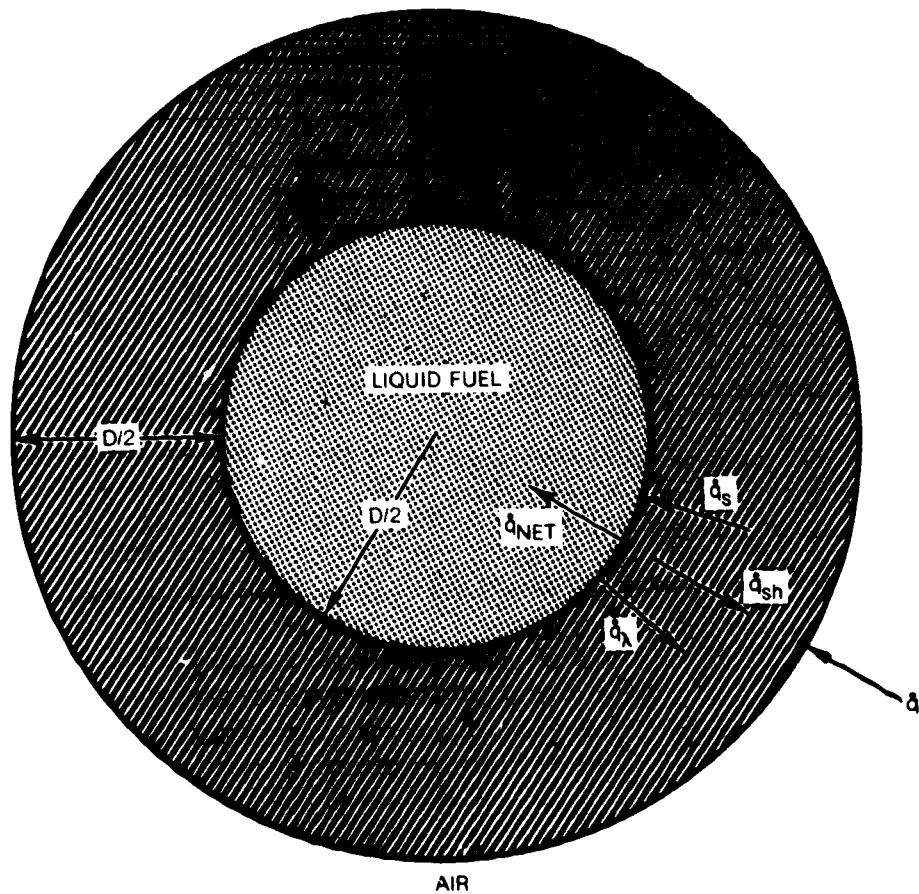
COLLISION INTEGRALS FOR CALCULATING BINARY DIFFUSION CO-EFFICIENTS

<u>T*</u>	<u>$\Omega(T^*)$</u>	<u>T*</u>	<u>$\Omega(T^*)$</u>
0.30	2.662	2.7	0.9770
0.35	2.476	2.8	0.9672
0.40	2.318	2.9	0.9576
0.45	2.184	3.0	0.9490
0.50	2.066	3.1	0.9406
0.55	1.966	3.2	0.9328
0.60	1.877	3.3	0.9256
0.65	1.798	3.4	0.9186
0.70	1.729	3.5	0.9120
0.75	1.667	3.6	0.9058
0.80	1.612	3.7	0.8998
0.85	1.562	3.8	0.8942
0.90	1.517	3.9	0.8888
0.95	1.476	4.0	0.8836
1.00	1.439	4.1	0.8788
1.05	1.406	4.2	0.8740
1.10	1.375	4.3	0.8694
1.15	1.346	4.4	0.8652
1.20	1.320	4.5	0.8610
1.25	1.296	4.6	0.8568
1.30	1.273	4.7	0.8530
1.35	1.253	4.8	0.8492
1.40	1.233	4.9	0.8456
1.45	1.215	5	0.8422
1.50	1.198	6	0.8124
1.55	1.182	7	0.7896
1.60	1.167	8	0.7712
1.65	1.153	9	0.7556
1.70	1.140	10	0.7424
1.75	1.128	20	0.6640
1.80	1.116	30	0.6232
1.85	1.105	40	0.5960
1.90	1.094	50	0.5756
1.95	1.084	60	0.5596
2.00	1.075	70	0.5464
2.10	1.057	80	0.5352
2.20	1.041	90	0.5256
2.30	1.026	100	0.5170
2.40	1.012	200	0.4644
2.50	0.9996	300	0.4360
2.60	0.9878	400	0.4170

SOURCE REF 4.6. pp 1126-1127

4.15 Figures

GEOMETRY OF DROPLET VAPORIZATION MODEL

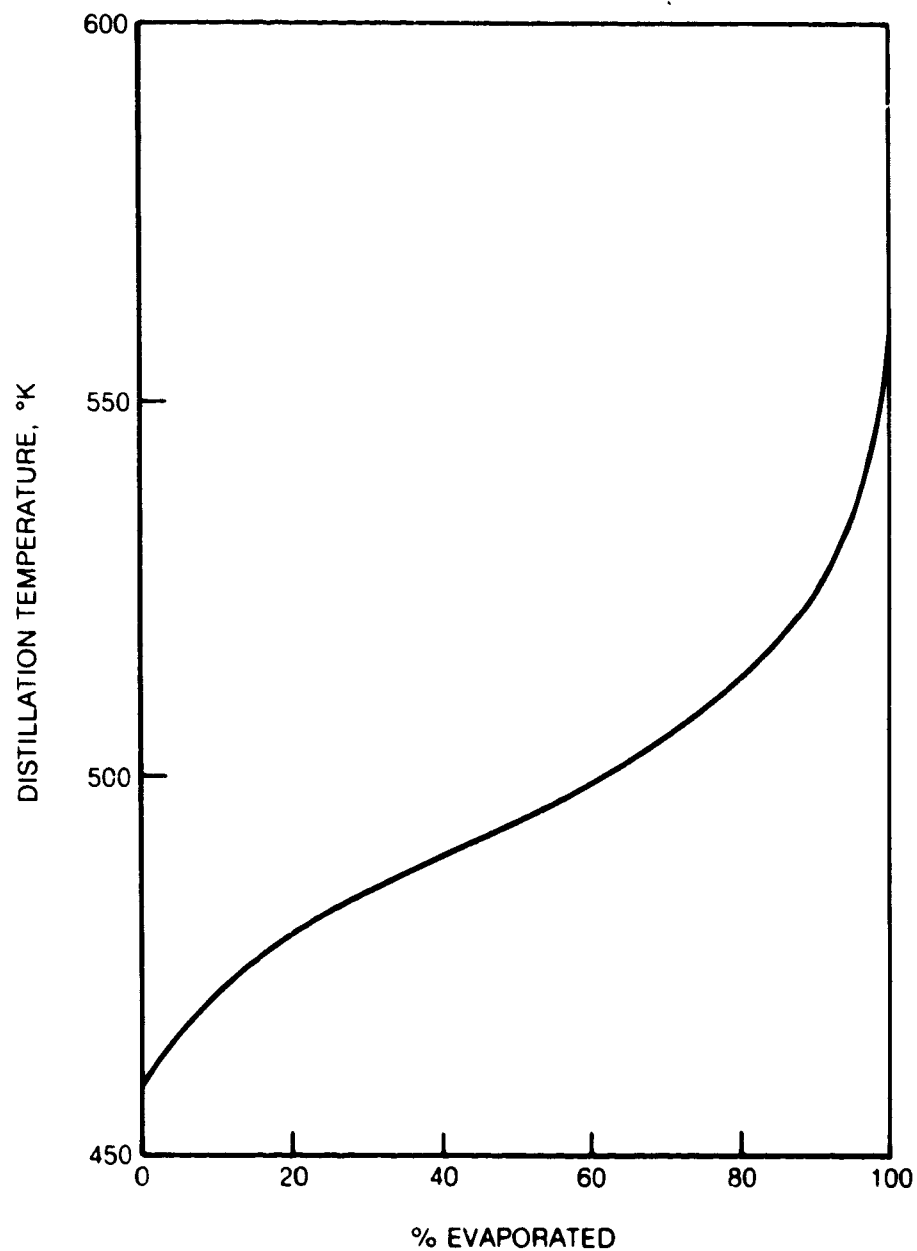


- \dot{q}_{NET} — NET HEAT TRANSFER TO LIQUID PHASE
 \dot{q}_s — HEAT TRANSFER TO DROPLET SURFACE
 \dot{q}_x — HEAT REQUIRED TO VAPORIZE FUEL
 \dot{q}_{sh} — SUPERHEAT REQUIRED TO HEAT FUEL VAPOR TO AMBIENT TEMPERATURE
 \dot{q}_t — TOTAL HEAT TRANSFER TO SYSTEM

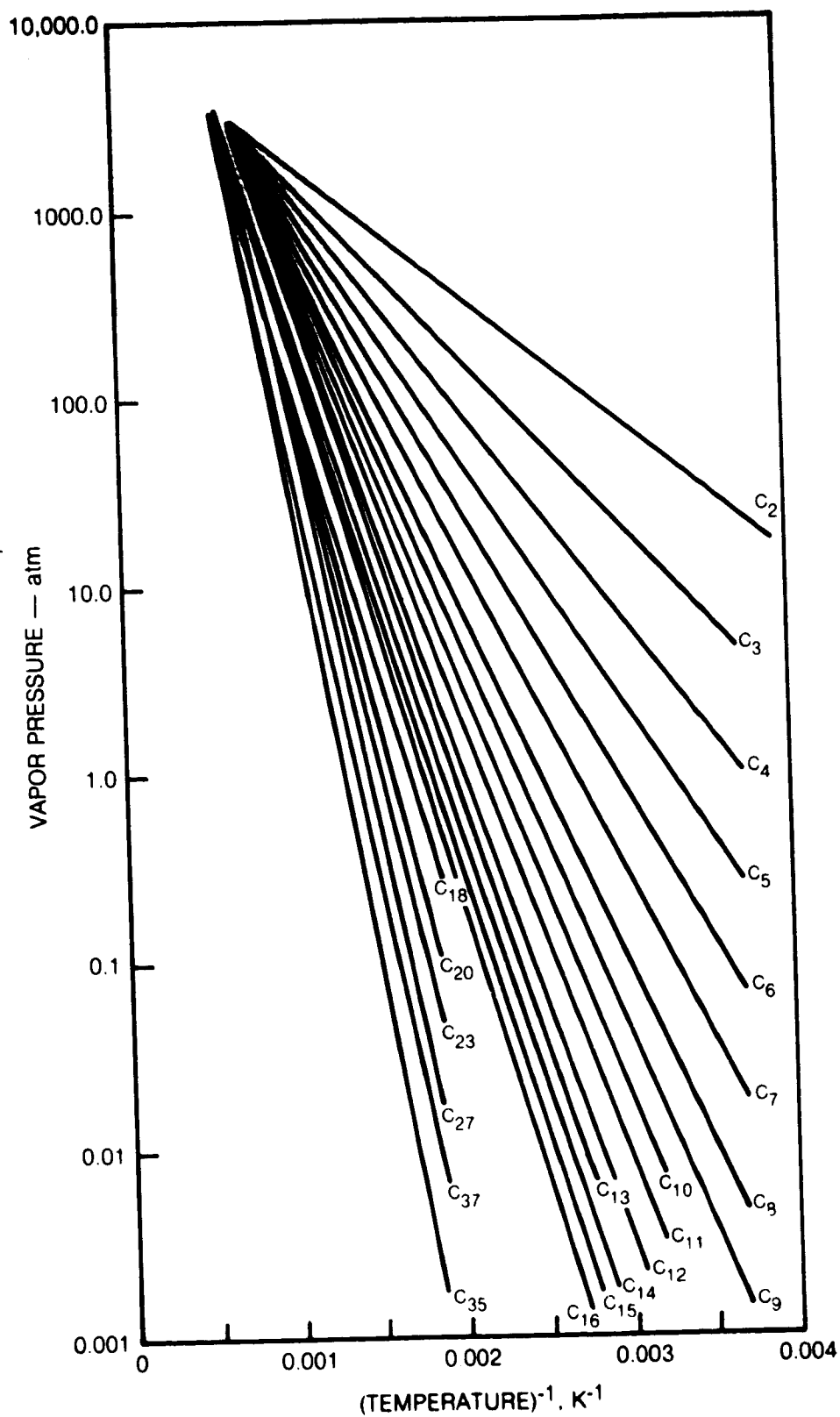
SOURCE REF 4 J

ORIGINAL PAGE IS
OF POOR QUALITY

REPRESENTATIVE DISTILLATION CURVE FOR JET-A

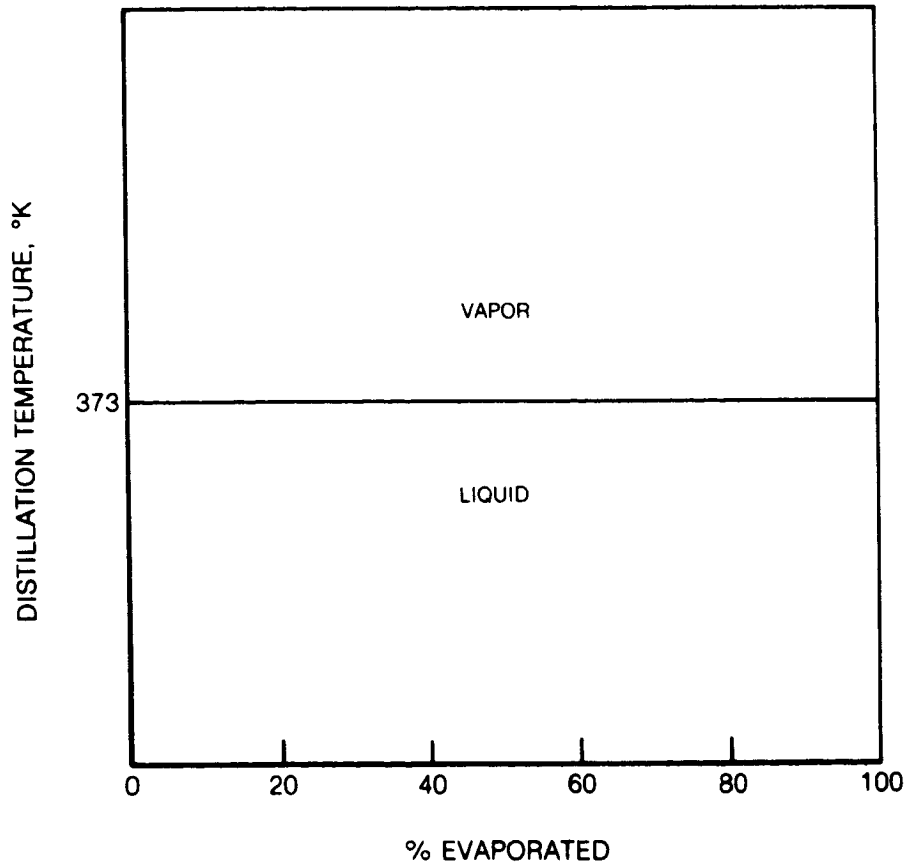


COX CHART FOR NORMAL PARAFFINS — C_nH_{2n+2}



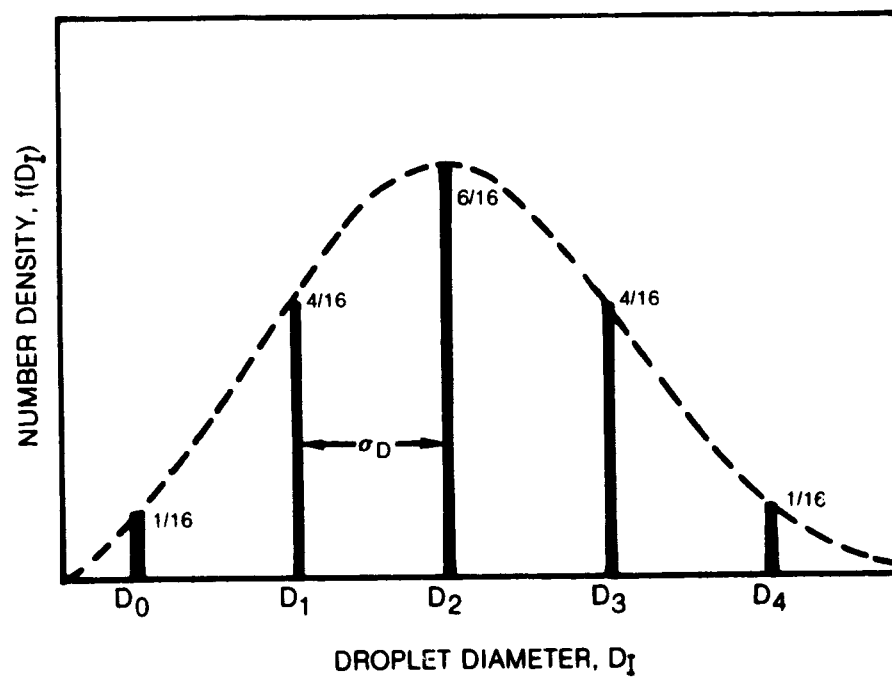
ORIGINAL PAGE IS
OF POOR QUALITY

DISTILLATION CURVE FOR WATER



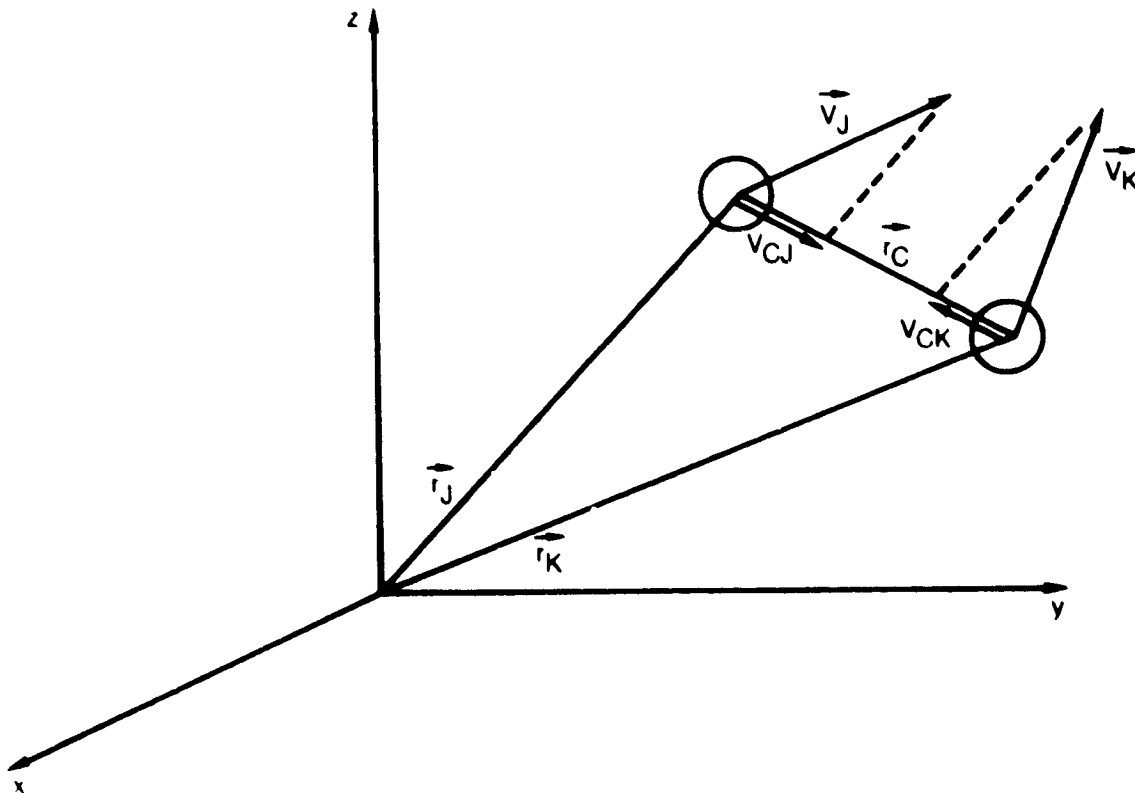
ORIGINAL PAGE IS
OF POOR QUALITY

DROPLET NUMBER DENSITY DISTRIBUTION



ORIGINAL PAGE IS
OF POOR QUALITY

VECTORIAL REPRESENTATION OF THE DYNAMICS OF DROPLET COLLISION



5.0 ANALYSIS OF DIFFUSION OF FUEL VAPOR

5.1 General Approach

Since the mass fraction of fuel vapor is small (lean equivalence ratio), the diffusion equations reduce to one equation for the mass fraction of fuel vapor diffusing into a known gas (air) flow field. The thermodynamic properties of the fuel vapor and air mixture are taken to be the thermodynamic properties of air. It is further assumed that the cloud of liquid fuel droplets does not interact with the fuel vapor other than to produce a source term in the diffusion equation due to evaporation and a source of diffusion flux at the wall due to evaporation of fuel from the wall. Since the flow field is turbulent, the turbulent diffusion coefficient is assumed to be proportional to the effective turbulent viscosity which is calculated in the solution of the air flow field. Under these conditions the diffusion equation reduces to a linear second order parabolic partial differential equation which can be solved by a forward marching integration technique. The Vapor Diffusion (VAPDIF) code is used to solve this diffusion equation.

Symbols used in this section are defined on page 71.

5.2 Fuel Vapor Diffusion Equation

If diffusion in the streamwise flow direction is neglected, then the diffusion equation in orthogonal streamline coordinates is given by:

$$v\rho U_s \frac{\partial C}{\partial s} + v\rho U_n \frac{\partial C}{\partial n} + \frac{\rho U_\phi}{r} \frac{\partial C}{\partial \phi} = \frac{v^2}{r} \left\{ \frac{\partial}{\partial n} \left[\frac{\mu_E}{S_c} r \frac{\partial C}{\partial n} \right] + \frac{\partial}{\partial \phi} \left[\frac{\mu_E}{S_c r v^2} \frac{\partial C}{\partial \phi} \right] \right\} + \dot{w}_f \quad (5.2.1)$$

$$J_n = - \frac{\mu_E}{S_c} v \frac{\partial C}{\partial n} = \dot{w}_{fw} \quad (5.2.2)$$

Since the gas flow field (ρ , U_s , U_n , U_ϕ) is known, from the ADD code calculation and \dot{w}_f and \dot{w}_{fw} are known from PTRAK calculation, Eq. (5.2.1) is a linear second order partial differential equation in the mass fraction of fuel C which can be solved by forward marching techniques with the boundary condition J_n at the wall given, and the initial conditions $C(n, \phi)$ prescribed.

5.3 Numerical Methods

The computational mesh is defined by

$$s_x = \Delta s(I-1) \quad (5.3.1)$$

$$n_j = n(j) \quad (5.3.2)$$

$$\phi_k = \Delta \phi(k-1) \quad (5.3.3)$$

$$\Delta n_j = n(j+1) - n(j) \quad (5.3.4)$$

where it is noted that the computational mesh in the n direction is not uniformly spaced. For a nonuniform mesh the difference formulae are given by

$$\frac{\partial f}{\partial n} = \left[f_{j+1,k} - (1-r^2) f_{j,k} - r^2 f_{j-1,k} \right] / d_1 \quad (5.3.5)$$

$$\frac{\partial^2 f}{\partial n^2} = \left[f_{j+1,k} - (1+r) f_{j,k} + r f_{j-1,k} \right] / d_2 \quad (5.3.6)$$

$$r = \Delta n_j / \Delta n_{j-1} \quad (5.3.7)$$

$$d_1 = \Delta n_j + r^2 \Delta n_{j-1} \quad (5.3.8)$$

$$d_2 = (\Delta n_j^2 + r \Delta n_{j-1}^2) / 2 \quad (5.3.9)$$

$$\frac{\partial f}{\partial s} = (f_{j,k}^{I+1} - f_{j,k}^I) / \Delta s \quad (5.3.10)$$

where f is any variable. These difference formulae are also applicable to a uniform grid where $r = 1$ in the ϕ direction.

Equation (5.2.1) is solved using the method of point successive over relaxation (see Roache (Ref. 5.1)). Let the difference formula for mass fraction C be given by

$$\frac{\partial C}{\partial n} = \left[C_{J+1,K}^v - (1-r^2)\tilde{C}_{J,K} - r^2 C_{J-1,K}^{v+1} \right] / d_1 \quad (5.3.11)$$

$$\frac{\partial^2 C}{\partial n^2} = \left[C_{J+1,K}^v - (1-r)\tilde{C}_{J,K} + r C_{J-1,K}^{v+1} \right] / d_2 \quad (5.3.12)$$

Then the difference formulae Eq. (5.3.5) through Eq. (5.3.12) can be applied to Eq. (5.2.1) and solved for $\tilde{C}_{J,K}$ as the unknown in terms of the value of C at neighboring points. The $v+1$ guess for $C_{J,K}^{v+1}$ is then

$$C_{J,K}^{v+1} = C_{J,K}^v + R(\tilde{C}_{J,K} - C_{J,K}^v) \quad (5.3.13)$$

The relaxation factor R as determined by Garabedian (Ref. 5.2) is given by

$$R = 2 / (1 + 3.014 \bar{h} / A^{1/2}) \quad (5.3.14)$$

where

$$\bar{h} = \sqrt{\left(\frac{n_{JL}}{JL-1}\right)^2 + \left(\frac{\phi_{KL}}{KL-1}\right)^2} \quad (5.3.15)$$

$$A = n_{JL} \phi_{KL} \quad (5.3.16)$$

Equation (5.3.13) is applied to all interior points. At the boundary, the one-sided difference formula is applied to Eq. (5.2.2). As an example, for $J = 1$

$$\frac{\partial C}{\partial n} = \left[-C_{3,K}^v + (1-r^2)C_{2,K}^v - r(r+2)C_{1,K}^{v+1} \right] / d_1 = \left(\frac{\dot{W}_{fw}}{V} \frac{Sc}{\mu E} \right) \quad (5.3.17)$$

which can be solved for $C_{J,K}^{v+1}$.

Iteration continues until

$$\left| \frac{C^{v+1} - C^v}{C^v} \right| < \epsilon \quad (5.3.18)$$

5.4 References

- 5.1 Roach, P. J.: Computational Fluid Dynamics, Hermosa Publishers, Albuquerque, N.M., 1972.
- 5.2 Garabedian, G.: Relaxation Solutions of $\nabla^2 \phi = 0$ Mathematical Tables and Other Aids to Computation, National Academy of Sciences, Vol. X, October 1956, No. 56.

5.5 List of Symbols

C	Mass fraction of fuel vapor (dimensionless)
f	Arbitrary variable
n	Normal coordinate (dimensionless)
r	Radius to axis of symmetry (cm)
S	Streamwise coordinate (dimensionless)
S_c	Schmidt number (dimensionless)
U_s, U_n, U	Air velocity components
\dot{w}_f	Evaporation rate per unit volume (gm/cm ³ /sec)
\dot{w}_{fw}	Evaporation rate per unit area (gm/cm ² /sec)
V	Metric scale coefficient (1/cm)
ϕ	Tangential coordinate (dimensionless)
μ_E	Effective turbulent viscosity (gm/cm/sec)
ρ	Density (gm/cm ³)

6.0 COMPUTER MODEL CALIBRATION

6.1 Calibration of Fuel Droplet Model

Task II of the present study consisted of calibrating the model, especially the particle tracking and vapor diffusion codes, by comparing predictions using the model with experimental data. These data were provided to UTRC by NASA which obtained them under a separate contract with Solar Turbines International (Ref. 6.1). These data were to be acquired at conditions simulating those occurring in premixing-prevaporizing ducts and were to be sufficiently detailed to include measures of the initial conditions required by the calculating procedures.

The experiments were conducted in an 8.89 x 8.89 cm square channel in which air flowed at pressures and temperatures representative of compressor discharge conditions. Fuel was injected through an orifice located on the downstream side of a circular tube at its mid-span point. The tube traversed the center of the duct and was shrouded by a thin symmetrical air foil over its entire length except in the vicinity of the orifice.

A Jet-A type aircraft gas turbine fuel was used in the experiments reported to UTRC. NASA obtained some properties of the batch of Jet-A fuel used in these tests and these are shown in Table 6.1. Fuel properties not supplied by NASA to UTRC for use in the calculations performed in Task II and Task III were estimated by UTRC from other sources.

Data were recorded at three axial positions that were located 7.5, 15 and 30 cm from the fuel injector. The stagnation pressure and stagnation temperature of air were measured at several points along bisectors of the duct both parallel and perpendicular to the axis of the fuel injector strut. Laser Doppler velocimetry (LDV) was used to determine the axial and radial components of air velocity, the axial and radial components of droplet velocity, and the fuel droplet size distribution at up to sixteen locations in the measuring half-plane at each axial station. A spillover technique was used to determine the local concentration of fuel vapor.

The data actually acquired in the experiments proved to be inadequate for model calibration. Only one set of data was provided to UTRC, and because of the large droplet sizes involved and hence very low levels of vaporization the data were of limited use in calibrating the model. Data were acquired at a pressure of 5 atm and at a temperature of 650K. The axial velocity of the air was approximately 40 m/sec. The radial velocity of the air was not reported because of problems with the data reduction equipment. Data for the fuel droplets indicated that the droplet axial velocity was typically 30 m/sec at the 7.5 cm measuring station. Droplet radial velocities were typically a few meters per second at this point. The spray velocity and mean particle size distributions were not

symmetric about the mid-plane of the duct parallel to the fuel-injector strut perhaps due to a misalignment of the fuel injector strut. The data indicated that the mean droplet size ($\sim 278 \mu\text{m}$ at the 7.5 cm measuring station) was essentially unchanged between the 7.5 to 30 cm locations. Fuel vapor concentration measurements were not reported to UTRC.

These data could not be used to calibrate the model since essentially no vaporization occurred between the 7.5 and 30 cm measuring station. The computer codes were used to verify this result. The geometry of the test section together with the air flow conditions were input into the Annular Diffuser Deck (ADD) code. The effects of the strut were ignored since it was believed that the strut would have no measurable impact on the calculated vaporization rates. The droplet axial and radial velocity components together with a mean droplet size and variance were input into the particle tracking (PTRAK) code at each of the twelve locations reported for the 7.5 cm measuring station. The program calculated that less than 3 percent of the fuel vaporized between the 7.5 cm and 30 cm axial positions.

The heat transfer, mass transfer and drag coefficients used for these calculations were those discussed in Section 4.4 and have been used by many other workers in this field. The procedure used to determine the vapor pressure of the fuel (Section 4.5) has not--as far as it is known--been used by other workers predicting fuel droplet vaporization behavior; however, the technique is a standard chemical engineering procedure. While it is comforting that the calculated and experimental results agree, it must be recognized that the vaporization and trajectory calculations can be expected to require calibration at least for flows at moderate pressures. Unfortunately, the test program had to be terminated before data could be acquired for calibration of the models used to determine the effects of droplet shattering, droplet coalescence, droplet-solid boundary interactions (other than simple elastic rebounds) and high gas stream pressure.

6.2 Model Sensitivity Study

The intent of the model sensitivity study was to assess the behavior of the model (the system of three computer programs) when flow conditions, empirical factors, and numerical factors were altered about selected mean values. Empirical factors, such as the heat and mass transfer coefficients used in the vaporization analysis, were to be determined (or verified) as part of the task of model calibration. Numerical factors are those parameters that control the mathematical progress of the codes such as those used to determine the step-size in forward-marching integration procedures.

There are three computer program used in the model. The gas flow field is determined by the Annular Diffuser Deck (ADD) code. The behavior of the fuel spray is calculated using the particle tracking (PTRAK) program. The resulting distribution of fuel vapor is estimated using the Vapor Diffusion (VAPDIF) deck. The results of VAPDIF are determined once the fuel vapor source terms and the computational grids established by the ADD and PTRAK codes are specified. The ADD code is a well-established code in use at several government and industrial sites. The sensitivity study was confined to evaluating the influence of changing air or fuel spray conditions on predictions made using the PTRAK code.

The baseline conditions used in the sensitivity study were essentially those of the calibration experiments; air stagnation pressure of 5 atm, air stagnation temperature of 650K, fuel injection temperature of 310K, and fuel droplet initial velocities of (approximately) 30 m/sec. The droplet velocity varied from point to point in the initial calculating plane similar to the experimentally-determined variation. The calculations were performed over a distance of 22.5 cm corresponding to the distance between the 7.5 cm and 30 cm measuring stations used in the calibration experiments.

Effect of Initial Droplet Diameter

The reported droplet Sauter mean diameter (SMD) for the calibration experiments (at the 7.5 cm measuring station) was 278 μm . The model predicted that less than three percent of the fuel evaporated over a distance of 22.5 cm. Calculations were also carried out for initial droplet Sauter mean diameters of 100 and 50 μm ; the model predicted that 13 percent and 39 percent, respectively, of the fuel would vaporize. All subsequent calculations were performed with an initial SMD equal to 50 μm .

Effect of Step-Size

Increasing the step-size in the particle tracking code by a factor of 2.5 above the value used in the baseline case had no effect on the calculated amount of fuel vaporized (39 percent). Step-size effects are expected to be significant only for cases in which the droplets are small and have velocities significantly different from the local air velocity.

Effect of Initial Fuel Temperature

If the fuel is preheated to 360K, the analysis indicates that 44 percent of the fuel vaporizes. This relatively small effect of fuel initial temperature is due to the droplets quickly reaching a temperature at which the rate of vaporization is just supported by the imposed heat flux. Thereafter, the droplet temperature in either case increases slowly. For droplets of pure substances evaporating in a uniform gas environment, the droplet temperature may reach a constant (wet-bulb) value. For droplets of a distillate fuel (the case analyzed here) in the same gas environment, the droplet temperature will never reach a constant value less than the ambient temperature, the droplet temperature will increase continuously as the more volatile components are evaporated. The calculated fuel droplet histories are shown in Fig. 6.1. For cases in which the initial droplet temperature transient is substantially longer, the results would differ more significantly.

Effect of Fuel Volatility

A more volatile fuel can be expected to vaporize more rapidly than a less volatile fuel. Fuel volatility was stimulated by reducing uniformly the fuel distillation curve by 50K. The analysis predicted that 55 percent of the fuel would vaporize.

Effect of Ambient Temperature

The stagnation temperature of the gas was increased from 650K to 750K. The air velocity was maintained at the original value. The ADD code was used to generate the new flow field. The PTRAK analysis calculated that 63 percent of fuel vaporized. This result is reasonable since the heat transfer rate to the droplet increases with increasing ambient temperature.

Effect of Initial Droplet Axial Velocity

The initial axial velocity of the droplets was reduced to 10 m/sec from 30 m/sec; the PTRAK code calculated that 48 percent of the fuel would vaporize. Some of this increase in fuel vaporization is due to the increased relative velocity and, hence Reynolds number, based on droplet relative velocity; the droplet heat and mass transfer coefficients used in the analysis (see Section 4.4) are strong functions of Reynolds number. Droplet residence times increase when the droplets have lower initial velocities, (Fig. 6.2), and the increase in residence time augments the effects of increased Reynolds number. For smaller droplets the effect of initial droplet velocity would be less important because these particles would accelerate more rapidly to the local gas velocity.

Effect of Ambient Pressure

As the ambient pressure of the gas is increased, the droplet Reynolds number increases and the heat and mass transfer coefficients increase in magnitude.

Thus, an increase in ambient pressure can be expected to increase the droplet vaporization rate. On the other hand, the drag force on the droplet also increases because the decrease in drag coefficient is more than offset by the increased dynamic pressure acting on the droplet. For a droplet with an initial velocity less than that of the air, the droplet accelerates more rapidly as the ambient pressure increases and the droplet residence time in the premixing passage decreases. The effect of increasing ambient pressure on the extent of fuel vaporized is the integrated result of an increased vaporization rate and a decreased residence time. No statement can be made a priori regarding the effect of increasing ambient pressure.

In the case analyzed the air stagnation pressure was increased from 5 to 10 atm. The extent of vaporization was reduced slightly from 39 to 38 percent. Evidently, the decrease in droplet residence time had a slightly greater influence than the increase in vaporization rate.

Simultaneous Effects of Ambient Pressure and Initial Droplet Velocity

In this case, the ambient pressure was again increased from 5 to 10 atm but the initial droplet axial velocity was decreased from 30 to 10 m/sec. The lower initial droplet velocity increased the residence time in the premixing passage and the PTRAK code calculated that 43 percent of the fuel vaporized.

6.3 Calibration of Vapor Diffusion Model

Calibration of the vapor diffusion model under Task II using the VAPDIF code was undertaken using experimental data provided to UTRC by NASA-Lewis Research Center. These data were obtained by NASA under a separate contract with Solar Turbines International.

The experiments were conducted in the test facility described in Section 6.1 with methane injected into the flow through a small orifice at the initial ($Z = 0$ cm) station. Methane concentrations were measured over the cross-section of the channel at the grid points shown in Fig. 6.3 at three downstream locations ($Z = 7.5, 15, 30$ cm, respectively). The average mass fraction and fuel flow rate at each station were determined by integrating the concentration data over the cross-sectional grid. These results are presented in Table 6.2 where it will be seen that the flow rate of methane increases by 60 percent from the first to third measuring station.

The VAPDIF code was run using the flow conditions presented in Table 6.2. For calculation purposes, the flow field was divided into a grid with 25×50 points at each of 38 axial locations. Convergence occurred in about 20 iterations with the residual less than 10^{-4} . Computing time was about 20 sec/station. Initial methane concentrations were obtained by curve fitting a function to the data recorded at the $Z = 7.5$ cm station.

The calculated methane concentration (mass fraction) distribution at the $Z = 30$ cm plane is shown in Fig. 6.4. This distribution is similar to the typical bell-shaped curve obtained from a point source. This result is not surprising since in the experimental program the methane was injected into the flow field through a small orifice located on the rig centerline. Comparisons of the calculated and measured concentration distributions are shown in Fig. 6.5. The data along the $X = 3.61$ cm grid line (see Fig. 6.4) was selected for comparison purposes. The results shown in Fig. 6.5 were obtained using a Schmidt number equal to 0.10. Only general agreement could be obtained.

Higher values of Schmidt number produced poorer agreement with the data. Generally, the turbulent Schmidt number is of the same order as the molecular Schmidt number (Ref. 6.2) which is about 0.8 for methane and air mixtures at the pressure and temperature presented in Table 6.2. Since the data indicate a lack of mass conservation and since the Schmidt number varies inversely with the mass diffusion coefficient, the VAPDIF computer program could not predict accurately the downstream concentration profiles given the concentration profile at the $Z = 7.5$ cm station.

6.4 References

- 6.1 Phase 1 of Data Acquisition in Low Emissions Combustor Model, Spectron Development Laboratories Inc. Report SDI No. 79-6505, Nov. 1979, Prepared for Solar Turbines International.
- 6.2 Jischa, M. and H. B. Rieke: About the Prediction of Turbulent Prandtl and Schmidt Numbers from Modeled Transport Equations, International Journal of Heat and Mass Transfer, Vol. 22, 1979, pp. 1547-1555.

6.5 Tables

TABLE 6.1

Properties of Jet-A Fuel Used in Calibration Experiments

Kinematic Viscosity	1.55 cs @ 311K
Specific Gravity	0.8096 @ 289K
Pour Point	211K
Flash Point	333K
Carbon Residue on 10 percent Residum	0.28 percent
Distillation Curve	
Initial Boiling Point	459K
10 percent distillation	472K
20 percent distillation	479K
50 percent distillation	494K
90 percent distillation	524K
End point (98.5 percent recovery)	560K

TABLE 6.2

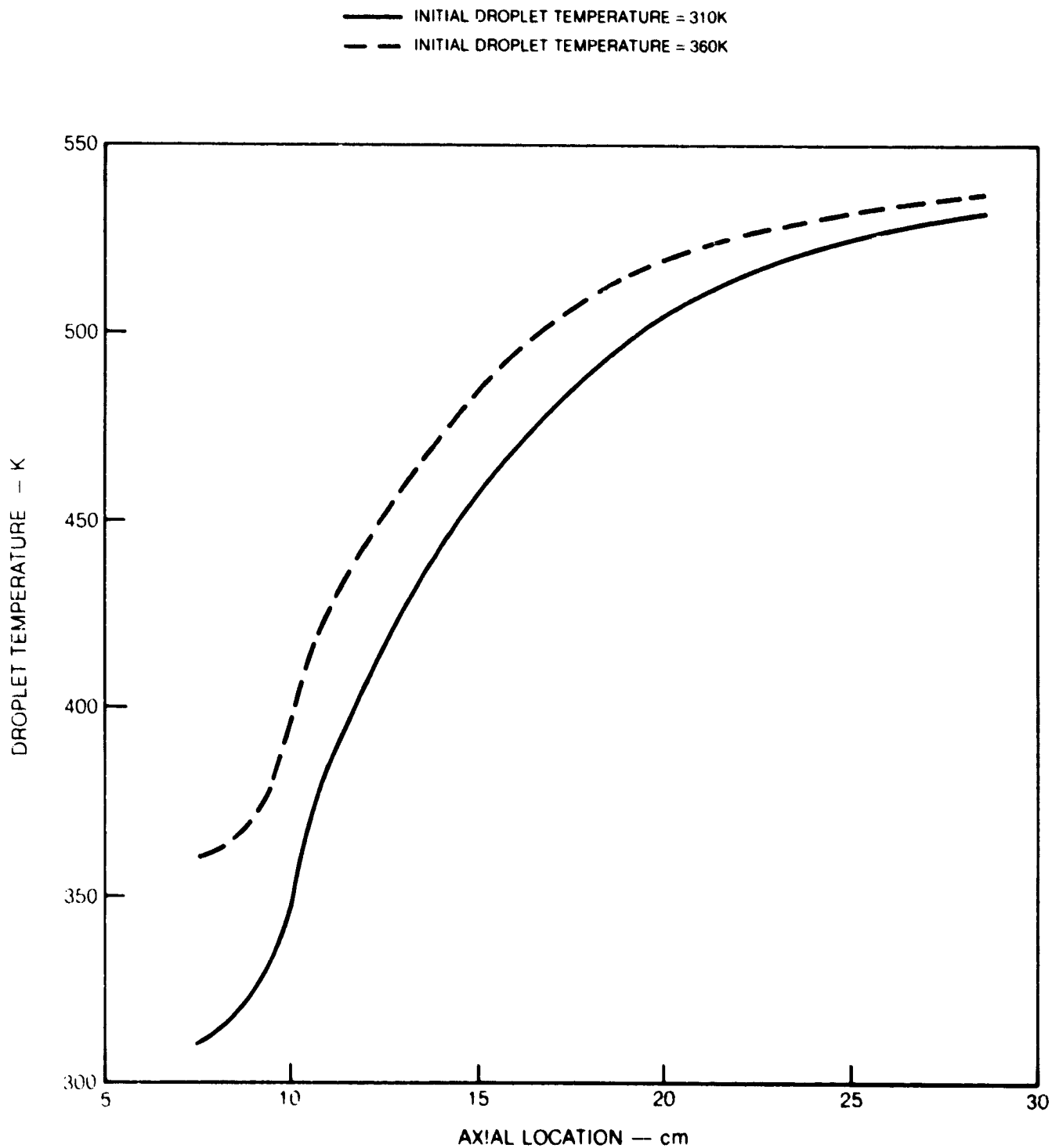
EXPERIMENTAL DATA

Methane Gas Diffusion Data

Air Velocity $V = 39.947$ m/secAir Density $\rho = 2.7929$ Kg/m³Duct Area $A = 79.02$ M²Weight Flow $W_a = .8816$ Kg/sec

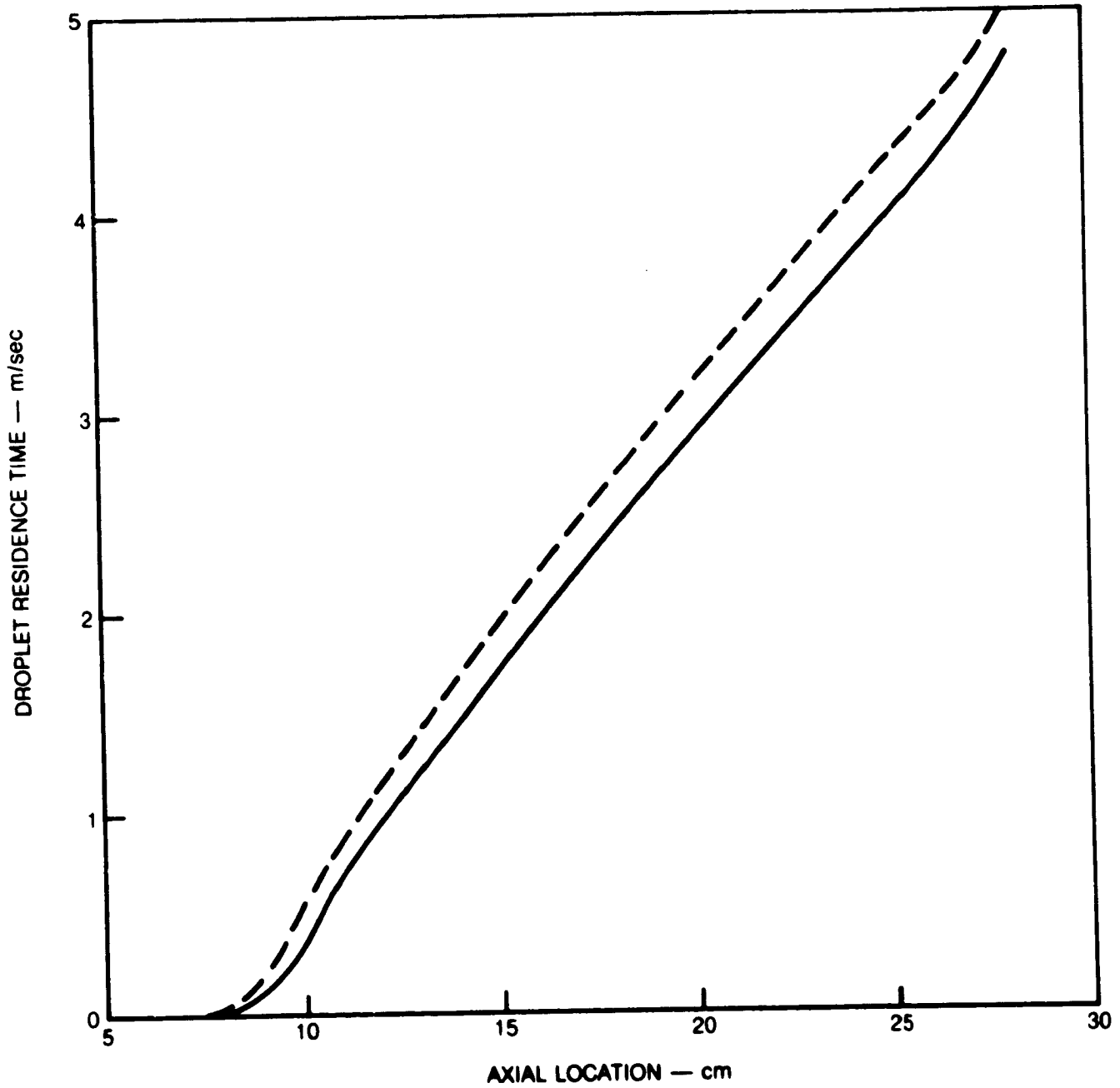
Z(cm)	$\bar{C} \times 10^4$	$W_f \times 10^4$ Kg/sec
7.5	.403	.355
15.0	.584	.515
30.0	.653	.571

CALCULATED DROPLET TEMPERATURE HISTORIES



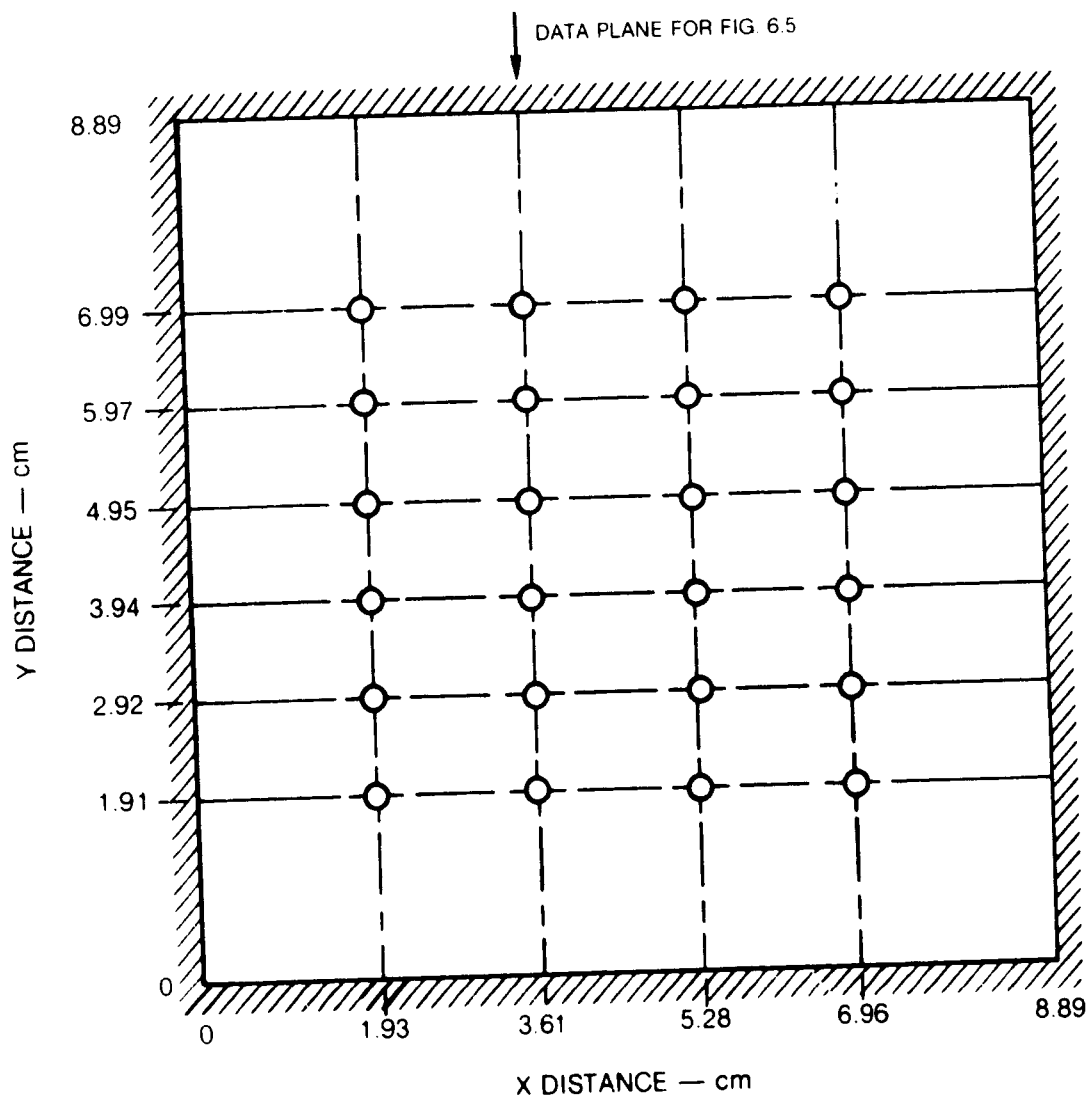
CALCULATED DROPLET RESIDENCE TIMES

— DROPLET INITIAL VELOCITY = 30 m/sec
- - DROPLET INITIAL VELOCITY = 10 m/sec

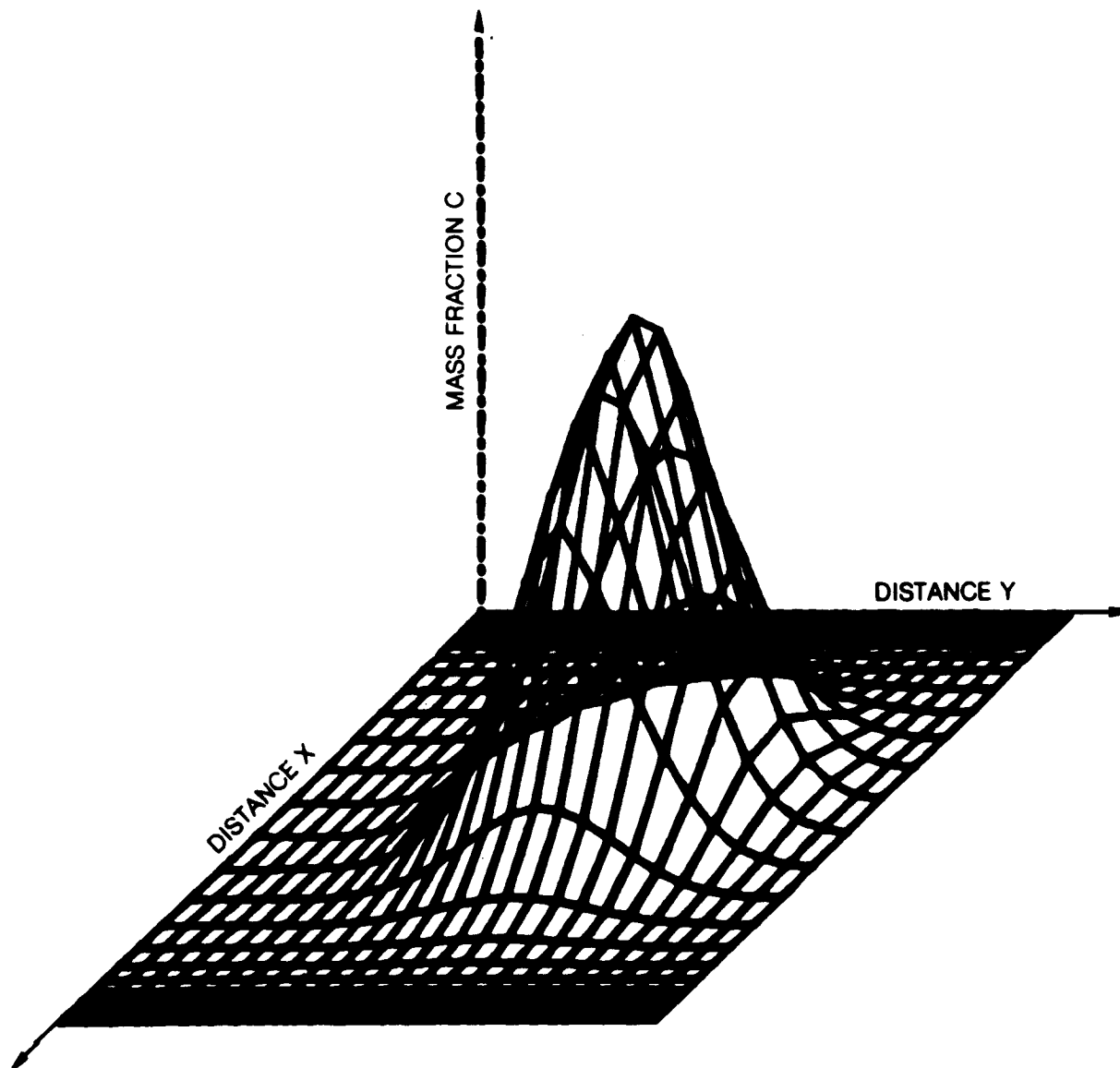


ORIGINAL PAGE IS
OF POOR QUALITY

LOCATION OF MEASUREMENT POINTS ON MEASUREMENT GRID

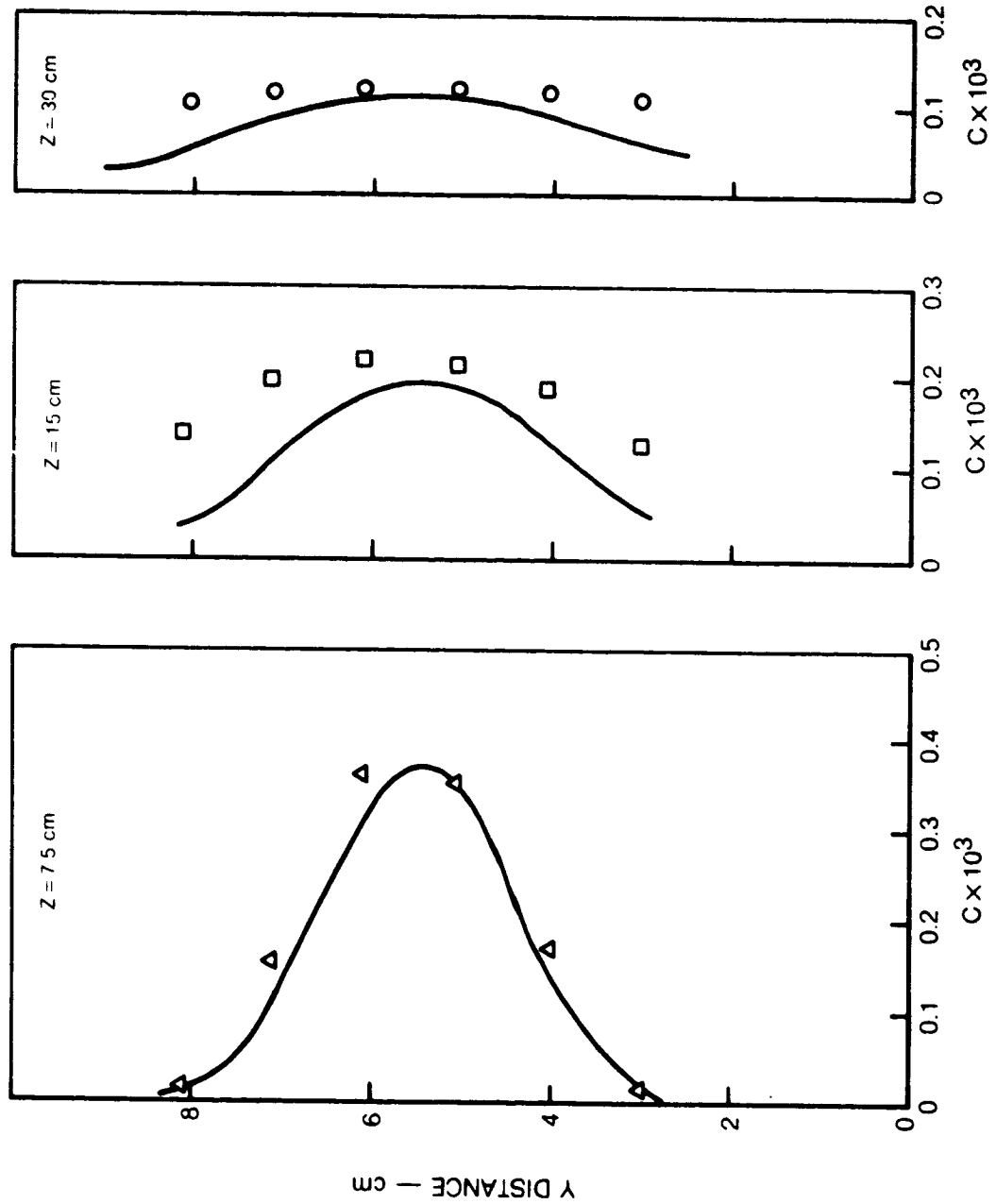


CALCULATED METHANE CONCENTRATION DISTRIBUTION AT Z = 30 cm PLANE



ORIGINAL PAGE IS
OF POOR QUALITY

COMPARISON OF CALCULATED AND MEASURED METHANE CONCENTRATION AT X = 3.61 cm



7.0 PARAMETRIC STUDIES

The model, consisting of three computer programs, was applied to the analysis of two configurations for premixing passages operating at conditions corresponding to Energy Efficient Engine (E³) cruise conditions. In the analysis of both designs, it was assumed that the inlet air stagnation temperature was 745K, the inlet air stagnation pressure was 11.1 atm, and the inlet air mean axial velocity was 54.9 m/sec. The equivalence ratio used in the analysis was different for each case.

Symbols used in this section are defined on page 92.

7.1 Swirl Tube Premixing Passage

In the swirl tube design, fuel is injected via a pressure atomizer along the centerline of an essentially cylindrical passage (5.9 cm initial diameter by 11.1 cm long); thirty of these passages are arranged at equal azimuthal positions at the upstream end of a single, annular burner (Fig. 7.1). A 15-deg swirl angle is imparted to the air. The fuel flow rate produces an overall equivalence ratio of 0.6.

The Annular Diffuser Deck (ADD) code was used to calculate the air flow field within the swirl tube using the assumed inlet air axial and tangential (swirl) velocity profiles shown in Fig. 7.2.

The Particle Tracking (PTRAK) code was used to estimate the spatial distribution of fuel vapor sources due to the vaporization of injected fuel. The fuel was divided into five classes distinguished by the angle of injection; each class contained twenty percent of the injected fuel. The Sauter mean diameter (SMD) for each class was 35 μm . Data for the pressure atomizer used in the swirl tube design indicate that the fuel spray is a hollow cone of 80-deg included angle with a variation of ± 10 deg. For the simulation, the droplets were assumed to be injected with angles of 30, 35, 40, 45 and 50-deg relative to the centerline of the passage. A fuel injection velocity of 17.6 m/sec (corresponding to the specified injector pressure drop of 1.22 atm) was assumed. (Because the initial diameter of the droplets is small, the droplets will accelerate rapidly to the freestream velocity so that the calculated results are insensitive to the choice of initial velocity in these cases.)

The calculations were performed using a 30-deg segment of each swirl tube. The fuel droplets acquire a tangential velocity component due to the swirl velocity of the air. The PTRAK code accounts for droplets exiting through one "boundary" of the segment by allowing identical droplets to enter at the opposite boundary of the segment. The radial and azimuthal variations of droplet position

for the droplet injected at an angle of 40 deg relative to the axial direction are shown in Fig. 7.3 where it can be seen that the fuel droplets are confined to the inner region of the flow. The calculations indicate that over 99 percent of the fuel is vaporized at the exit of the swirl tube (Fig. 7.4).

The Vapor Diffusion (VAPDIF) code was used to calculate the fuel vapor concentration profiles throughout the segment of the swirl tube. A turbulent Schmidt number ($Sc_t = \mu/\rho D_t$) of unity was assumed. A contour plot of equivalence ratio at the exit of the swirl tube (and, hence, entrance to the annular burner) is shown in Fig. 7.5; it is noted that little diffusion of fuel vapor has occurred. There is published evidence to suggest that the turbulent Schmidt number should be about 1.0 (Ref. 7.1); however, unpublished Corporate-sponsored analytical and experimental efforts at UTC suggest that a lower value (0.5) may be more appropriate. A lower Schmidt number corresponds to a higher rate of diffusion. In addition, the average value of eddy viscosity calculated by the ADD code is lower (by about a factor of 3.0) than anticipated based upon the use of other eddy viscosity models at UTC. The uncertainty in the calculated equivalence ratio contours due to the uncertainty in the proper choice of turbulent Schmidt number and eddy viscosity can be reduced only through the conduct of experiments to calibrate properly the model.

The available evidence indicates that the rate of mixing of the fuel vapor and air is probably understated in these calculations. However, if the calculated profiles of equivalence ratio are at all representative of conditions within a swirl tube, then it can be concluded that the design does not produce a profile satisfactory for use with the lean, premixed combustion concept. On the other hand, the design is capable of achieving nearly complete vaporization, a result is not expected to be affected by a different choice of mixing parameters (μ_t and Sc_t).

7.2 Series Staged Premixing Passage

In the series staged configuration, fuel is injected through sixty fuel injectors spaced at equal azimuthal locations within a premixing passage that is concentric with the axis of the engine (Fig. 7.6). No swirl is imparted to either the air or the fuel. The fuel injector is a simple streamlined shape (Fig. 7.7) with orifices at four equal azimuthal positions; the fuel is injected normal to the local flow direction. The axis of the fuel injector is parallel to the local flow direction. At the cruise condition, the fuel flow rate in the premixing passage produces an overall equivalence ratio of 0.55.

The ADD code was run with the uniform inlet air conditions described above and the geometry shown in Fig. 7.6 up to the point where the premixing passage just enters the combustor. Four classes of droplets were used in the PTRAK analysis. Each class had an initial SMD of 25.14 μm . Each class of droplets was injected at an angle nearly normal (80-deg) to the local freestream direction but at four equal azimuthal angle locations (corresponding to the four orifice positions) around the injector. A 6-deg segment of the annular premixing passage was analyzed. The calculations indicate that all of the fuel is vaporized upstream of the exit of the passage (Fig. 7.8).

The fuel concentration profiles were estimated using the VAPDIF code. Contour plots of equivalence ratio are shown in Fig. 7.9; as in the case of the swirl tube design, it is seen that little mixing of the fuel and air has occurred. The turbulent Schmidt number was assumed to be unity and the average eddy viscosity calculated by the ADD code was lower than the anticipated level. Thus, for reasons similar to those presented in the discussions of the swirl tube design, the degree of mixing may be understated in the series staged design.

7.3 Reference

- 7.1 Jischce, M. and H. B. Rieke: About the Prediction of Turbulent Prandtl and Schmidt Numbers for Modeled Transport Equations, International Journal of Heat and Mass Transfer, Vol. 22, 1979, pp. 1547-1555.

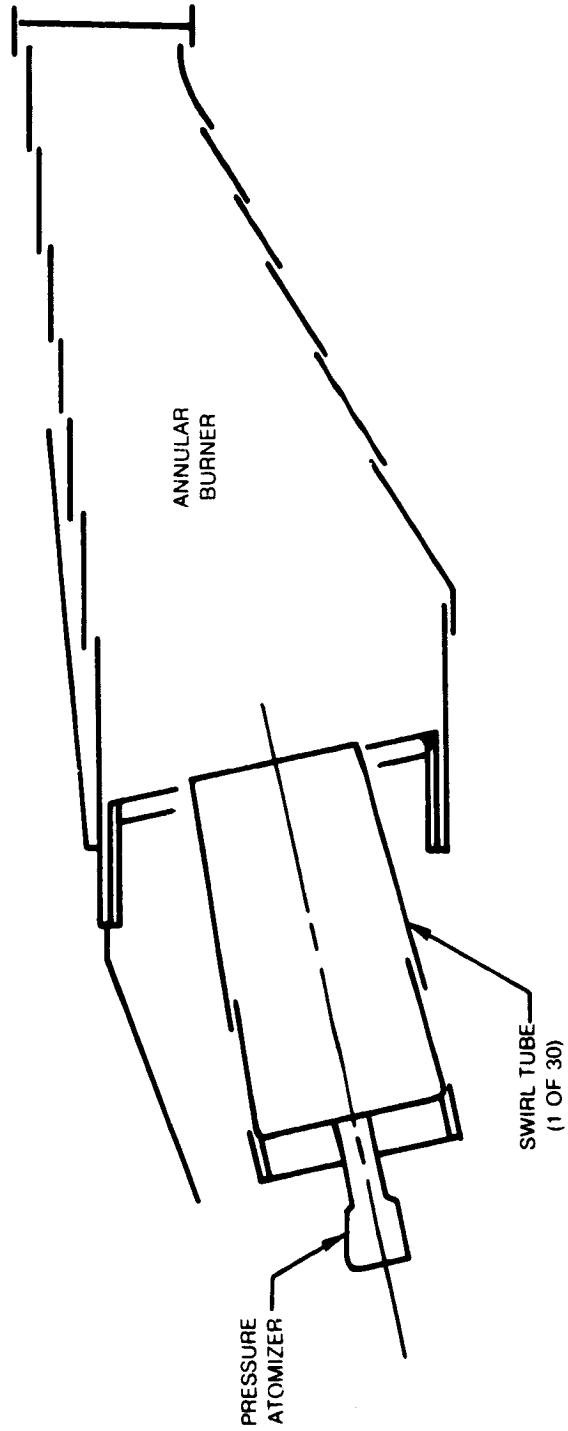
7.4 List of Symbols

\mathcal{D}_t	Turbulent mass diffusivity (cm ² /sec)
Sc_t	Turbulent Schmidt number $\mu_t/\rho\mathcal{D}_t$
μ_t	Eddy viscosity (gm/cm-sec)
ρ	Density (gm/cm ³)

SWIRL TUBE PREMIXING PASSAGE GEOMETRY

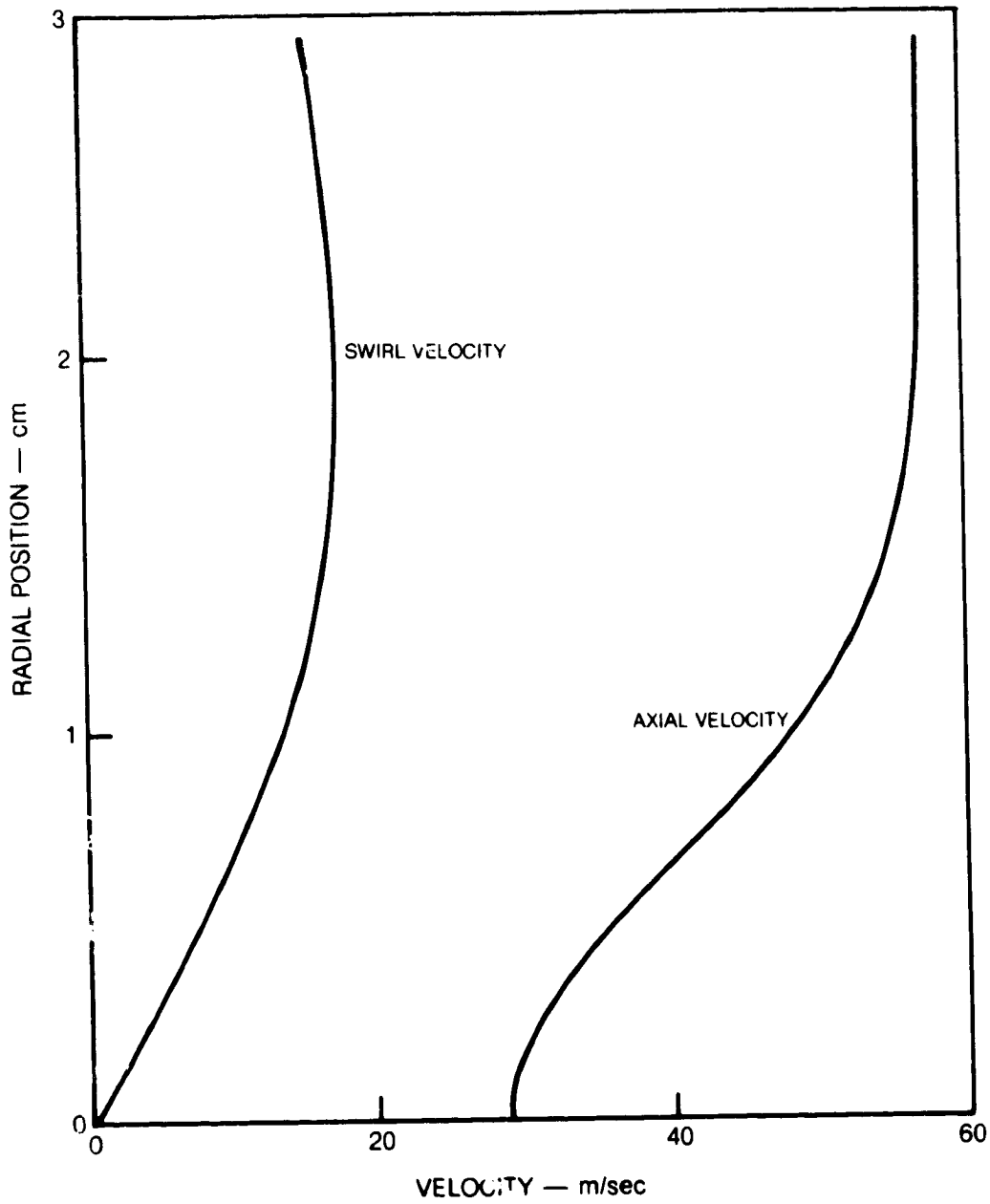
REFERENCE LINE PARALLEL TO ENGINE CENTER LINE

ORIGINAL PAGE IS
OF POOR QUALITY



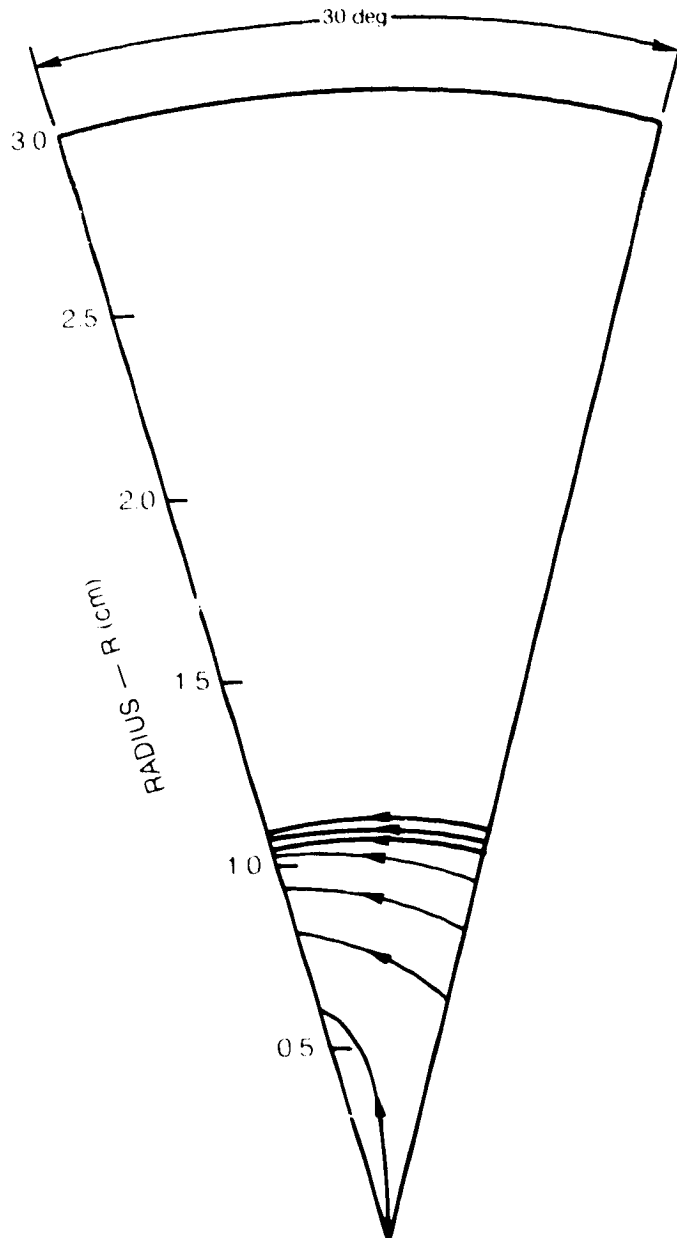
ORIGINAL PAGE IS
OF POOR QUALITY

INLET AIR VELOCITY PROFILES FOR SWIRL TUBE PREMIXING PASSAGE



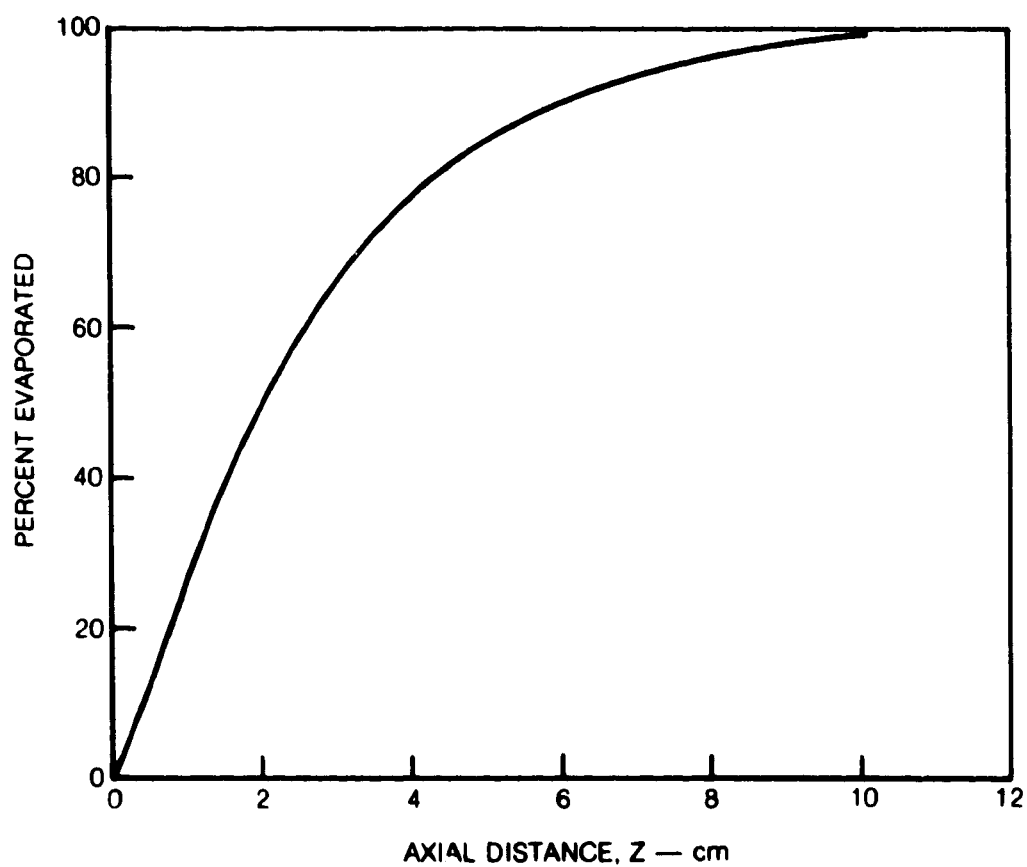
C-2

TRAJECTORY OF DROPLET INJECTED AT 40 deg ANGLE INTO
THE SWIRL TUBE PREMIXING PASSAGE

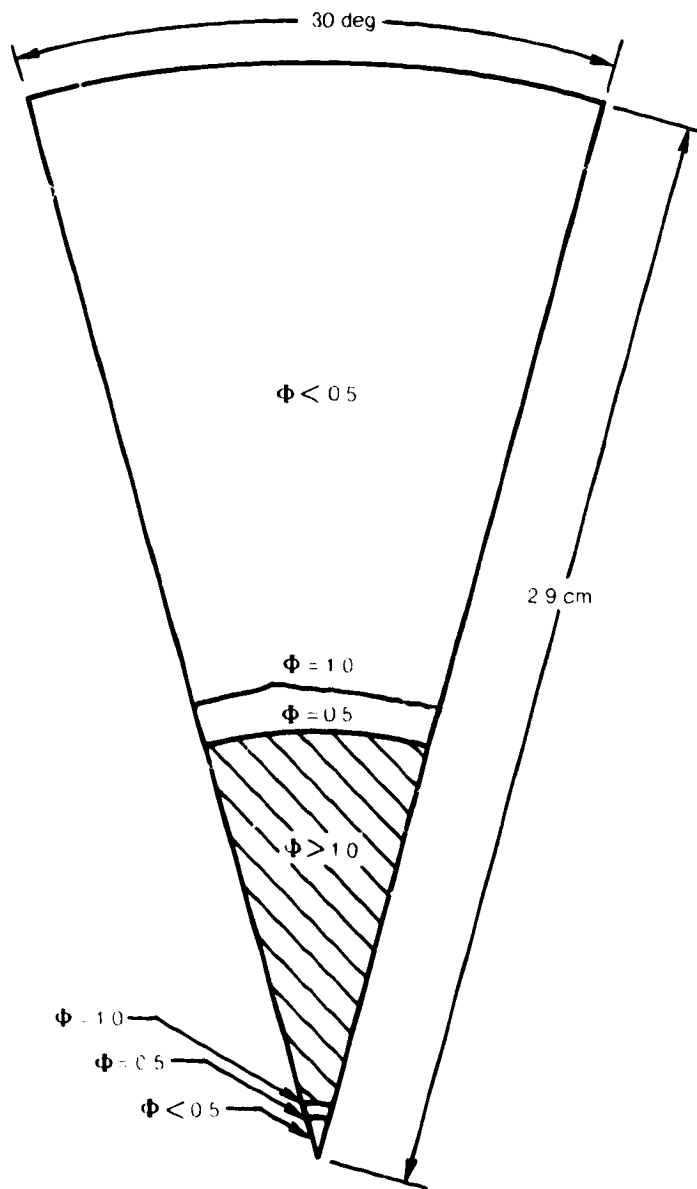


ORIGINAL PAGE IS
OF POOR QUALITY

**AXIAL VARIATION IN THE EXTENT OF FUEL EVAPORATED
IN THE SWIRL TUBE PREMIXING PASSAGE**



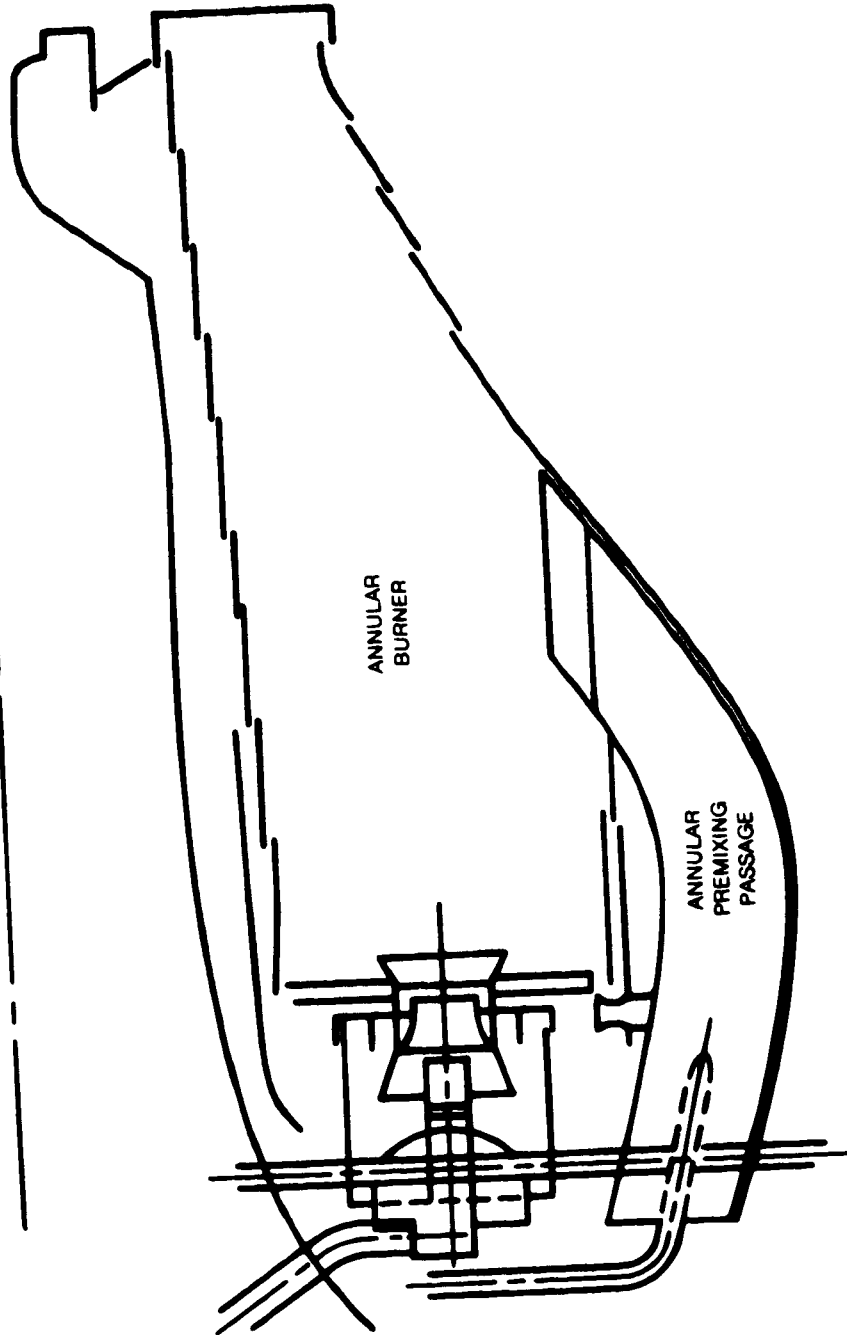
**EQUIVALENCE RATIO CONTOURS AT EXIT OF
SWIRL TUBE PREMIXING PASSAGE**



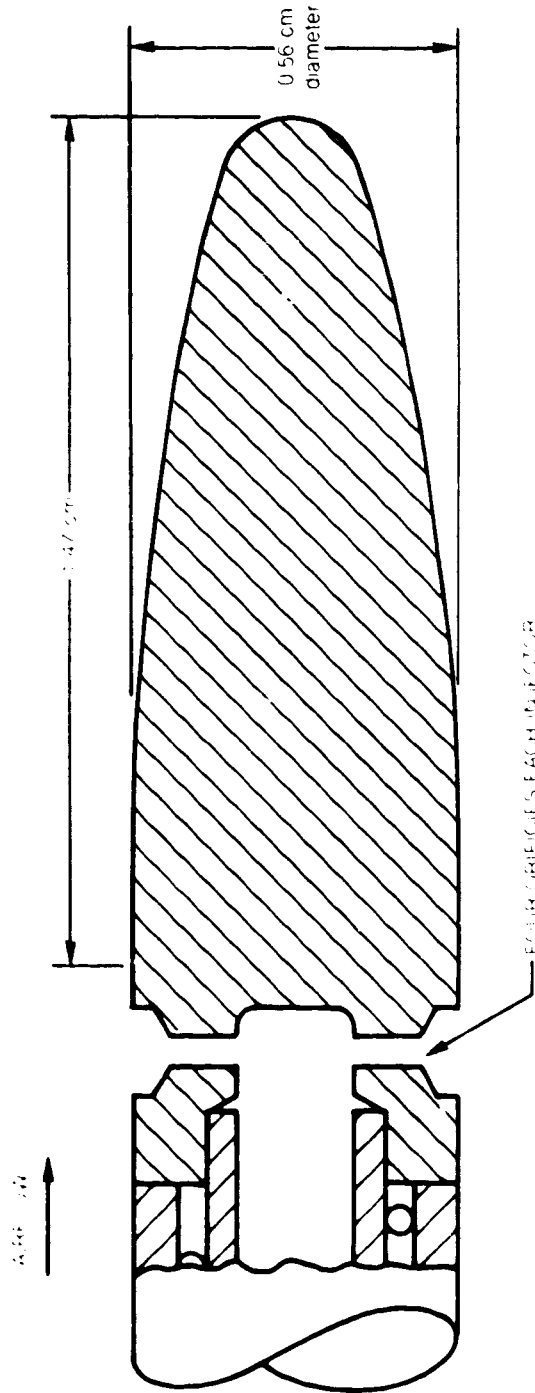
ORIGINAL PAGE IS
OF POOR QUALITY

SERIES STAGED PREMIXING PASSAGE GEOMETRY

REFERENCE LINE PARALLEL TO ENGINE CENTER LINE



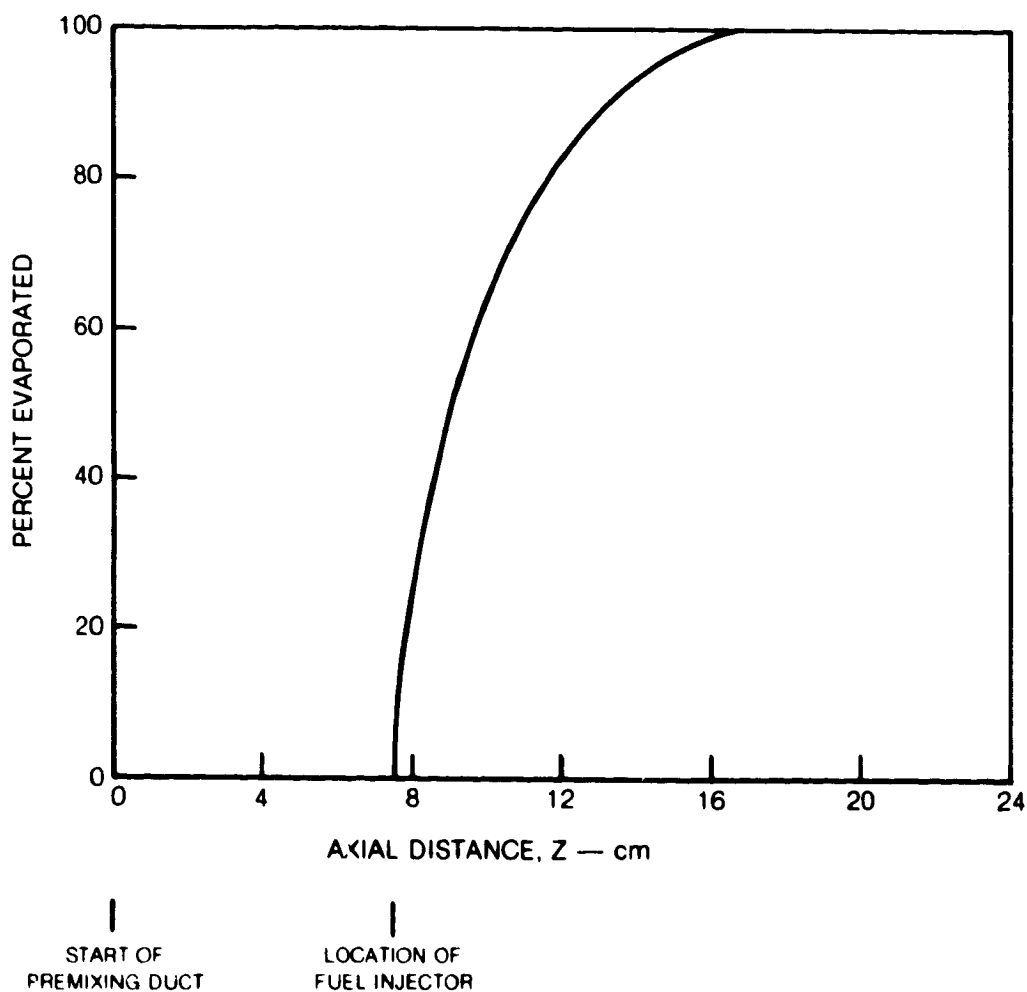
FUEL INJECTOR FOR SERIES STAGED PREMIXING PASSAGE



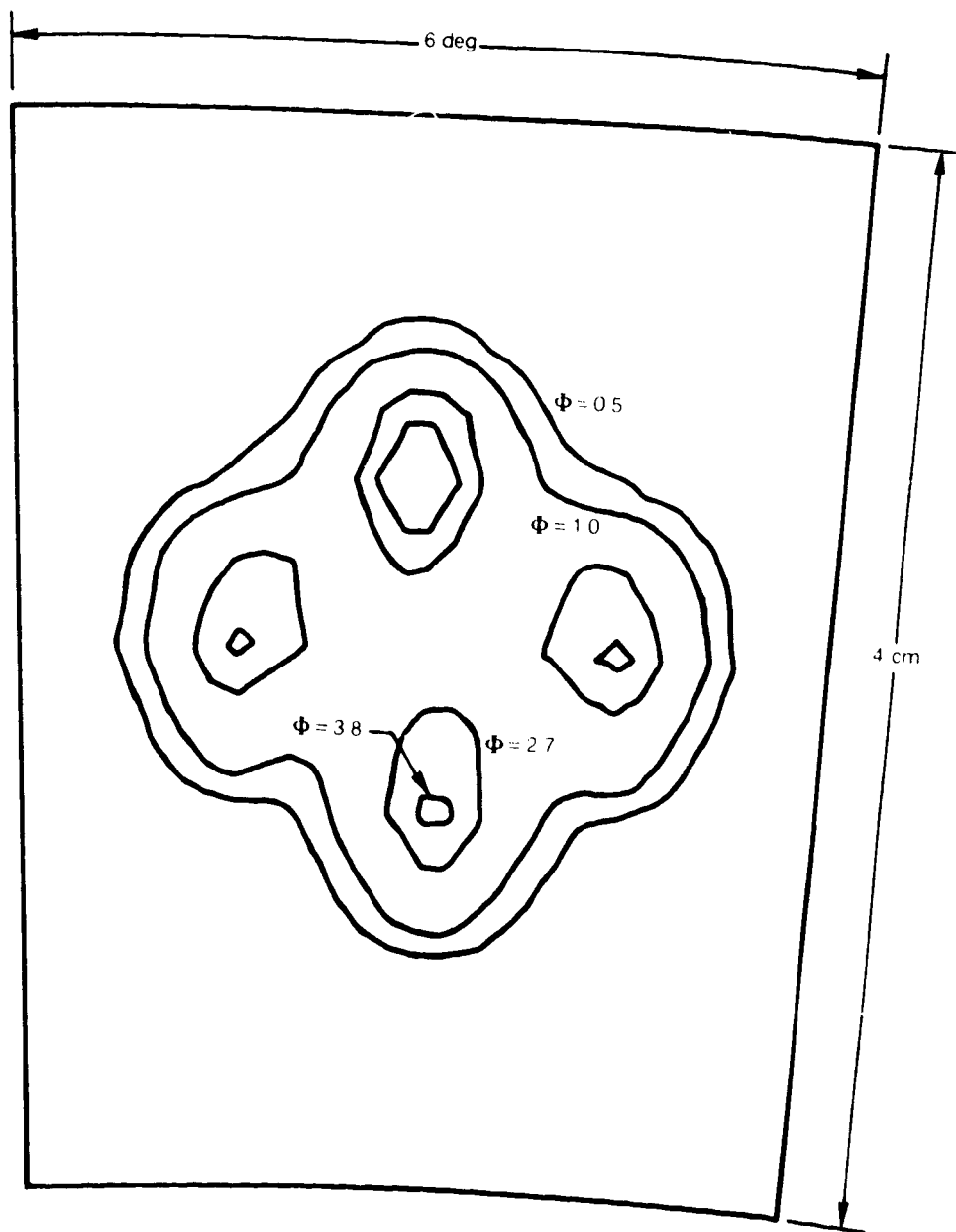
ORIGINAL PART IS
OF POOR QUALITY

ORIGINAL PAGE IS
OF POOR QUALITY

**AXIAL VARIATION IN THE EXTENT OF FUEL EVAPORATED IN THE
SERIES STAGED PREMIXING PASSAGE**



**EQUIVALENCE RATIO CONTOURS AT THE EXIT OF THE
SERIES STAGED PREMIXING PASSAGE**



3.0 ANALYSIS OF AUTOIGNITION

8.1 General Approach

The analysis described in Sections 3.0 through 5.0 provides a method for predicting the performance of an LPP design with respect to fuel vaporization and mixing. This section describes a method for predicting the occurrence of autoignition in turbulent two-phase flow within practical premixing section designs. A literature review conducted to identify the important characteristics that influence the occurrence of autoignition and to aid in the development of autoignition models is presented in the Appendix.

Two autoignition models are described in this section. In either model, it is assumed that the progress of the pre-ignition chemical reactions can be related to the level or rate of change of concentration of a critical, intermediate chemical species. The characteristics of this species and the autoignition criterion are specified for each model. As was done in the previous sections of this report, the weak interaction assumption is made so that the determination of the occurrence of autoignition can be carried out in successive steps. First, the viscous flow field for the carrier gas (air) is determined by use of the ADD code as described in Section 3.0. Second, the liquid fuel droplet heating and evaporation rates are calculated by the PTRAK code as described in Section 4.0. Third, the fuel vapor concentration distribution is calculated using the fuel vapor source terms and the VAPDIF code as presented in Section 5.0. Finally, with the distribution of fuel vapor known, the net production and turbulent mixing of critical species in the vapor phase can be calculated as described below and an estimate of autoignition time in realistic LPP mixing passage can be made. The models described in this section permit the calculation of the net production of critical species in a two-phase fuel-air mixture in which critical species are produced and consumed both throughout the diffusing fuel vapor-air mixture and within the fuel vapor film surrounding the liquid droplets. This second source of critical species is a function of fuel droplet heating and vaporization rates. The basic assumption of weak interaction has been applied throughout this formulation of the general problem of premixing passage flow analysis. For the autoignition analysis, it is assumed that the production of critical species does not affect the fuel vapor concentration. The significance of this assumption on the ignition delay times predicted by each of the two autoignition criteria is discussed below. An exception to the weak interaction has been made in that the temperature depression due to fuel evaporation is taken into account. That is, the energy which is extracted from the carrier gas and which is used to heat the fuel droplets and to evaporate the fuel results in a decrease in the temperature of the gas. This can significantly affect the pre-ignition chemical reaction rates. The amount of heat extracted from the gas is calculated in the PTRAK code and must be equal to the change in internal energy of the flow passing through a given volume of the flow field. Because the mass flux is also known, the temperature change can be calculated.

Symbols used in this section are defined on pages 114-115.

8.2 Basic Equations

It is assumed that autoignition is controlled by the level or rate of change of a critical intermediate species. The equation relating the production, convection, and turbulent mixing of this species (for which the mass fraction is designated C_2) is given by the diffusion equation

$$\frac{DC_2}{Dt} - \nabla^2 C_2 = S_g + S_d \quad (8.2.1)$$

where the convection term is

$$\frac{DC_2}{Dt} = \left[\frac{\rho u_1}{h_1} \right] \frac{\partial C_2}{\partial y_1} + \left[\frac{\rho u_2}{h_2} \right] \frac{\partial C_2}{\partial y_2} + \left[\frac{\rho u_3}{h_3} \right] \frac{\partial C_2}{\partial y_3} \quad (8.2.2)$$

and the diffusion term is

$$\begin{aligned} \nabla^2 C_2 = & \left[\frac{\mu_E}{S_c} \frac{1}{h_2^2} \right] \frac{\partial^2 C_2}{\partial y_2^2} + \left[\frac{\mu_E}{S_c} \frac{1}{h_3^2} \right] \frac{\partial^2 C_2}{\partial y_3^2} \\ & + \left[\frac{1}{h_1 h_2 h_3} \frac{\partial}{\partial y_2} \left(\frac{h_1 h_3 \mu_E}{h_2 S_c} \right) \right] \frac{\partial C_2}{\partial y_2} \\ & + \left[\frac{1}{h_1 h_2 h_3} \frac{\partial}{\partial y_3} \left(\frac{h_1 h_2 \mu_E}{h_3 S_c} \right) \right] \frac{\partial C_2}{\partial y_3} \end{aligned} \quad (8.2.3)$$

The terms within the brackets are known a priori from previous calculations (see Section 5.0). The source term S_g represents the net rate of formation (production minus consumption) per unit time per unit volume of critical species in the diffusing fuel vapor-air mixture. The source term S_d represents the net rate of formation per unit time per unit volume of critical species in the fuel vapor film surrounding the droplet. The source term S_g is calculated from

$$S_g = M_2 \frac{dx_2}{dt} \quad (8.2.4)$$

where dx_2/dt is the rate of change of molar concentration of the critical species due to chemical reaction (see Section 8.3). The molar concentration and mass fraction for critical species are related by

$$x_2 = \frac{\rho C_2}{M_2} \quad (8.2.5)$$

The source term S_d is obtained by integrating dx_2/dt over the time Δt in which the droplet resides in the volume dV , integrating over the volume of vapor film surrounding the droplet, and summing over all droplet classes.

$$S_d = M_2 \frac{n \Sigma f_i}{dV} \left\{ \int_{r_d}^{r_d+b} 4nr^2 \int_1^{1+\Delta t} \frac{dX_2}{dt} dt dr \right\} \quad (8.2.6)$$

Eq. (8.2.6) is evaluated at the local temperature and fuel concentration (partial pressure) of the vapor surrounding each droplet. The radial variations in temperature and fuel vapor partial pressure are determined in accordance with the model presented in Section 4.0 which is based upon the model described in Ref. 8.1. The radial variation in film temperature is given by

$$T_f = \frac{\dot{q}_s}{hA_s z} \left\{ \exp \left[z \frac{r-r_s}{r_s} \right] - 1 \right\} + T_s \quad (8.2.7)$$

It can be shown that the Lewis number within the fuel vapor film is generally not equal to unity so that the thicknesses of the heat and mass transfer boundary layers surrounding the droplet differ. However, the heat transfer and mass transfer coefficients used in the model developed in Ref. 8.1 are determined from correlations that use droplet diameter as the length scale; this convention has the practical effect of defining the heat and mass transfer boundary layer thicknesses as equal. Essentially, the model presented in Ref. 8.1 is used to derive a functional form for the vaporization rate and then a mass transfer coefficient correlation is used to obtain the constant of proportionality. Consistent with this approach, the functional form for the radial variation of fuel vapor partial pressure is derived assuming that the heat and mass transfer boundary layer thicknesses are equal.

$$P_f = P_0 - (P_0 - P_{f,s}) \exp [A(r - r_s)] \quad (8.2.8)$$

where

$$A = \frac{1}{r_s} \ln \left(\frac{P_0}{P_0 - P_{f,s}} \right) \quad (8.2.9)$$

Then the molar concentration of fuel is:

$$X_1 = P_f / (R_0 T_f) \quad (8.2.10)$$

The decrease in temperature of the carrier gas (air) due to the heat extracted by droplet heating and vaporization is calculated from the energy equation. If it is assumed that diffusion and crosswise convection can be neglected, then

$$\left[\frac{\rho u_1 C_p}{h_1} \right] \frac{dT}{dy_1} = -n \frac{\Sigma f_i}{dV} \left\{ \int_1^{1+\Delta t} \dot{q}_s dt \right\} \quad (8.2.11)$$

where the sink term on the right-hand side is obtained by integrating the droplet heat transfer rate over the time the droplet resides in the volume dV and then summing these integrals for all droplet classes.

8.3 Autoignition Models

The first autoignition model described in this section (designated Model I) is based on a kinetics scheme proposed by Hautman, et al. (Ref. 8.2) who examined data for the autoignition of several paraffin fuels and determined that during the pre-ignition period (1) the fuel molecule decomposes into ethene and other chemical species and (2) the maximum ethene concentration corresponds in time to the time at which a sudden rise in gas temperature occurs. Thus, the time of maximum ethene concentration is defined by the authors as the autoignition time. It is assumed in the model described in Ref. 8.2 that all of the fuel is in the vapor phase, that the amount of fuel is specified as an initial condition, and that all chemical reactions occur in the vapor phase at the molecular level. It is assumed herein that this model can be generalized to two-phase flows consisting of mixtures of liquid fuel droplets and fuel vapor convected by a carrier gas such as air. The rate of change of the molar concentration of ethene is given by

$$\frac{dx_2}{dt} = \frac{\eta}{2} R_F X_{O_2}^{\alpha_F} X_1^{\beta_F} X_2^{\gamma_F} - R_B X_{O_2}^{\alpha_B} X_1^{\beta_B} X_2^{\gamma_B} \quad (8.3.1)$$

(where X_1 and X_2 represent the concentrations of fuel and critical species, respectively) and the reaction rate constants are of the form

$$R_F = A_F \exp(-E_F/R^*T) \quad (8.3.2)$$

$$R_B = A_B \exp(-E_B/R^*T) \quad (8.3.3)$$

Although Eq. (8.3.1) has the formal structure consistent with forward and reverse reactions, it could represent the net production and depletion of ethene by distinct processes. In terms of mass fraction, Eq. (8.3.1) becomes

$$S_g = \frac{\eta}{2} \bar{R}_F X_{O_2}^{\alpha_F} C_1^{\beta_F} C_2^{\gamma_F} - \bar{R}_B X_{O_2}^{\alpha_B} C_1^{\beta_B} C_2^{\gamma_B} \quad (8.3.4)$$

where

$$\bar{R}_F = \frac{M_2 \rho^{\beta_F + \gamma_F} R_F}{M_1^{\beta_F} M_2^{\gamma_F}} \quad (8.3.5)$$

and

$$\bar{R}_B = \frac{M_2 \rho^{\beta_B + \gamma_B} R_B}{M_1^{\beta_B} M_2^{\gamma_B}} \quad (8.3.6)$$

In the model described in Ref. 8.2, the rate of depletion of fuel is calculated according to:

$$\frac{dx_1}{dt} = -R_F x_{O_2}^{\alpha_F} x_1^{\beta_F} x_2^{\gamma_F} \quad (8.3.7)$$

Eqs. (8.3.1) and (8.3.7) are solved simultaneously. Since β_B is negative, then the ethene concentration will (eventually) reach a maximum and decrease thereafter. The time of maximum ethene concentration (as indicated by dx_2/dt equal to zero) is designated as the autoignition time.

Due to the weak interaction assumption, no fuel depletion chemical reaction is included in the present analysis. Thus, the concentration of ethene will approach asymptotically a maximum value and an autoignition criterion different from that used in Ref. 8.2 must be developed. In the present analysis, autoignition is assumed to occur when the time rate of change of ethene due to chemical reaction becomes less than some specified fraction of the local ethene concentration; i.e.,

$$\frac{dx_2/dt}{x_2} < \omega \quad (8.3.8)$$

It has been estimated by the present authors using the data presented in Ref. 8.2 that ω is of the order of 5000 sec^{-1} . A refined estimate of ω would require calibration of the criterion used herein with the numerical results reported in Ref. 8.2

It should be noted that the model described in Ref. 8.2 is based upon data obtained using a shock tube operated at stagnation temperatures typically in excess of 1200K whereas the present analysis is intended for use in the analysis of premixing passages (stagnation temperatures between 400 and 900K). The constants used in the model described in Ref. 8.2 were obtained by calibrating the model with these shock tube data. It is well-known that different rate-controlling processes may be important at high and low temperatures. The present authors estimate that the use of the model constants presented in Ref. 8.2, when applying the model to the analysis of flows within premixing passages, will produce unrealistically large values of ignition delay time. Clearly, calibration of this model for the lower temperature (and higher pressure) levels characteristic of flows within premixing passages is required and therefore, there is no basis for selecting a value of the autoignition criterion (ω) for these conditions.

In the second model for autoignition (Model II), it is assumed that autoignition occurs when the concentration of an unknown, critical species reaches a critical value. This approach is essentially the same as that described in Ref. 8.3. Model constants are obtained by comparing the calculated autoignition time with experimental data. Thus, if X_2 represents molar concentration of critical species and if X_{2c} is its critical value, then ignition occurs when

$$X_2 \geq X_{2c} \quad (8.3.9)$$

ORIGINAL PAGE IS
OF POOR QUALITY

or equivalently,

$$\frac{x_2}{x_{2c}} \geq 1 \quad (8.3.10)$$

It is assumed that the normalized rate of production of critical species is given by an expression of the form:

$$\frac{d(x_2/x_{2c})}{dt} = A_F e^{-E_F/R^*T} x_f x_{O_2} \phi_T^{\delta} \quad (8.3.11)$$

and that the production of X_2 has negligible effect on the concentration of fuel and oxidizer.

In order to use Eq. (8.3.11) in the diffusion equation, Eq. (8.2.1), it is necessary either (1) to know the value of x_{2c} or (2) to express both the source terms and the diffusion equation in terms of normalized concentrations. Because in this model the characteristics of the critical species are unknown, the second approach is taken. The source terms given by Eqs. (8.2.4) and (8.2.6) can be expressed as:

$$S_g = x_{2c} f_g \left[d(x_2/x_{2c})/dt \right] \quad (8.3.12)$$

and

$$S_d = x_{2c} f_d \left[d(x_2/x_{2c})/dt \right] \quad (8.3.13)$$

and the diffusion equation can be written as:

$$\frac{D(C_2/C_{2c})}{Dt} - \tilde{\nabla}^2 (C_2/C_{2c}) = \frac{x_{2c}}{C_{2c}} (f_g + f_d) \quad (8.3.14)$$

then, using Eq. (8.2.5),

$$\frac{D(C_2/C_{2c})}{Dt} - \tilde{\nabla}^2 (C_2/C_{2c}) = -\frac{\rho}{M_2} (f_g + f_d) \quad (8.3.15)$$

It is evident from examination of Eqs. (8.2.4), (8.2.6), and (8.3.15) that the computed relative mass fraction distribution is independent of M_2 , the molecular weight of the critical species.

The constants appearing in Eq. (8.3.11) are obtained by first deriving an expression for the ignition delay time for a uniform fuel-air mixture in a constant temperature, constant pressure flow and then comparing the result to the appropriate

ORIGINAL PAGE IS
OF POOR QUALITY

ignition delay time correlation for this simple flow situation. The autoignition time τ is defined such that

$$\int_0^{\tau} \frac{d(X_2/X_{2c})}{dt} dt = 1 \quad (8.3.16)$$

or

$$A_{Fe}^{-E_F/R^*T} X_f X_{O_2} \phi^{\delta} T^{\nu} \tau = 1 \quad (8.3.17)$$

and therefore

$$\tau = \frac{A_{Fe}^{-1} e^{E_F/R^*T}}{X_f X_{O_2} \phi^{\delta} T^{\nu}} \quad (8.3.18)$$

As an example of the method used to determine the constants in Eq. (8.3.11), consider the ignition delay time data for various fuels obtained by Spadaccini and TeVelde (Ref. 8.4) and recently correlated in terms of mixture temperature and equivalence ration (Ref. 8.5). A suggested correlation assuming second-order pressure dependence is, for example only:

$$\tau = \frac{k e^{E/RT}}{P^2 \phi} \quad (8.3.19)$$

The temperature appearing in Eq. (8.3.19) is the mixture temperature corresponding to the equivalence ratio, ϕ . The equivalence ratio is related to the molar concentrations of fuel and oxygen by

$$\phi = \frac{X_f/X_{O_2}}{1/n_{ST}} \quad (8.3.20)$$

so that

$$X_f = X_{O_2} \phi / n_{ST} \quad (8.3.21)$$

and

$$X_{O_2} = y_{O_2} \frac{P}{R_0 T} \quad (8.3.22)$$

Thus, Eq. (8.3.19) becomes

$$\tau = \frac{R_0^2 n_{ST}}{A_{Fe}^2} \frac{e^{E_F/R^*T}}{P^2 \phi^{1+\delta} T^{2-\nu}} \quad (8.3.23)$$

Then, comparing Eqs. (8.3.19) and (8.3.23), the constant used in the model are

$$A = \frac{R_0^2 n_{st}}{Y_0^2 K}$$

$$E_F = E$$

$$\delta = 0$$

$$v = 2$$

8.4 Numerical Methods

The source term S_d given by Eq. (8.2.6) and the energy sink term in Eq. (8.2.11) are calculated in the PTRAK code using a predictor-corrector method described in Section 4.11. This method is second-order accurate over the time step Δt . The volume integration in Eq. (8.2.6) is obtained using the trapezoidal rule which is also second-order accurate.

The solution of the non-linear diffusion equation, Eq. (8.2.1), is obtained using the numerical methods described in Section 5.3 and is included as part of the VAPDIF code. The source term S_g requires special treatment when Model I is used since Eq. (8.3.4) is nonlinear in C_2 . The authors of the model described in Ref. 8.2 recommend an integration step-size on the order of one microsecond whereas the typical integration step-size (in terms of flow residence time) used by the VAPDIF code is at least one order of magnitude larger. Presently, the source term S_g is determined from

$$S_g = M_2 \frac{\Delta X_2}{\Delta t} \quad (8.4.1)$$

where

$$\frac{\Delta X_2}{\Delta t} = \frac{1}{\Delta t} \int_{\Delta t} \frac{dX_2}{dt} dt \quad (8.4.2)$$

such that the integration step-size is approximately 1 μsec in the volume whose residence time is Δt .

Since the source term is not a function of C_2 (or equivalently, X_2) for Model II, it is not necessary to calculate S_g using Eqs. (8.4.1) and (8.4.2). Instead, a single calculation is performed using Eqs. (8.3.11) and the source term is then determined using Eq. (8.2.4). For moderate to large numbers of computational grid points, the use of Model II can result in a significant savings in computational time.

8.5 Results and Discussion

Autoignition Model I was used to analyze the flow within the Series Staged Premixing Passage described in Section 7.2. The constants used in this model were obtained from Ref. 8.2 and are presented in Table 8.1. Figure 8.1 shows the calculated axial variations of ethene mass fraction along several coordinate lines, which in the present approach approximate the actual streamlines. These streamlines are located at approximately 20, 40, 60 and 80 percent of the distance from the inner to the outer wall of the passage in the plane of symmetry. The results presented in Fig. 8.1 show a rapid increase in ethene mass fraction in the region where the fuel droplets are evaporating. The ethene mass fraction increases at a less rapid rate as droplet vaporization is completed and then appears to increase more rapidly near the duct exit where only the gas-phase reaction occurs. These calculated results were obtained for two-phase flow and include the effects of droplet evaporation, turbulent diffusion, and chemical reaction both in the gas phase and in the film surrounding the liquid fuel droplets.

The autoignition criterion proposed for Model I, Eq. (8.3.8), states that autoignition occurs when the rate of change of ethene concentration due solely to chemical reaction becomes less than some fraction of the ethene concentration. The axial variation of the minimum rate of change in ethene concentration due to chemical reaction relative to the local ethene concentration is shown in Fig. 8.2. For a completely premixed, prevaporized fuel air mixture at the point of injection, as assumed in Ref. 8.2 and as assumed in deriving the autoignition criterion, the autoignition criterion should decrease monotonically. However, the mixture within the Series Staged duct is neither completely prevaporized nor premixed at the point of injection so that the behavior of the autoignition parameter shown in Fig. 8.2 is quite different. Furthermore the absolute level of this parameter is much less than that suggested by examining its behavior for the relatively high temperature flow situations described in Ref. 8.2. Therefore, without further calibration it is not possible at the present time to use Model I and autoignition criterion, Eq. (8.3.8), to determine the likelihood of autoignition in the Series Staged passage.

Autoignition Model II was then used to analyze the flow within the Series Staged Premixing Passage (described in Section 7.2). The constants used in this model were obtained by applying the procedure described in Section 8.3 to an unpublished correlation of the ignition delay data for Jet-A fuel presented in Ref. 8.4.

$$\tau = \frac{8.59 \times 10^{-12} e^{36614/R \cdot T}}{P^2 \phi} \quad (8.5.1)$$

The constants for Model II are presented in Table 8.2. Calculations made using this correlation indicate that autoignition within the Series Staged Premixing Passage does not occur for the assumed flow conditions if the flow therein is uniform. The contours of relative mass fraction, calculated using Model II and shown

in Fig. 8.3, indicate that autoignition may occur near the exit of the duct in the relatively fuel-rich interior of the flow (see Fig. 7.9). Since the calculated profiles of equivalence ratio and mixture temperature are non-uniform, a direct comparison of calculated autoignition times made using Model II and the correlation based upon uniform flow conditions (Eq. 8.5.1) is not possible at present without additional calibration of the model.

8.6 References

- 8.1 El Wakil, M. M., O. A. Uyehara and P. S. Myers: A Theoretical Investigation of the Heating Up Period of Injected Fuel Droplets Vaporizing in Air, NACA TN 3179, May 1954.
- 8.2 Hautman, D. J., F. L. Dryer, K. P. Shug and I. Glassman: A Multiple Step Overall Kinetic Mechanism for the Oxidation of Hydrocarbons, Combustion Science and Technology, Vol. 25, 1981, pp. 219-235.
- 8.3 Faeth, G. M. and D. R. Olson: The Ignition of Hydrocarbon Fuel Droplets in Air, SAE Paper No. 68045, May 1968.
- 8.4 Spadaccini, L. J. and J. A. TeVelde: Autoignition Characteristics of Aircraft-Type Fuels, NASA Contractor Report CR-159886, June 1980.
- 8.5 Spadaccini, L. J. and J. A. TeVelde: Autoignition Characteristics of Aircraft-Type Fuels, Combustion and Flame, 1982 (to be published).

8.7 List of Symbols

A	Constant (1/cm)
A_F, A_B	Reaction rate constants
b	Film thickness \equiv droplet radius (cm)
c_p	Specific heat at constant pressure (cal/gm/K)
C	Mass fraction
E_F, E_B, E	Activation energy (cal/mole)
h	Heat transfer coefficient (cal/cm ² /K/sec)
h_1, h_2, h_3	Metric scale coefficients (1/V, 1/V, r, see Section 3.7)
K	Constant
M	Molecular weight
n	Droplet number density (1/sec)
n_{st}	Stoichiometric oxidizer to fuel mole ratio (dimensionless)
P	Pressure (atm)
$R_F, R_B, \overline{R_F}, \overline{R_B}$	Reaction rate constants
R_o	Universal gas constant (82.0575 cm ³ -atm/mole/K)
R^*	Universal gas constant (1.98717 cal/mole/K)
S_c	Schmidt number (dimensionless)
S_d, S_g	Source terms for critical species (gm/cm ³ /sec)
t	Time (sec)
T	Temperature (K)
U_1, U_2, U_3	Velocity components (m/sec)
V	Metric scale coefficient (inverse of potential flow velocity)
X	Molar concentration (moles/cm ³)

Y_1, Y_2, Y_3	Coordinates (dimensionless)
Y_{O_2}	Mole fraction of oxygen (dimensionless)
z	Blowing parameter
$\alpha, \beta, \gamma, \delta, \nu$	Reaction rate exponents (dimensionless)
Δt	Residence time in volume element (sec)
μ_E	Effective turbulent viscosity (gm/cm/sec)
n	Carbon number of fuel (dimensionless)
ϕ	Equivalence ratio (dimensionless)
ρ	Density (gm/cm ³)
τ	Residence time (sec)
ω	Autoignition criterion (sec ⁻¹)

Subscripts

a	Air
c	Critical value
f	Fuel
B	"Reverse" reaction - depletion of critical species
F	"Forward" Reaction - production of critical species
O ₂	Oxygen
s	Droplet surface
1	Fuel
2	Critical species

TABLE 8.1

Autoignition Model I Constants Used in the
Analysis of the Series Staged Premixing Passage

n	12		
A_F	$1.0 \times 10^{17.32}$	B_B	$1.0 \times 10^{14.70}$
E_F	49600	E_B	50000
α	1.07	α_B	1.18
β	.5	β_B	-.37
γ	.4	γ_B	.90

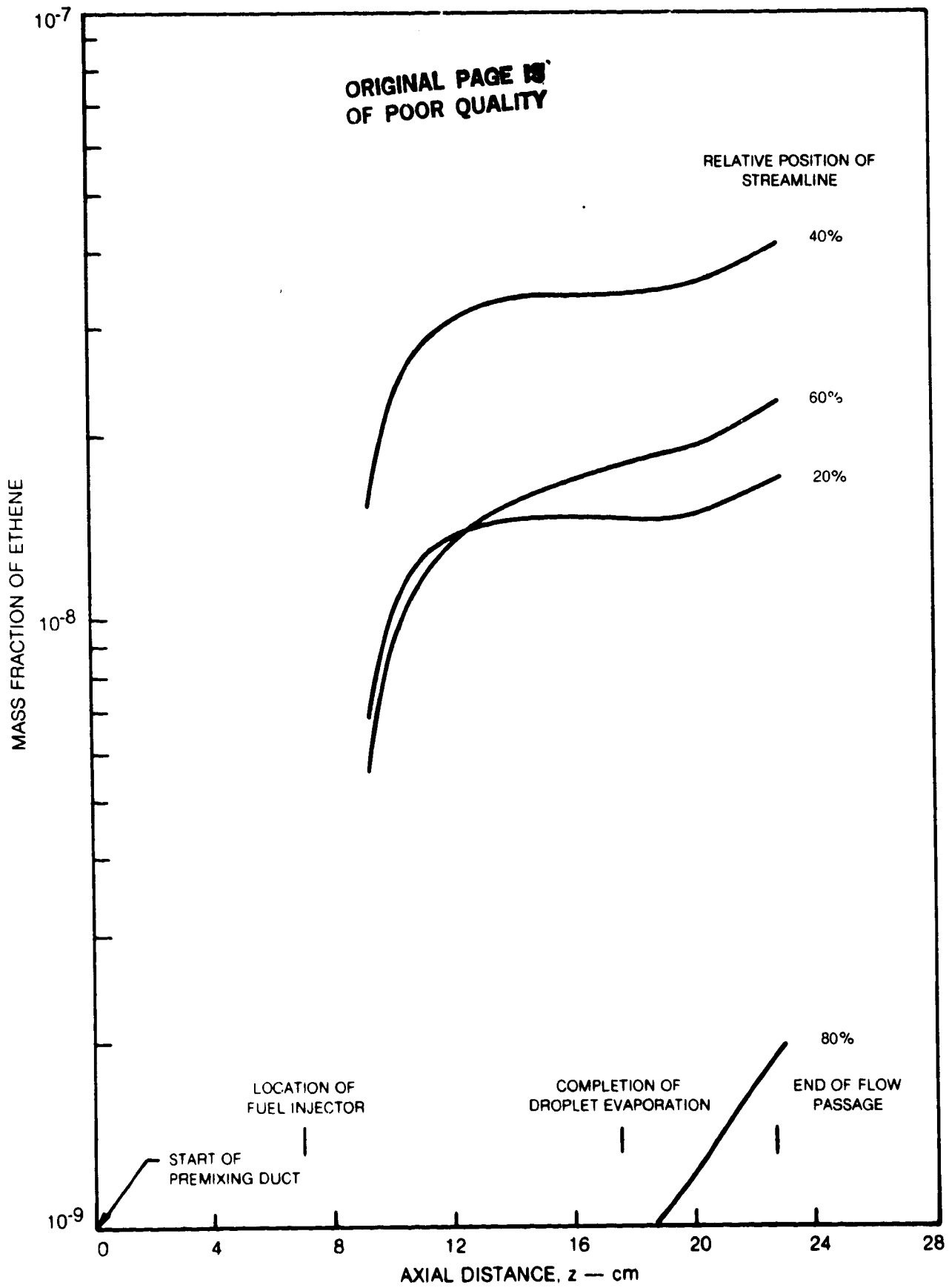
TABLE 8.2

Autoignition Model II Constants Used in the
Analysis of the Series Staged Premixing Passage

n	12
A	3.05×10^{17}
E	36614
α	1.0
β	1.0
δ	0.0
ν	2.0

FIG. 8.1

AXIAL VARIATION OF MASS FRACTION OF ETHENE



82-3-38-1

ORIGINAL PAGE IS
OF POOR QUALITY

**AXIAL VARIATION OF MINIMUM RATE OF CHANGE OF ETHENE PER UNIT
CONCENTRATION OF ETHENE FOR SERIES STAGED PREMIXING PASSAGE**

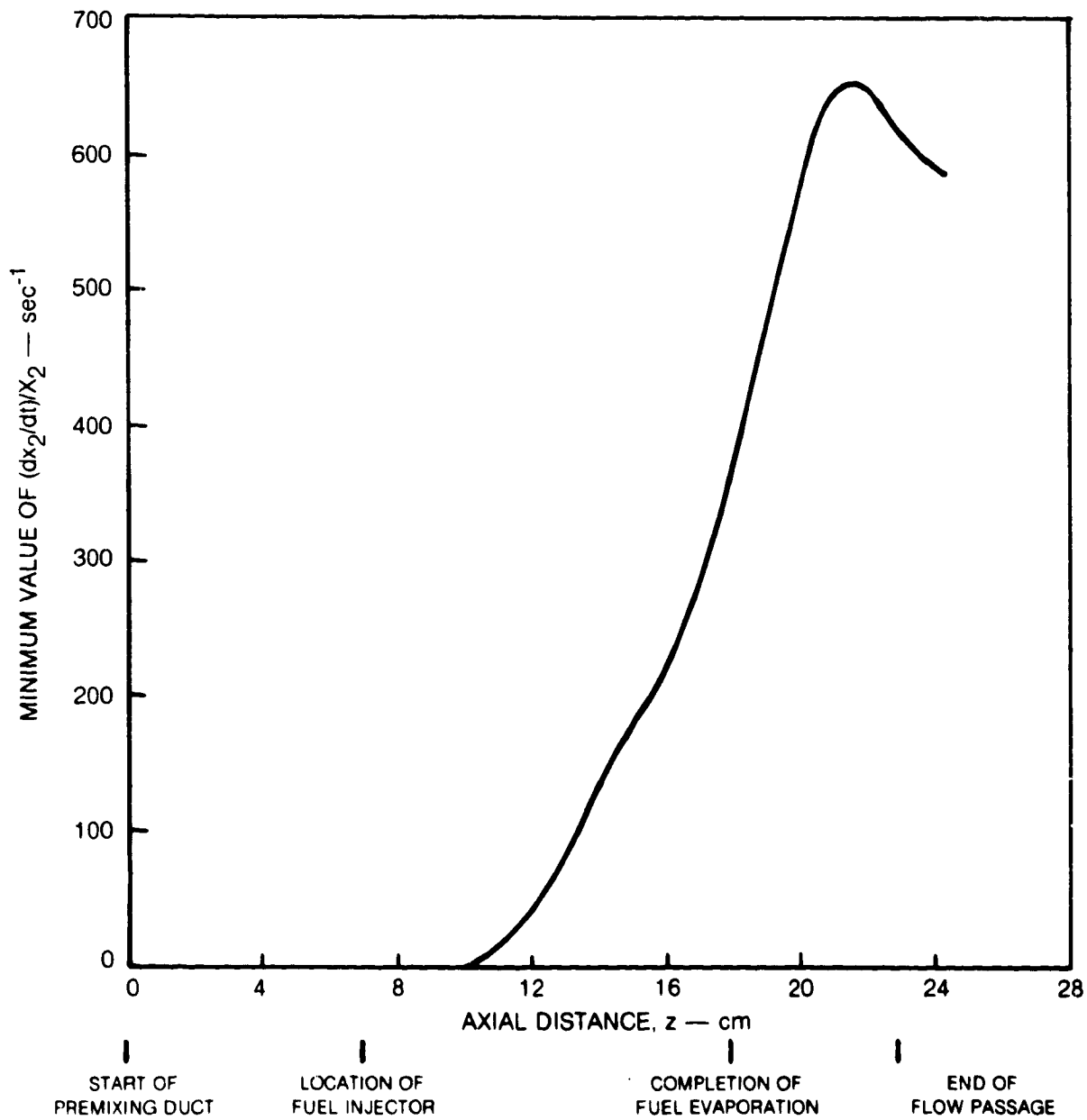
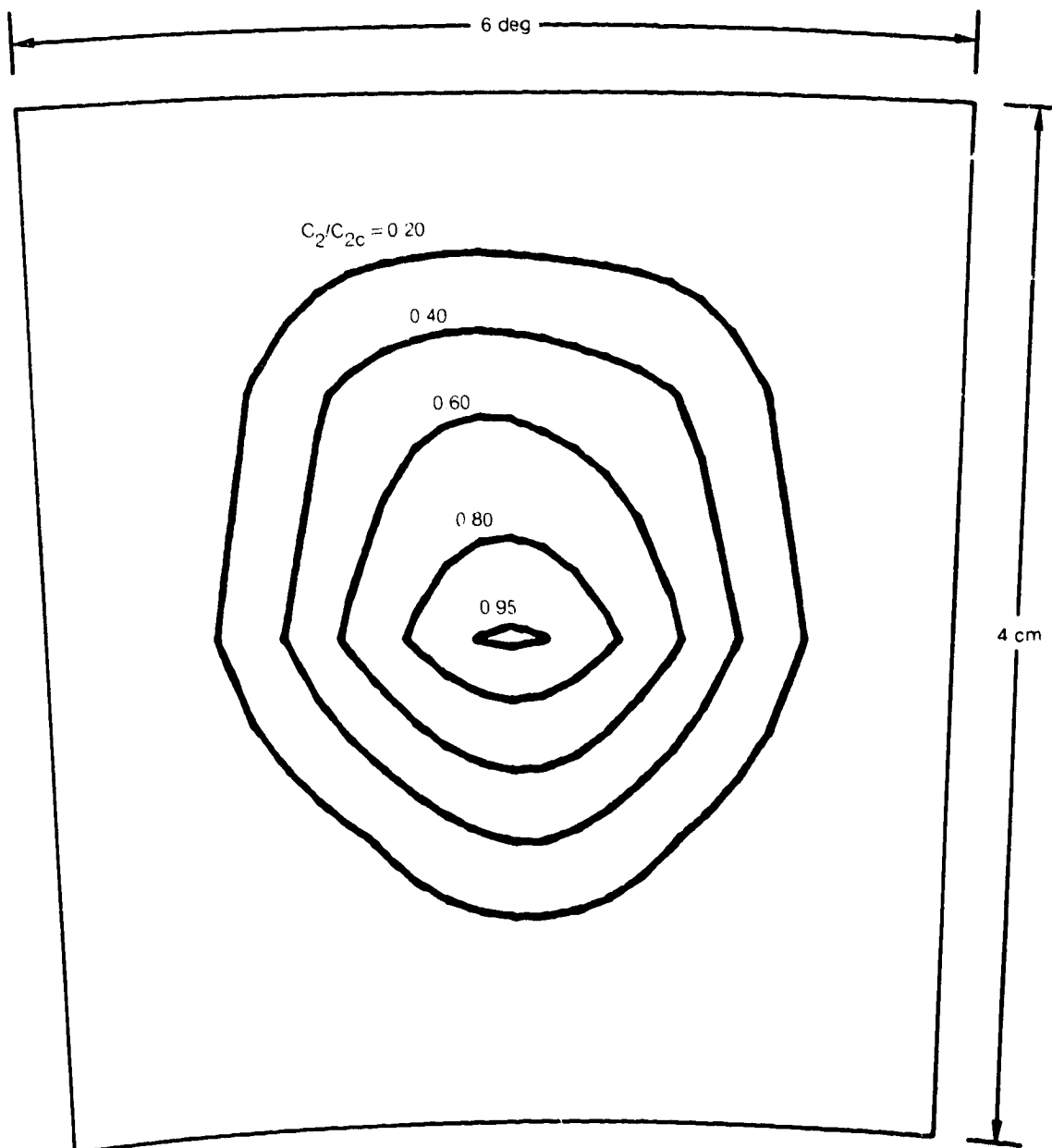


FIG. 8.3

**RELATIVE MASS FRACTION CONTOURS AT THE EXIT
OF SERIES STAGED PREMIXING PASSAGE**

**ORIGINAL PAGE IS
OF POOR QUALITY**



9.0 CONCLUDING REMARKS

1. The analytical approach for modeling the operational characteristics of premixing-prevaporizing fuel-air mixing passages developed herein (i.e., the successive application of the ADD, PTRAK, and VAPDIF computer codes) produces results which are physically realistic. Insufficient data exists for calibrating the fuel droplet evaporation model (PTRAK) and the vapor diffusion model (VAPDIF). Predictions of the evaporation model, however, are consistent with the available data. Results of calculations performed by the diffusion model indicate that the turbulence levels and diffusion rates are lower than levels anticipated on the basis of general experience. Data on turbulence levels and turbulent diffusivities are required to calibrate the turbulence models.
2. The model sensitivity study indicates that the more important parameters for determining the fuel droplet evaporation rate are initial droplet size, fuel volatility, and ambient temperature, while the less important parameters are initial fuel temperature and initial droplet velocity.
3. The model was used to analyze two designs of premixing-prevaporizing fuel-air passages. The model predicted that both designs produce essentially complete vaporization. For the levels of turbulence calculated by the model, it was determined that neither design produces a uniform vapor fuel-air ratio profile at the exit of the passage.
4. Two autoignition models have been described and these models have been incorporated into the analysis. One model embodies the framework required for the incorporation of multi-step chemical kinetic reaction mechanisms. The other is based on application of a simple global expression for describing the progress of the autoignition process. Both models were applied to the analysis of a premixed-prevaporized fuel-air mixing passage; however, only a qualitative assessment of the computed results was possible since further calibration of these models is required before a quantitative assessment can be made. Presently, a single rate expression is employed in the first model; with further development of the VAPDIF code, simplified multi-step mechanisms for hydrocarbon fuel oxidation appearing in the literature could be incorporated. In addition, further calibration and refinement of the autoignition models used in the present calculations are needed which account for the depletion of fuel and for the influence of turbulence on pre-ignition reaction rates.

APPENDIX A - LITERATURE SURVEY

LITERATURE SURVEY CONDUCTED IN SUPPORT OF
THE DEVELOPMENT OF A MODEL FOR AUTOIGNITION

INTRODUCTION

A literature survey was conducted to provide information in support of the formulation and calibration of an analytic model capable of predicting the onset of autoignition within the premixing passage of lean, premixing, prevaporizing (LPP) combustors. These models have been incorporated into the computer programs used to analyze the LPP combustor premixing passage flows. These computer codes are described in the previous sections. The results of the literature survey are presented herein.

Symbols used in this section are defined on page 136.

Background

The application of the LPP concept presents several design problems a major problem being prevention of autoignition. It is well known that autoignition time (ignition delay time) decreases with increasing pressure and gas temperature. Therefore, the severity of the autoignition problem increases as the design pressure ratio of modern gas turbine engines increase. For most proposed designs, autoignition in the premixing passage must be prevented because the uncooled engine hardware in this duct can undergo catastrophic failure as a result of the sudden large heat release following autoignition. Clearly, the exploitation of the LPP concept requires that the residence time within the fuel preparation passage be long enough to achieve essentially complete vaporization and mixing of the fuel and yet short enough to preclude the occurrence of autoignition. The analysis described in Sections 3 through 5 (1980) provides a method for predicting the performance of an LPP design with respect to fuel vaporization and mixing. It is desired to incorporate within the analysis a model of the autoignition process such that it will be possible to determine whether autoignition occurs in a given fuel preparation duct. This model must be sufficiently comprehensive to address all of the processes which could affect the progress of the pre-ignition reaction in the turbulent, two phase flow field characteristic of practical premixing section designs.

The first objective of this effort was to review the literature from the point of view of identifying the characteristics of the flow which can influence the

PRECEDING PAGE BLANK NOT FILMED

occurrence of autoignition. The following factors were projected to be of significance:

1. mixture pressure;
2. mixture temperature;
3. degree of fuel vaporization and mixture ratio;
4. droplet initial temperature;
5. droplet size;
6. mixture turbulence characteristics including the intensity, scale and distribution of turbulence;
7. fuel chemical composition.

Attention was given to examining the literature from the standpoint of defining the appropriate functional relationships between autoignition time and these factors. Attention was also given to literature which might point to factors of significance other than those listed above.

When conducting the survey, primary consideration was given to papers dealing specifically with autoignition or ignition delay phenomena. However, related information may prove useful in developing this model; therefore, information on the autoignition temperature, the mixture below which autoignition is not possible, and on the minimum energy which an external source (e.g., a spark) must apply in order to ignite a fuel-air mixture is cited where such information is believed to be of significance.

The experimental procedures employed in various efforts to obtain autoignition data were not directly of interest in this survey; the reader interested in these techniques is referred to Spadaccini and TeVelde (1980). However, as emphasized by Spadaccini and TeVelde, the interpretation of reported data does, in fact, require an appreciation of the influence of the experimental technique used upon the data obtained.

The review of the experimental literature on autoignition is given in the following section of this report. A second objective of this task was to review previously published models of the autoignition process. The results of that phase of the effort are given in the final section of this appendix.

Procedures

This survey was conducted by reviewing the contents of the United Technologies Corporation Library. In addition, computer-assisted searches were conducted of the National Technical Information Service, Science Citation Index, and Current Contents.

REVIEW OF EXPERIMENTAL DATA

1. Effect of Mixture Pressure

It is reasonable to expect that the rates of gas phase chemical reactions vary directly with the concentration of the reactants. For pre-ignition reactions of air and fuel in the range of mixture ratios of interest, it follows that reaction rates should vary directly with pressure. Because ignition delay time is related inversely to the pre-ignition reaction rates, ignition delay time will vary inversely with mixture pressure. Likewise, autoignition temperatures and minimum ignition energy should vary inversely with mixture pressure.

Many ignition delay time experiments have involved injection of liquid fuels into hot gas streams; therefore, to interpret the results in terms of the pressure effect on gas phase reactions, consideration must be given to how pressure variations could influence the results other than through the effect on gas-phase reaction rates. In particular, the extent of fuel vaporization of the liquid spray is a function of mixture pressure. As pressure increases, droplet vaporization rates are influenced by two factors: 1) enhanced heat transfer from the gas phase to the liquid phase, and 2) decreased heat transfer due to a reduced temperature differential when the droplet reaches its higher equilibrium temperature. At the same time, the drag on the droplet due to the relative motion between the droplets and the gas increases because of the increased dynamic pressure. Assuming that the droplet is injected with a velocity less than that of the air stream, then the residence time of the droplet within a fuel preparation passage of fixed length decreases with increasing pressure. The amount of fuel vaporized is the integrated product of vaporization rate and residence time. Calculations performed at UTRC for representative conditions indicate that the amount of fuel vaporized within a fixed duct length changes only slightly with changing pressure [see, for example, Anderson, et al. (1980)]. It is therefore reasonable to assume that the pressure effects reported in the literature for experiments conducted with both liquid and gaseous fuels can be attributed primarily to the effects of pressure on gas-phase kinetics.

Correlations of the effects of pressure on ignition delay are usually expressed in the form:

$$\tau \approx 1/p^n \quad (1)$$

A summary of the correlations found in the literature for fuel injected into flowing air streams is presented in Fig. A.1. The number in parentheses next to each data correlation is the value of the exponent, n . Spadaccini and Tevelde (1980) provided correlations of their data using values of the exponent n equal to 1 and 2; both sets of correlations are shown in Fig. A.1. As can be seen, the body of data available in the literature indicates a suitable value for n lies in the range from 1 to 2; a more precise generalization cannot be made.

Numerous experiments on related phenomena supported the findings reported for the flowing air stream experiments. For example, Halstead, et al. (1977) report ignition delay data for various liquid fuels in reciprocating engines. These data indicate that ignition delay time varies inversely with mixture density to the first or second power. Since both pressure and pre-ignition delay temperature vary during the compression stroke, the effect of pressure on the ignition time data reported from such experiments is not easily determined. However, the variation of ignition delay time with density implies a variation not inconsistent with the pressure behavior presented in Fig. A.1. Data for the variation of autoignition temperature reported by Ingebo (1974) for fuel-air mixtures in a combustor environment and for minimum ignition energy reported by Satcunanathan (1971) for individual droplets in an oxidizing environment also show an inverse correlation with mixture pressure.

2. Effect of Mixture Temperature

It is generally accepted that gas phase chemical reaction rate behavior can be represented using reaction rate constants having the form:

$$k = Ae^{-E/RT} \quad (2)$$

This form of expression reflects the fact that as mixture temperature increases, the kinetic energy of the reactant molecules increases, intermolecular collisions become more energetic, and the probability of reaction increases. Indeed, it has been the practice by most experimenters to use expressions of the form:

$$\tau \sim e^{E/RT} \quad (3)$$

to correlate experimental results. It is important to recognize that the value of the activation energy, E , reported by the experimenters is in reality a correlation coefficient and not the activation energy for a specific reaction. Thus, if the experimental data is to be used to specify the constants appearing in a global or single-step rate expression, the form of the rate expression must reflect the form of the expression used to correlate the experimental data. Specifically, if an activation energy is obtained from a set of experiments in which the data is correlated using the form

$$\tau = ap^2 e^{E/RT} \quad (4)$$

then the reported activation energy should only be used in an expression which shows a second order pressure dependence. For example, Spadaccini and TeVelde (1980) report values of activation energy obtained from regression analysis employing either first or second order pressure dependence and show that the activation energy values obtained assuming first order dependence are approximately 15 percent lower than those obtained assuming second order dependence.

It is also important to recognize that the experimentally-determined values of activation energy in general reflect phenomena other than gas-phase chemical reactions

due to the imperfect nature of the experiments. Obviously, for those experiments in which liquid fuel is injected into a flowing air stream, increased mixture temperature affects droplet vaporization rates and therefore the concentration profiles between the point of injection and the point of ignition will differ for different air temperatures.

Data from a representative group of experiments is presented in Fig. A.2. The slope of each correlation curve is a measure of the activation energy; the calculated value of activation energy is given by the value in parentheses adjacent to each curve. Note that the data group corresponds to those experiments which were correlated assuming a pressure exponent, n , of 1.0. A wide variation in magnitude of activation energy is observed and is probably wider than the variation due to fuel chemistry alone. Differences in experimental technique which result in different rates of fuel-air mixing and different rates of spray variation certainly influence the experimental results. An example is the work of Myasaka and Mizutani (1975) where the apparent activation energy is reported as a function of fuel injection rate. Because experimenters are unable to separate these effects from the gas-phase kinetic effects, the amount of experimental bias is unknown in all cases. The behavior of the reported data indicate that a dependence of ignition delay time on temperature of the form given by Eq. (3) is suitable for modeling, but the appropriate activation energy can only be determined by conducting calibration experiments using an apparatus similar in configuration to the fuel preparation system of interest.

An important finding reported by numerous researchers is that although expressions of the form of Eq. (3) are useful for correlating data, the range of temperatures over which a given correlation applies is limited due to changes in the rate-controlling reaction steps as temperature changes. For example, Yashizawa, et al. (1978) present data and a reaction rate expression that shows that different values of activation energy apply above and below approximately 1200K for butane, hexane, and octane. Myers and Bartle (1969) show similar results for propane. Brokaw (1965) has examined the reaction system responsible for the exponential growth of OH radicals during the ignition delay period and provides illustrations of how the changing dominant reactions control delay in both the long (millisecond to second) and short (less than millisecond) ignition delay regions. The important point is that correlations or reaction rate mechanisms developed from high temperature experiments cannot be used at low temperature conditions without the risk of serious errors.

3. Effects of Degree of Vaporization and Mixture Ratio

It is clear that the increasing extent of vaporization of a fuel spray as time increases will affect the rate of progress of the ignition delay reactions through the effect of increasing reactant concentrations on reaction rates. These concentration effects are treated as pressure effects where the pressure represents the partial pressure of the reactants. Additionally, as the spray vaporizes, the fuel to oxidizer ratio increases; the mixture ratio may or may not have an effect on reaction rates. Also, within a vaporizing spray, two phases are present. No evidence exists in the literature, however, which would indicate that heterogeneous reaction

phenomena are of significance. As a result, the only new effect which the degree of vaporization may introduce is the effect of mixture ratio.

With respect to mixture ratio effects, Yashizawa, et al. (1978) obtained ignition delay time data in gaseous mixtures of n-butane, n-hexane, and n-octane for equivalence ratios between 0.05 and 1.0 and determined that ignition delay time did not vary with equivalence ratio. Correlations of ignition delay time with equivalence ratio have also been reported by Marek, et al. (1977) and Halstead, et al. (1977) and Spadaccini and TeVelde (1980) for liquid fuel injection. However, as noted in these works, the temperature of the fuel vapor-air mixture decreases within the vicinity of the fuel droplets due to fuel vaporization; and it is apparently the effect of this mixture temperature decrease on ignition delay time which is expressed by correlations of ignition delay time with equivalence ratio. Spadaccini and TeVelde (1980) presented ignition delay time data both as a function of inlet air temperature and as a function of the mixture temperature assuming complete mixing and vaporization; the data for each equivalence ratio correlate with the mixture temperature corresponding to that equivalence ratio. On the basis of the limited data available, it is concluded that, for the range of mixture ratios of interest in LPP systems, mixture ratio does not have a large effect on the autoignition process.

4. Effect of Fuel Initial Temperature

If the liquid fuel is heated prior to injection, then the fuel will vaporize more rapidly than would unheated fuel. Also, the mixture temperature decrease associated with a given degree of fuel vaporization will be less for the heated fuel than for the cold fuel. Based on the remarks in the preceding sections, ignition delay time would be expected to decrease with increasing fuel injection temperature. The data of Spadaccini and TeVelde (1980) for Jet-A fuel preheated to 400K prior to injection show little effect of initial fuel temperature on ignition delay time. The lean, premixing prevaporizing concept requires that essentially all of the fuel vaporize within the premixing passage. Achievement of a high degree of fuel vaporization within is dependent on the atomization of the fuel into small droplets ($d < 100 \mu\text{m}$). Small droplets will be heated rapidly by the air stream so that the effect of injection temperature should be minimal. The estimated Sauter mean diameter of the Jet-A fuel injected in the tests described by Spadaccini and TeVelde (1980) was approximately $30 \mu\text{m}$; these droplets are small enough to be heated rapidly by the air at conditions representative of those that exist within the LPP passage and therefore the reported results are reasonable.

The data reported by El Wakil and Abdou (1966) shows about a two-fold decrease in ignition delay times as the fuel injection temperature is increased from 330K to 380K. However, these data were obtained using droplets with initial diameters of $1650 \mu\text{m}$; droplets of this size are not characteristic of LPP system sprays. Preheating of the fuel in the case of large droplets helps to overcome the large thermal inertia of the droplets.

5. Effect of Droplet Size

It is reported in the literature that the presence of droplets in a fuel-oxidizer stream can have a significant effect on the onset of ignition. That is,

ignition may occur more readily in a stream containing droplets than a stream of the same overall fuel air ratio in which the fuel is completely vaporized. Wood and Rosser (1969) have shown that ignition within a system produced by a droplet falling through a hot gaseous oxidizer can occur either in the wake of the droplet or in the fuel-air mixture envelope surrounding the droplets depending on conditions. With all except droplet size remaining the same, ignition delay times remained the same as droplet size was decreased until a critical size was reached, then ignition delay times increased. It was observed that this increase was associated with a shift in the point of ignition from the droplet fuel-air mixture envelope to the droplet wake. These experiments indicate that the presence of droplets can have a controlling effect and that effect is dependent on the droplet size. The droplet diameters used in the experiments ranged in size from 100 to 300 microns. It was concluded that the smaller droplets evaporate before ignition occurred in the vapor-fuel/oxidizer mixture in the droplet wakes. For the larger droplets, pre-ignition reactions progressed to the point of ignition in the envelope surrounding liquid fuel droplets; both the rate of progress of the pre-ignition reactions and the rate of diffusion of intermediate species into the environment played a role in this process.

Other experiments in which the effect of droplet size on ignition delay were investigated include the work of El Wakil and Abdou (1966) who determined experimentally that ignition delay time can be correlated as

$$\tau \sim D_o^{0.85} \quad (5)$$

for single droplets in the size range from 1200 to 1800 microns for several paraffins (n-octane, n-decane, n-dodecane, n-tetradecane, and n-hexadecane) suspended in a hot air stream; in these experiments the temperature of the air was varied between 1000 and 1250K. The authors concluded that the observed dependence on droplet diameter could be explained on the basis of consideration of the physical (droplet heating, diffusion) and chemical processes occurring in the envelope surrounding the droplet. An analysis based on a spherically symmetric field is presented. These authors also observed that ignition could occur either in the droplet envelope or in the droplet wake; at higher droplet-air velocities, burning occurred in the droplet wake. Kadota, et al. (1976) reported no correlation of ignition delay time with droplet diameter for single droplets of n-heptane which are plunged into a quiescent furnace. The contrasting result obtained by these two experiments with respect to the role of the size of the droplet on ignition delay is probably not of significance because of the imprecision associated with the small droplet size range studied and the difference in experimental conditions. These experiments were carried out with isolated droplets in an infinite oxidizer environment. A definitive experiment in which autoignition times have been measured for systems with and without presence of droplets at overall fuel-oxidizer ratios in the range of interest for gas turbine combustion systems has not been conducted.

6. Effect of Turbulence

No data were located which show the effect of turbulence on ignition delay time. There have been studies which show that increasing turbulence level decreases the

ease with which ignition is achieved [e.g., Ballal and Lefebvre (1979)] or increases the tendency for a flame to blowout [Radhakrishnan (1979)]. In the case of ignition, the increased turbulence causes the local rate of dissipation of thermal energy to increase relative to the local rate of energy release due to reaction. When dissipation rate exceeds the heat release rate, propagation of the reaction front, which is required for ignition, cannot occur. In the case of blowout of a premixed flame, the role of turbulence is to exchange cold reactants with hot combustion products. Because reaction rates are exponentially dependent on temperature and dependent on reactant concentration to a lesser degree, the increased rate of exchange of cold reactants with hot products always causes a decrease in heat release in the flame stabilization wake or pilot region; hence increased turbulence is not favorable to blowout limits. In both the ignition and blowout cases, the essential feature of the flow is the non-uniformity of the temperature field which the turbulence tends to dissipate. In the case of the LPP system, the temperature non-uniformities will be a result of non-uniform work performed on the gas during the compression process and the temperature depression associated with the injection of cold fuel into the hot air. Gradients in the temperature field due to these effects should be small and hence the influence of turbulence on redistributing the thermal energy will be small. On the other hand, the concentration gradients resulting from imperfect premixing can be large both on the scale of the duct and on the scale of the eddies associated with the turbulent mixing of fuel and air. As stated previously, no data exist by which the significance of these non-uniformities and the role which turbulence plays on dissipating these non-uniformities has been generated for the case of autoignition of premixed systems. At best, theoretical models which treat the general class of turbulent chemical reactions are available; these models are reviewed in the following section of this report.

7. Effect of Fuel Chemical Composition

The chemical composition of a fuel can affect ignition delay time in at least two ways. First, the rate of fuel vaporization, and hence the fuel vapor concentration, is determined by the volatility of the fuel; in the case of a multi-component fuel (e.g., a distillate fuel), the rate is determined by the relative proportions of high-volatility and low-volatility compounds in the blend. A procedure to calculate the vaporization rate of multi-component fuel blends is described by Anderson, et al. (1980). Second, the pre-ignition reaction system probably consists of a number of chemical reactions involving chemically simple molecules and radicals together with one or more steps in which the large, complicated fuel molecules thermally decompose into these simpler structures. For example, Edelman, et al. (1972) proposed an ignition delay model based upon the assumption that the fuel decomposes into methane, ethane, and propane for which ignition delay reaction systems are known; this model was applied by Siminski and Wright (1972) to the analysis of the ignition delay data for a number of heavy hydrocarbon fuels. Hautman, et al. (1981) present a model for the oxidation of paraffin-series hydrocarbons in which the hydrocarbons are assumed to be converted to ethene which further reacts to form products of combustion. Empirical coefficients used in the model have been determined using the results of shock tube measurements. A method of deducing the ignition delay period from the calculated behavior of the ethene concentration is proposed. Halstead, et al. (1975) have determined a rate limiting mechanism for

calculating the ignition delay time for a number of fuels used in reciprocating engines; they have determined the type of destruction reactions that limit the production of certain chain branching radicals. Affens and Carhart (1974) have attempted to relate the influence of chain branching radical distribution to fuel chemical characteristics. They have found that autoignition temperature increases with decreasing number of carbon atoms in a hydrocarbon molecular chain and with increasing cyclicity or aromaticity; these findings indicate that ignition delay time increases with increasing complexity of the molecule's bond structure.

It has also been determined by Ballal and Lefebvre (1979) that the minimum ignition energy for various liquid hydrocarbon fuels tends to increase with increasing molecular complexity and decreasing fuel volatility. It is possible to evaluate the relative importance of each effect from the data presented.

Experimental studies have been carried out to determine the effect of fuel type and hence composition on ignition delay time. As indicated earlier, for those experiments conducted using liquid fuel sprays, it is not possible to separate fuel chemistry effects from physical effects (e.g., evaporation rate). Yashizawa, et al. (1978) conducted shock tube experiments using n-butane, n-hexane, and n-octane and concluded that, in the temperature range over which the experiments were conducted (900-1700K), there was no discernible difference in ignition delay time among these fuels. In comparing their results with other results, Yashizawa, et al. conclude that with the exception of the lighter hydrocarbons, methane and ethane, all saturated hydrocarbons exhibit nearly the same ignition delay values. Compared to the heavier saturated (paraffin-series) hydrocarbons, methane exhibits longer delay times while ethane exhibits shorter ignition delay times--times comparable to those observed for hydrogen and acetylene. These results suggest that differences in the ignition delay time behavior of liquid fuel sprays of the heavy hydrocarbon fuels will arise from the different physical characteristics alone; chemical effects can be ignored.

ANALYTICAL METHODS FOR AUTOIGNITION MODELS

On the basis of the experimental observations reviewed in the previous section, a model for the autoignition of fuel injected into a lean, premixing, prevaporizing fuel-air mixing passage must treat the occurrence of autoignition both in the vicinity of vaporizing droplets and in the fuel vapor-air mixture generated as the fuel vapor diffuses throughout the airstream. No analytic model was located during this literature survey in which this dual single-phase and two-phase autoignition problem has been modeled. However, a number of reports were obtained in which some important aspect of the overall problem has been treated. For convenience, the discussion of the results of the literature survey for analytical methods is divided into three parts: (1) a discussion of models in which no liquid phase is present, (2) a discussion of models applicable to the occurrence of autoignition in the droplet boundary layer, and (3) a brief discussion of turbulent reacting flow modeling.

Single Phase Models for Autoignition

Two methods have been used to model the autoignition of fuel-air mixtures in which no droplets are present. In the first method, the reactants are assumed to be thoroughly mixed locally and a system of elementary reaction rates describing the pre-ignition process is assumed to apply. For example, it has been assumed that any large fuel molecule undergoes a one-step thermal decomposition process into various proportions of methane, ethane and propane [Edelman, et al. (1972)]; the calculation of ignition delay time is based upon a ten reaction rate system derived from autoignition data for these three simpler molecules. A similar model is described by Halstead, et al. (1975). However, in this case, the fuel molecule participates directly in the system of reactions by contributing hydrocarbon atoms and (upon partial oxidation of the fuel) hydroxyl radicals. Recently Hautman, et al. (1981) proposed a four-step kinetic mechanism for the oxidation of paraffin-series hydrocarbons in which the fuel first decomposes to ethene. The authors have shown that the onset of significant heat release corresponds to the time at which the ethene concentration reaches a maximum; therefore a criterion serving to designate the ignition delay period exists. All of these models have produced results in reasonable agreement with data for particular ranges of temperature and concentration.

In the second approach to modeling autoignition in the absence of fuel droplets, the restriction that the fuel and air are locally premixed is removed [Dopazo and O'Brien (1974)]. Fuel and air are assumed to be contained in individual fluid eddies; intermixing of these eddies is controlled by the turbulence of the flow. The amount of contact time between the fuel and air is calculated from an assumed form of probability density function. The rate of reaction of fuel with air during the time intervals in which both reactants are mixed is estimated using a one-step, second order chemical reaction rate. Autoignition is indicated if the local temperature begins to increase rapidly, a phenomenon to which the authors refer as "thermal runaway". Thus, although the flow may appear to be premixed on the basis of time-mean fuel and air concentrations, different reaction rates can be calculated depending upon the turbulence level and the assumed probability density function.

Models for Autoignition in the Presence of Droplets

Models for the autoignition of mixtures in which the fuel is injected initially as liquid droplets can be divided into two classes: (1) models that include the detailed structure of the mass and thermal boundary layers surrounding a droplet (referred to as in this report as boundary layer models), and (2) models that ignore these boundary layers except for the use of mass and heat transfer rates calculated a priori from knowledge of these structures.

In the boundary layer models, the fuel vapor concentration and temperature profiles in the boundary layer are calculated at each instant during the vaporization process. These profiles are used together with other criteria to determine the ignition delay time. In some cases, the pre-ignition period is divided into a number of subintervals with each subinterval characterized by a single rate controlling

process. For example, El Wakil and Abdou (1966) divided the pre-ignition period into physical delay and chemical delay subintervals. They defined the physical delay time as the time that elapses from the injection of the fuel droplet into the air stream to the development within the boundary layer of a fuel vapor concentration corresponding to the lean combustion limit. The chemical delay time is the time that elapses after the physical delay time until the occurrence of a rate of oxidation of fuel that is some fraction of the reaction rate at stoichiometric conditions. Calculation of the chemical delay time requires knowledge of a gas-phase global reaction rate for oxidation of the fuel. Satchunanathan (1971) presents a similar analysis which uses additional subintervals to define the ignition delay time.

There are several boundary layer models in which the ignition delay time is not divided into subintervals. For example, Kadota, et al. (1976) first calculated the temperature and fuel vapor concentration profiles for the droplet and then estimated the ignition delay time at several positions within the boundary layers; the ignition delay time, τ , is calculated as a function of the local temperature and fuel vapor concentration using correlations obtained from gas-phase experiments also described in their paper. The entire calculation is repeated for several times during the droplet vaporization process. Ignition is assumed to occur when

$$\int_0^t \frac{dt}{\tau} \geq 1 \quad (6)$$

at some position within the boundary layers. This expression indicates that ignition has occurred when the residence time of the fuel-air mixture at a fixed position relative to the droplet center has exceeded the ignition delay time. With the additional assumption that ignition is most likely to occur near stoichiometric fuel-air concentrations within the boundary layer, Law and Chung (1980) have developed a criterion for autoignition which specifies the relationship between a critical Damköhler number (rate of chemical reaction to rate of heat transfer) and parameters describing the droplet environment.

In some boundary layer models, it is assumed that the pre-ignition reaction rates are controlled by the rate of production of an intermediate, but unknown, species X_I ; for example, this species may be an important chain branching species, or it may be a species that destroys important chain branching species. Faeth and Olsen (1968) developed a model for autoignition in which the rate of production of the intermediate species is calculated using a single-step rate expression for the formation of X_I as a function of local fuel and air concentrations, temperature and pressure. The calculation is performed at various points within the boundary layer and several time intervals throughout the vaporization process. The rate expression is calibrated by adjusting the coefficients in the expression to give agreement with experimentally-derived correlations of ignition delay time data for the vapor of the same fuel in air. Ignition is assumed to occur when the normalized concentration of X_I (the concentration of X_I divided by its value at the end of the pre-ignition period) exceeds unity. A similar approach has been used by Sangiovanni (1976) but the model described therein accounts for the diffusion of the intermediate species throughout the boundary

layer; under similar conditions, the effect of diffusion can be expected to increase the calculated value of ignition delay time relative to the value which is calculated using the model of Faeth and Olsen. It should be noted that since the models employed by Faeth and Olsen and by Sangiovanni are calibrated using gas-phase ignition delay time correlations, they are essentially similar in approach to the method employed by Kadota, et al. (1976).

There are autoignition models that do not consider the details of the fuel vapor concentration and thermal boundary layers surrounding the droplet. Instead, these models make certain simplifying assumptions and use expressions for the instantaneous droplet vaporization and heating rates; it should be noted that the derivation of these rates requires knowledge of the concentration and temperature profiles around the droplet. Rao and Lefebvre (1981) calculated the ignition delay time as the sum of a vaporization delay time and a chemical delay time. They defined the vaporization delay time as the time required to completely vaporize the fuel droplet; this time interval is estimated by the ratio of initial droplet mass to a constant value of calculated vaporization rate. Implicit in this model is the assumption that the pre-ignition reactions are unimportant until the fuel is completely vaporized. The rationale for the derivation of the expression for chemical delay time used in this model is ambiguous. Model constants are estimated from the available data.

Turbulent Reacting Flow Modeling

If the fuel vapor and air are mixed thoroughly on the molecular scale, then it should be possible to derive models for autoignition from an understanding of the important rate controlling processes and the available data; the assumption that reactions are thoroughly mixed is basic to the models presented by Edelman, et al. (1972) and by Halstead, et al. (1975) described earlier. If the flow is turbulent, then this assumption may not be justified. Each reactant may be contained in individual eddies of fluid; the time-mean reactant concentration may indicate that the reactants are premixed, but the instantaneous concentrations may indicate that the reactants are unmixed for a significant portion of the time. If the latter situation prevails, the calculated reaction rate will be less than that calculated for the premixed system.

In modeling turbulent reacting flow, it is necessary to specify the dependent variables (velocities, temperature, pressure, species concentrations, etc.) for which fluctuations represent important departures from the mean values. For example, the instantaneous value of a dependent variable may be represented as $u = \bar{u} + u'$. Expressions for u together with similar expressions for the other dependent variables are then substituted into the equations of motion. After a number of algebraic manipulations that may include subtracting the corresponding equations for the mean values and neglecting certain higher order terms, one obtains a system of equations in terms of convective and diffusive terms for the fluctuating components together with products of two or more fluctuating components. These products are often termed correlations. Models for turbulent flow tend to be differentiated by (1) the number of fluctuating variables selected, (2) the order of the resulting equations, and (3) the models used to calculate the correlations. A recent review of

turbulent flow models is presented by Libby and Williams (1981). Another review, together with papers on both analytical and experimental techniques in turbulent reacting flows is presented in a special issue of Combustion Science and Technology (1976).

Most of the papers cited in modeling turbulent reacting flows [e.g., Spalding (1971), Bilger (1976), Magnussen and Hjertager (1976), Lockwood (1977), Lockwood and Syed (1979) and Gosman and Ioannideo (1981)] are concerned with the rate of consumption of reactants. An exception is the model of Dopazo and O'Brien (1974) which is based upon solutions to the turbulent equations of motion using a statistical approach for the modeling of the effects of the fluctuations in temperature of the reactants. During the pre-ignition period, negligible amounts of reactants are consumed, although the reactants that are consumed produce the intermediate products important to autoignition. It is difficult to extend these models for reactant consumption to obtain an autoignition model because of the lack of data suitable for calibrating the model. For example, Magnussen and Hjertager propose that the rate of fuel consumption be calculated by an expression of the form:

$$\frac{d\bar{X}_F}{dt} = A\bar{X}_F \epsilon/\kappa \quad (7)$$

where ϵ and κ are determined from the solution of the turbulent equations of motion. The constant A varies from a value of 4 to 32 depending on the extent to which the reactants, fuel and air, are mixed. If it is assumed that the rate-controlling intermediate species are produced at a similar rate (say)

$$\frac{d\bar{X}_I}{dt} = B\bar{X}_F \epsilon/\kappa \quad (8)$$

then data are required to determine B. Alternatively, a system of equations, analogous to Eq. (7), can be generated that are similar to the systems of equations describing autoignition reaction rates in flows in which the effects of turbulence are neglected. The constants appearing in such a system would be adjusted to give reasonable agreement with the available data. Unfortunately, no ignition delay time data which include the effects of turbulence have been published.

Apparently, attempts have been made to model the fuel oxidation process by starting with reaction rate expressions in the form (for example):

$$\frac{dX_i}{dt} = A X_j e^{E/RT} \quad (9)$$

Upon introducing the variables

$$T = \bar{T} + T'$$

$$X_k = \bar{X}_k + X_k' \quad (k = i, j)$$

into Eq. (9), turbulent forms of the reaction rate expressions are obtained. The fluctuating components of temperature and species concentration are obtained from the turbulent energy and species equations. Lockwood (1977) has stated that this approach is not useful because of the strong influence of temperature fluctuations due to the exponential term. This method can be useful in formulating a model for autoignition if (1) temperature fluctuations in the fuel preparation passage are negligible, (2) the appropriate pre-ignition reactions can be identified, and (3) data can be located relating ignition delay time to turbulence parameters. Since the system of rate equations must be solved at each point in the three-dimensional flow field, machine computation time requirements are likely to be so large as to make application of this approach impractical.

CONCLUDING REMARKS

The results of the literature survey indicate that the factors which are most significant in effecting the ignition delay time of fuel-air systems are the mixture pressure (reactant concentration), mixture temperature, and the presence of fuel droplets. Fuel composition and mixture ratio are of secondary importance. The role of turbulence has not been clearly defined. Analysis of the results of experiments in which liquid fuel is injected into hot flowing gas streams for the purpose of isolating the individual effects noted above is not possible because of the complexity of the flows and the resulting lack of knowledge concerning flow details (e.g., the initial spray droplet size distribution, the temperature profiles within the flow, etc.). The existing experimental results can best be utilized to support the development of the analytical model through comparisons of the analytical results obtained when applying the model to the experimental conditions with the published experimental data. Obviously, a degree of engineering judgment will necessarily be employed in setting up the cases to be modeled because of lack of detail concerning the experiments; also judgments will be required to select which of the many empirical factors to be employed in the model should be changed in order to achieve agreement between experiment and theory.

The results of this survey indicate that experimental data are lacking even for the most significant of factors controlling the process of autoignition of vaporizing fuel sprays. No definitive work on vaporization of fuel sprays has been performed. The kinetic mechanisms controlling autoignition of fuel at low (non-shock tube) temperatures is unknown. The role of the presence of droplet sprays (as opposed to single droplets or a series of individual droplets) is unknown. The analysis described in Section 8 reflects this stage of knowledge through the use of the most simple and straight-forward models of the individual processes as can reasonably be believed to account for observed experimental trends.

LIST OF SYMBOLS

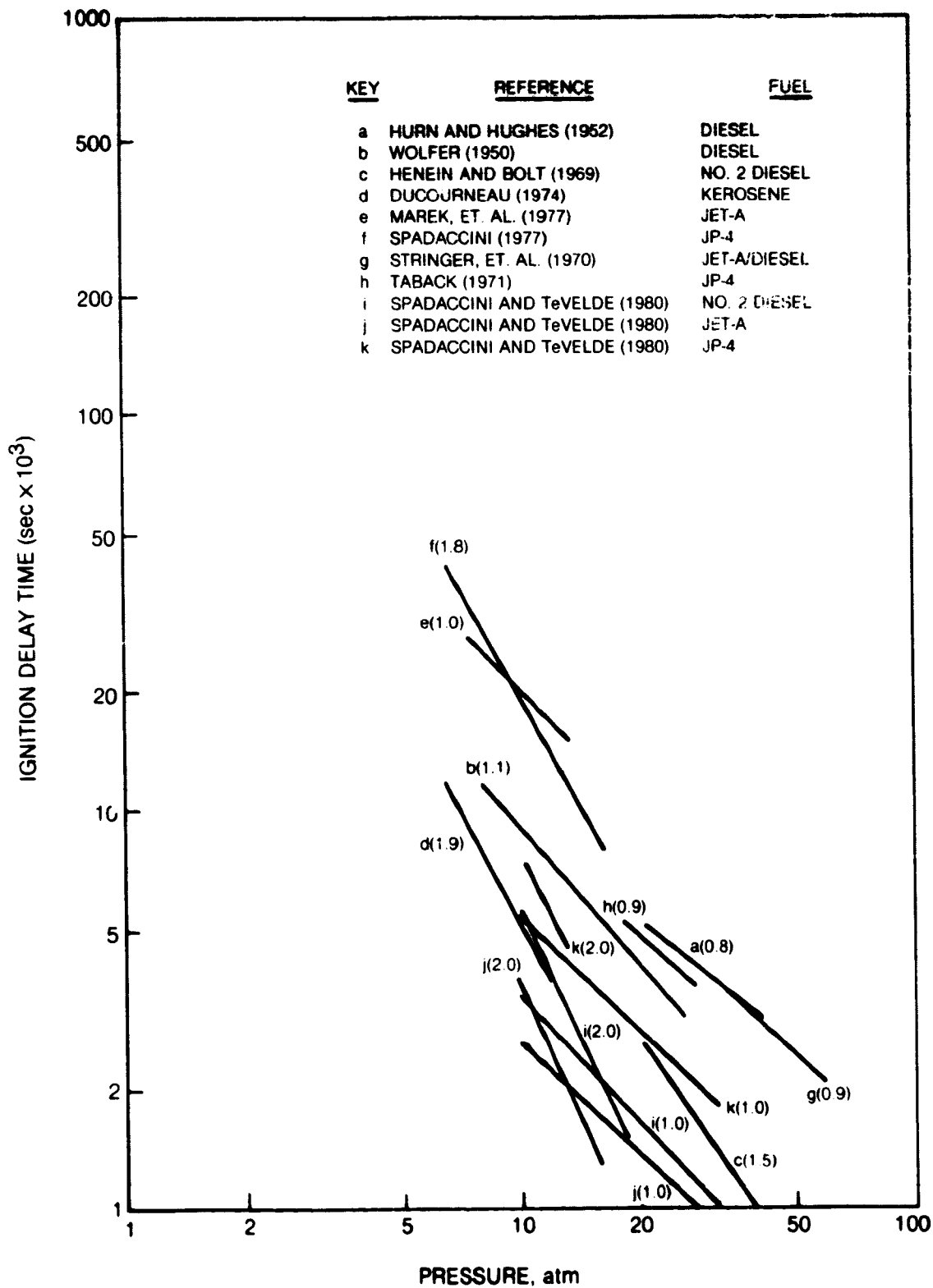
A, a, B	Constants
D_0	Droplet initial diameter
E	Activation energy
k	Reaction rate constant
n	Pressure exponent
P	Pressure
R	Universal gas constant
T	Temperature
t	Time
u	Velocity, dependent variable
X	Concentration
ϵ	Turbulent energy dissipation rate
K	Turbulent kinetic energy
τ	Ignition delay time
<u>Subscripts</u>	
F	Fuel
I	Intermediate species
i, j, k	Referring to i, j, k chemical species
<u>Superscripts</u>	
$\bar{}$	Mean value
$\delta $	Fluctuation

REFERENCES

- A.1 Affens, W. A. and H. W. Carhart: Ignition Studies - Part VII, The Determination of Autoignition Temperature, Naval Research Laboratory, NRL-7665, April 1974.
- A.2 Ballal, D. R. and A. H. Lefebvre: Ignition and Flame Quenching of Flowing Heterogeneous Fuel-Air Mixtures, Combustion and Flame, Vol. 35, 1979, pp. 155-168.
- A.3 Bilger, R. W.: The Structure of Diffusion Flames, Combustion Science and Technology, Vol. 13, Nos. 1-6, 1976, pp. 155-170.
- A.4 Brokaw: R. S.: Analytic Solutions to the Ignition Kinetics of the Hydrogen-Oxygen Reaction, Tenth Symposium (International) on Combustion, The Combustion Institute, 1965, pp. 269-278.
- A.5 Dopazo, C. and E. O'Brien: An Approach to the Autoignition of a Turbulent Mixture, Acta Astronautics, Vol. 1, 1974, pp. 1239-1266.
- A.6 Ducourneau, F.: Inflammation Spontanee de Melanges Riches Air-Kerosene, Entropie, N°59, 1974.
- A.7 Edelman, R., C. Economou and O. Fortune: Research on Methods of Improving the Combustion Characteristics of Liquid Hydrocarbon Fuels, Vol. II - Kinetics Modeling and Supersonic Testing, General Applied Sciences Laboratories, Technical Report AFAPL-72-24, Volume II, February 1972.
- A.8 El Wakil, M. M. and M. I. Abdou: The Self-Ignition of Fuel Drops in Heated Air Streams, Parts I-III, Fuel, Vol. 45, 1966, pp. 177-205.
- A.9 Faeth, G. M. and D. R. Olson: The Ignition of Hydrocarbon Fuel Droplets in Air, SAE Paper No. 68045, May 20-24, 1968.
- A.10 Gosman, A. D. and E. Ioannides: Aspects of Computer Simulation of Liquid Fueled Combustors, AIAA Paper No. 81-0323, January 1981.
- A.11 Halstead, M. P., L. J. Kirsch, A. Prothero and C. P. Quinn: A Mathematical Model for Hydrocarbon Autoignition at High Pressures, Proc. Royal Society of London, Series A, Vol. 346, 1975, pp. 515-538.
- A.12 Hautman, D. J., F. L. Dryer, K. P. Shug and I. Glassman: A Multiple Step Overall Kinetic Mechanism for the Oxidation of Hydrocarbons, Combustion Science and Technology, Vol. 25, 1981, pp. 219-235.

- A.13 Henein, N. A. and J. A. Bolt: Ignition Delay in Diesel Engines, SAE Paper 670007, 1967.
- A.14 Hurn, R. W. and K. J. Hughes: Combustion Characteristics of Diesel Fuels as Measured in a Constant-Volume Bomb, SAE Trans., Vol. 6, pp. 24-35, 1952.
- A.15 Ingebo, R. D.: Spontaneous Ignition Temperature Limits of Jet-A Fuel in Research Combustor Segment, NASA TM X-3146, November 1974.
- A.16 Kadota, T., H. Hiroyasu and H. Oya: Spontaneous Ignition Delay of a Fuel Droplet in High Pressure and High Temperature Gaseous Environments, Bulletin JSME, Vol. 19, No. 130, April 1976, pp. 437-445.
- A.17 Law, C. K. and S. H. Chung: An Ignition Criterion for Droplets in Sprays, Combustion Science and Technology, Vol. 22, 1980, pp. 17-26.
- A.18 Libby, P. A. and F. A. Williams: Some Implications of Recent Theoretical Studies in Turbulent Combustion, AIAA J., Vol. 19, No. 3, March 1981, pp. 261-274.
- A.19 Lockwood, F. C.: The Modeling of Turbulent Premixed and Diffusion Combustion in the Computation of Engineering Flows, Combustion and Flame, Vol. 29, 1977, pp. 111-122.
- A.20 Lockwood, F. C. and S. A. Syed: Consideration of the Problem of Combustion Modeling for Engineering Applications; Combustion Science and Technology, Vol. 19, 1979, pp. 129-140.
- A.21 Magnussen, B. F. and B. H. Hjertager: On Mathematical Modeling of Turbulent Combustion with Special Emphasis on Soot Formation and Combustion, Sixteenth Symposium (International) on Combustion. The Combustion Institute, 1976, pp. 719-729.
- A.22 Marek, C. J., L. C. Papathakos and P. W. Verbulecz: Preliminary Studies of Autoignition and Flashback in Premixing-Prevaporizing Flame Tube Using Jet-A Fuel at Lean Equivalence Ratios, NASA TM X-3526, May 1977.
- A.23 Mestre, A. and F. Ducourneau: Recent Studies of the Spontaneous Ignition of Rich Kerosene-Air Mixtures, Combustion Institute European Symposium, 1973.
- A.24 Miyasaka, K. and Y. Mizutani: Ignition of Sprays by an Incident Shock, Combustion and Flame, Vol. 25, 1975, pp. 177-186.
- A.25 Mullins, B. P.: Studies on the Spontaneous Ignition of Fuels Injected into a Hot Airstream; Parts I - VIII, Fuel No. 32, 1953.
- A.26 Myers, B. F. and E. R. Bartle: Reaction and Ignition Delay Time in the Oxidation of Propane, AIAA Journal, Vol. 7, 1969, pp. 1862-1869.

- A.27 Radhakrishnan, K., J. B. Heywood and R. J. Tabacsynski: Premixing Quality and Flame Stability: A Theoretical and Experimental Study, NASA Contractor Report 3216, December 1979.
- A.28 Rao, K. V. L. and A. H. Lefebvre: Spontaneous Ignition Delay Times of Hydrocarbon Fuel/Air Mixtures, Unpublished, Presented at NASA-Lewis Research Center, 1981.
- A.29 Sangiovanni, J. J.: A Model for the Nonsteady Ignition and Combustion of a Fuel Droplet, American Chemical Society, Symposium on Evaporization-Combustion of Fuel Droplets, San Francisco, CA, August 29-September 3, 1976.
- A.30 Satcunanathan, S.: Ignition Delay of Individual Liquid Fuel Droplets. Industrial and Engineering Chemistry Process Design and Development, Vol. 10, No. 3, 1971, pp. 297-304.
- A.31 Siminiski, V. J. and F. J. Wright: Research on Methods of Improving the Combustion Characteristics of Liquid Hydrocarbon Fuels, Vol. I - Experimental Determination of Ignition Delay Times in Subsonic Flow Systems, General Applied Sciences Laboratories, Technical Report AFAPL-72-24, Volume I, February 1972.
- A.32 Spadaccini, L. J.: Autoignition Characteristics of Hydrocarbon Fuels at Elevated Temperatures and Pressures, Journal of Engineering for Power, Trans. ASME, Vol. 99, Series A, January 1977.
- A.33 Spadaccini, L. J. and J. A. TeVelde: Autoignition Characteristics of Aircraft Type Fuels, NASA CR-159866, June 1980.
- A.34 Spadaccini, L. J. and J. A. TeVelde: Autoignition Characteristics of No. 2 Diesel Fuel, NASA CR-165315, June 1981.
- A.35 Spalding, D. B.: Concentration Fluctuation in a Round Turbulent Free Jet, Chemical Engineering Science, Vol. 26, 1971, pp. 95-107.
- A.36 Stringer, F. W., A. E. Clarke and J. S. Clarke: The Spontaneous Ignition of Hydrocarbon Fuels in a Flowing System, Proc. Auto. Div., Institution of Mechanical Engineers, 1970.
- A.37 Taback, E. D.: The Autoignition Characteristics of JP-4 at High Temperature and Pressure, P&WA TDM-2284, 1971.
- A.38 Wolfer, H. H.: Ignition Lag in Diesel Engines, Trans. by R. A. E., No. 358, 1950.
- A.39 Wood, B. J. and W. A. Rosser, Jr.: An Experimental Study of Fuel Droplet Ignition, AIAA Journal, Vol. 7, No. 12, December 1969, pp. 2288-2292.
- A.40 Yoshizawa, Y., H. Kowada, K. Shigihara, K. Yamada and Y. Takagishi: A Shock Tube Study on the Combustion Process Hydrocarbon Fuels, Bulletin JSME, Vol. 21, No. 153, March 1978, pp. 486-493.

SUMMARY OF DATA CORRELATIONS SHOWING
EFFECT OF PRESSURE ON IGNITION DELAY TIME

**SUMMARY OF DATA CORRELATIONS SHOWING
EFFECT OF TEMPERATURE ON IGNITION DELAY TIME**

